ANOMALOUS AND NONLINEAR EFFECTS IN INDUCTIVELY COUPLED PLASMAS

A Thesis Submitted
to the College of Graduate Studies and Research
in Partial Fulfillment of the Requirements
for the Degree of Doctor of Philosophy
in the Department of Physics & Engineering Physics
University of Saskatchewan

by

Yuriy O. Tyshetskiy

Saskatoon, Saskatchewan, Canada

PERMISSION TO USE

In presenting this thesis in partial fulfillment of the requirements for a Postgraduate degree from the University of Saskatchewan, it is agreed that the Libraries of this University may make it freely available for inspection. Permission for copying of this thesis in any manner, in whole or in part, for scholarly purposes may be granted by the professors who supervised this thesis work or, in their absence, by the Head of the Department of Physics and Engineering Physics or the Dean of the College of Graduate Studies and Research at the University of Saskatchewan. Any copying, publication, or use of this thesis, or parts thereof, for financial gain without the written permission of the author is strictly prohibited. Proper recognition shall be given to the author and to the University of Saskatchewan in any scholarly use which may be made of any material in this thesis.

Request for permission to copy or to make any other use of material in this thesis in whole or in part should be addressed to:

Head of the Department of Physics and Engineering Physics
116 Science Place
University of Saskatchewan
Saskatoon, Saskatchewan, S7N 5E2
Canada

ACKNOWLEDGEMENTS

ABSTRACT

In this thesis the nonlinear effects and heating are studied in inductively coupled plasma (ICP) in a regime of anomalous skin effect (nonlocal regime). In this regime the thermal motion of plasma electrons plays an important role, significantly influencing the processes associated with the penetration of electromagnetic field into plasma, such as the ponderomotive effect and heating of plasma by the field. We have developed a linear kinetic theory that describes the electron dynamics in ICP taking into account the electron thermal motion and collisions of electrons. This theory yields relatively simple expressions for the electron current in plasma, the ponderomotive force, and plasma heating. It describes correctly the thermal reduction of ponderomotive force in the nonlocal regime, which has been previously observed experimentally. It also describes the collisionless heating of plasma due to resonant interaction between the electromagnetic wave and plasma electrons. There is a good overall agreement of the results of our theory with the experimental data on ponderomotive force and plasma heating. Using our theory, we predicted a new effect of reduction of plasma heating compared to the purely collisional value, occurring at low frequencies. This effect has not been previously reported.

The nonlinear effects of the electromagnetic field on the electron distribution function and on plasma heating, that are not accounted for in the linear kinetic theory, have been studied using a quasilinear kinetic theory, also developed in this thesis. Within the quasilinear approximation we have formulated the system of equations describing the slow response of plasma electrons to the fast oscillating electromagnetic field. As an example, these equations have been solved in the simplest case of cold plasma with collisions, and the nonlinear perturbation of the electron distribution function and its effect on the plasma heating have been found. It has been shown that the nonlinear modification of plasma heating occurs mainly due to the nonlinear effect of the magnetic

component of the electromagnetic field. It has also been shown that at high frequencies the nonlinear effects vanish, and the heating is well described by the linear theory.

To verify the predicted new effect of plasma heating reduction at low frequencies, as well as to investigate the nonlinear effect of the magnetic field on plasma heating for arbitrary amplitudes of electromagnetic field in plasma, we have developed a 1d3v Particle-In-Cell (PIC) numerical simulation code with collisions. The collisions were implemented into the PIC code using two different techniques: the direct Monte-Carlo technique for the electron-atom collisions, and the stochastic technique based on the Langevin equation for the electron-electron collisions. The series of numerical simulations by this code confirmed the results of our linear theory, particularly the effect of heating reduction at low frequencies that we predicted theoretically. Also, the nonlinear effects of electromagnetic field on plasma heating were studied using the PIC code in the cases of weak and strong electromagnetic fields. It has been shown that in the case of weak electromagnetic fields (corresponding to weak nonlinearity) the nonlinear effects lead to some enhancement of heating (compared to the linear theory) at low frequencies, followed by a small reduction of heating at higher frequencies. This observed nonlinear perturbation of heating in warm plasma with collisions is similar to that predicted by the quasilinear theory for the case of cold plasma with collisions. In the case of strong electromagnetic fields (corresponding to strong nonlinearity) the nonlinear effects lead to a further reduction of heating (compared to the linear theory) at low frequencies, as shown by the simulation, thus adding to the effect of reduction of heating predicted by the linear theory. The nonlinear effects are shown to vanish at high frequencies, as expected.

Table of Contents

List of Figures

ix

List of Tables

List of Symbols

Comments:

1. This list of symbols is complementary to the explanations of the meanings of the symbols in the text.

2. Vector quantites are indicated by bold face.

3. Perturbed quantites are indicated by different means. Examples are $\tilde{f}$ (tilde over the symbol representing the quantity), f_1 (subscript), and δf.

Operators:

∇	Gradient operator
$\langle ... \rangle$	Averaging in time over period of field oscillations; also used as averaging over distribution function
$\overline{(...)}$	Averaging over velocity directions
$\hat{S}$	Collisional operator
$\hat{S}_{ee}$	Collisional operator for electron-electron collisions
$\hat{S}_{ei}$	Collisional operator for electron-ion collisions
$\hat{S}_{en}$	Collisional operator for electron-atom collisions
$\hat{S}_{ql}$	Quasilinear operator

Latin symbols:

$\mathbf{A}$	Random isotropic vector
$\mathbf{B}$	Magnetic field
B_x, B_r, B_z	Axial and radial components of magnetic field in cylindrical model, z - component of magnetic field in planar model
c	Speed of light in vacuum
D_{ij}	Tensor of electron diffusion in velocity phase space

$\mathbf{E}, E_y, E_\theta$	Electric field, y - and θ - components of electric field
E_k	Fourier component of electric field
E_0	Amplitude of electric field in plasma
$\mathrm{Ei}\,(...)$	Exponential integral
$\mathrm{erf}\,(...)$	Error function
$\mathrm{erfc}\,(...)$	Complementary error function
$\mathbf{F}_p, F_p$	Ponderomotive force
F_M	Miller ponderomotive force
$\mathbf{F}_L$	Lorentz force
e_α	Electric charge of particles of the α species
e	Elementary charge
f_α	Distribution function of particles of the α species
f_{0e}, F_0	Equilibrium (background) distribution function of electrons
δF	Nonlinear perturbation of electron distribution function
$\widetilde{f}$	Oscillating perturbation of electron distribution function
$f^{(+)}$	Perturbation of distribution function of electrons moving away from the plasma boundary
$f^{(-)}$	Perturbation of distribution function of electrons moving towards the plasma boundary
f_k	Fourier component of electron distribution function
f_n	n-th temporal harmonic of perturbed electron distribution
f_M	Maxwell distribution function
$\mathbf{H}$	Magnetic induction
$\mathbf{j}$	Current density
j_y	y - component of current density
j_k	Fourier component of current density
J_1	Cylindrical Bessel function of the first order
k	Wave number
L	Length of discharge
m_e, m_i, m_n	Mass of electron, mass of ion, mass of neutral atom
N	Number of simulation particles
n_α	Number density of particles of the α species
n_0	Equilibrium plasma density
p_α	Pressure of plasma component of the α-th sort
$\mathbf{p}$	Wave momentum
P, P_{pl}	Discharge power

Q	Heating source
Q_L	Linear heating source
δQ	Nonlinear perturbation of heating source
q_i	Charge of i-th simulation particle
r, r_i, r_t, r_θ, r_φ	Random numbers in the range $[0,1]$
R	Radius of cylindrical discharge chamber; also coefficient of reflection
s	Parameter of nonlocality of discharge regime
S	Absorbed power flux
S_{tot}	Total absorbed power flux
S_{coll}	Purely collisional absorbed power flux
T_α	Temperature of particles of the α species
T_e	Temperature of electrons
t	Time
Δt	Timestep in PIC simulation
U, U_p	Ponderomotive potential
U_M	Miller ponderomotive potential
$\mathbf{v}$, v_x, v_y, v_z	Velocity and its components
$\mathbf{v}_\alpha$	Velocity of particles of the α species
v_E	Oscillatory velocity of electrons in electromagnetic field
v_{Te}	Thermal velocity of electrons
v_{ph}	Phase velocity of wave
V	Plasma potential
w	Absorbed power density
w_k	Spectral density of absorbed power
W	Coefficient of absorption
x, y	Spatial coordinates
x_i	Spatial coordinate of i-th simulation particle
Δx	Length of spatial grid cell in PIC simulation
X_j	Position of j-th gridpoint in PIC simulation
$Z(p)$	Plasma dispersion function
Z_H	Surface impedance

Greek symbols:

γ	Complex wave vector
γ_0	Adiabatic index
δ	Skin depth; characteristic scale of field inhomogeneity in plasma
δ_a	Anomalous skin depth
ε	Electron kinetic energy, average electron kinetic energy
η	Ratio of total plasma heating to purely collisional heating
θ	Azimuthal coordinate
κ	Imaginary part of complex wave vector
Λ	Fundamental measure of plasma nonlocality, similar to s
$\ln \Lambda_{ee}$	Coulomb logarithm
λ_D	Debye length
λ_E	Characteristic depth of penetration of electric field into plasma
λ_H	Characteristic depth of penetration of magnetic field into plasma
λ_{eff}	Effective mean free path
$\mu,\ \mu_0$	Magnetic permittivity of plasma and of vacuum
ν_α	Effective frequency of collisions of particle of species α
ν_e	Effective electron collision frequency
ν_{en}	Electron-atom collision frequency
$\xi,\ \xi_{B=0}$	Ratio of nonlocal perturbation of plasma heating to linear heating, with and without magnetic field
ρ	Charge density
σ	Plasma conductivity
Σ_a	Anomalous plasma conductivity
$\sigma_a(k)$	Fourier image of anomalous plasma conductivity
$\phi_E,\ \phi_J$	Phases of electric field and electric current in plasma
ω	Frequency of electromagnetic field oscillations
ω_{pe}	Electron plasma frequency
ω_c	Electron cyclotron frequency

Chapter 1

Introduction

1.1 Inductively Coupled Plasma (ICP) Sources

In this thesis we study the phenomena occurring in low-pressure high density plasmas in the regime of anomalous skin effect. To introduce the object of our study to the reader, we will start from the general definition of plasma. There is a number of various definitions of plasma at various levels, the most basic and the less informative of which is the definition "plasma is the fourth state of matter". A more informative definition is that plasma is an ionized gas – a gas in which some or all atoms lost one or more electrons, thus becoming charged (these charged atoms are called ions). As a result, the ionized gas contains some number of charged particles – electrons and ions – that make it conductive. The Coulomb interaction between the charged particles is long-ranged, therefore the ionized gas may exhibit a collective behavior which is far more complex than that of usual, neutral gases. However, not any ionized gas is plasma. An important property of plasma is quasineutrality – an overall electrical neutrality of the plasma media. This means that the total charge of negatively charged particles should be approximately equal to the total charge of positively charged particles within any selected volume of plasma (the volume of a size that is large compared to the characteristic distance between the

1

plasma particles). A related important phenomenon, which is sometimes used to define the plasma state, is the screening of electric fields within plasma at a characteristic length called the Debye length. The Debye length is an important characteristic of plasma that depends on plasma electron temperature T_e and density n, $\lambda_D = (k_B T_e / 4\pi n e^2)^{1/2}$, where k_B is the Boltzmann constant, e is the elementary charge (here and hereafter we use the CGS system of units). The derivation of the Debye length as the length of screening of electric field in plasma can be found, for example, in [1].

The requirement for the plasma state to occur is that the kinetic energy of electrons in the system significantly exceeds their potential energy. Mathematically this requirement can be expressed in terms of number of charged particles N_D within a sphere of radius equal to the Debye length λ_D (a so-called Debye sphere), which should be large:

$$N_D = n \frac{4\pi}{3} \lambda_D^3 >> 1. \tag{1.1}$$

Most of a matter in the Universe is in plasma state; examples are the sun and stars, interstellar gas, Earth's ionosphere and magnetosphere, visible part of lightning bolts, etc. Plasma can also be created in laboratory by various means, such as heating of a gas until the mean kinetic energy of the gas particles is comparable to the ionization potential of the gas atoms or molecules. At very high temperatures, from about $50000\,K$ upwards, collisions between gas particles cause cascading ionization of the gas. Another way of creating plasma in laboratory is heating a gas by an applied electric field (fluorescent lamps are an example), which accelerates charged particles that are already in the gas until they gain the kinetic energy necessary to ionize the gas atoms. This way of creating plasma does not require high temperature, and thus it is more favorable for applications. The temperature of neutral component of such gas plasma may remain quite low as the plasma particles are continually colliding with walls of the gas container and between each other, causing cooling and recombination (the process of recreating neutral atoms from ions and

2

electrons; this process is opposite to the ionization). In such cases ionization is only partial and requires a large energy input. In thermonuclear reactors an enormous plasma temperature necessary to maintain the thermonuclear fusion reactions is created by launching a strong heating electric current through the plasma being confined away from the container walls by magnetic field.

The applications of plasmas range from material processing (deposition of films onto substrate, etching, etc.) and manufacturing of microchips, to generation of energy by thermonuclear fusion reactions. The number of plasma applications is constantly and rapidly growing.

In this thesis we will be dealing with the low-temperature plasmas ($T_e <$ 10 eV), which are mostly used in semiconductor manufacturing, material processing, and in lighting sources. Such plasmas are produced by different types of the so-called glow discharges, apparently called so because of the glow coming from the plasma created. Currently, there is a trend toward low-pressure (< 10 mTorr) operation of these discharges to provide better plasma uniformity over large area substrates. Low operating pressures require high plasma densities to maintain productivity of industrial manufacturing and processing devices. A number of different types of low pressure high-density plasma discharges are being developed, among them inductively coupled plasma (ICP) discharges, which are particularly attractive due to their relatively simple design.

In the ICP discharges, the plasma is created by ionizing of a working gas by a time varying electric field $\mathbf{E}(t)$, which is induced by a time varying magnetic field $\mathbf{B}(t)$ through Faraday's law

$$\nabla \times \mathbf{E}(\mathbf{r},t) = -\frac{1}{c}\frac{\partial \mathbf{B}(\mathbf{r},t)}{\partial t}. \tag{1.2}$$

The magnetic field $\mathbf{B}(t)$ is created by a time varying electric current running through an antenna coil located *outside* of a gas-containing chamber.

There are two principal configurations of the ICP discharges: a configuration with a cylindrical coil and a configuration with a planar coil. The schemes

3
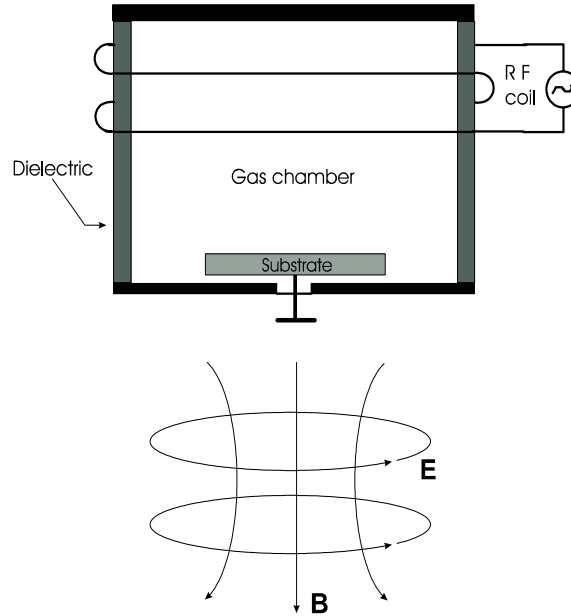
Figure 1.1: Configuration of ICP discharge with cylindrical coil.

of both configurations along with the sketches of the electromagnetic fields in plasma are shown in Fig. 1.1 (cylindrical coil configuration) and Fig. 1.2 (planar coil configuration).

In the cylindrical coil configuration, the radio frequency (RF) current coil is wound around the cylindrical chamber containing the working gas, while in the planar coil configuration the coil, resembling the stovetop heating coil, is located on top of the cylindrical gas chamber. In both configurations the coil is separated from the chamber by dielectric wall in order to allow the electromagnetic fields to penetrate into the gas chamber volume. The plasma is created in the region of the most intense electric fields through the ionization process similar to the process described above for the fluorescent lamps.

From the electrodeless design of the ICP discharges follows one of their advantages – absence of contamination of plasma by the electrode material. Another advantageous feature of ICP discharges is the possibility to achieve higher densities of ions at lower pressures. Also, the plasma created in ICP

4
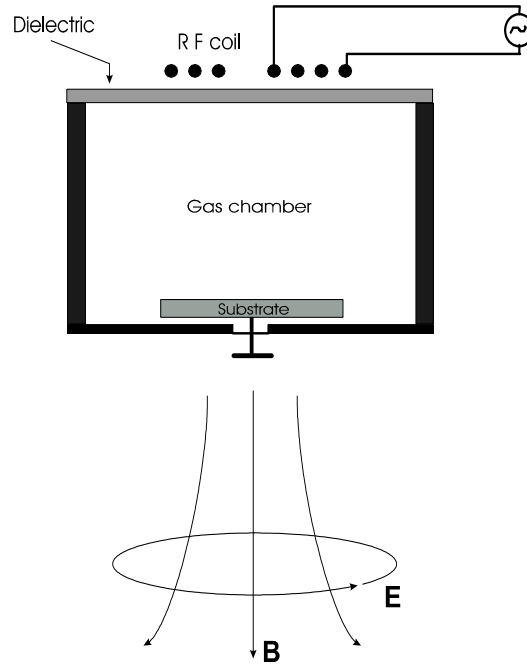
Figure 1.2: Configuration of ICP discharge with planar coil.

discharges has a high degree of uniformity, which is typically a requirement in plasma processing and semiconductor manufacturing.

The typical parameters of ICP discharges are given in Table 1.1.

Pressure, mTorr	Plasma density, cm^{-3}	Driving frequency, MHz	Electron temperature, eV	Electron-atom collision frequency, s^{-1}	Discharge power, W
0.1-100	10^{10}-10^{12}	0.1-20	1-10	10^6-10^8	50-500

Table 1.1: Ranges of typical parameters of ICP discharges.

The ICP discharges have found many applications. Among them, there is an application in plasma processing, which is a vital step in producing large-scale integrated chips. Another application is in mass-spectrography, where the

ICP discharges are used as plasma sources. Recently, the ICP has found an application in the area of electrodeless fluorescent lamps, being manufactured by OSRAM Sylvania and Phillips. Because these lamps are electrodeless, they have significantly longer lifetime than conventional fluorescent lamps – up to 8 years compared to 3 years for the conventional fluorescent lamps.

Recently, there has been a trend towards lower driving frequencies used in the ICP discharges. This reduces the cost of power supply for the plasma discharge. Low driving frequencies, together with the low pressures and significant electron temperature regimes, drive the plasma into a regime of the so-called anomalous skin effect, also called a nonlocal regime [2, 3, 4, 5, 6]. This regime, its features and difference from the regime of classical skin effect will be discussed in the next section of this chapter.

1.2 Penetration of Electromagnetic Wave into Plasma: A Brief Review

At first, we will review briefly a process of penetration of electromagnetic wave into plasma. A self-consistent system of equations describing the penetration of electromagnetic field into plasma consists of Maxwell's equations:

$$\nabla \times \mathbf{E} = -\frac{1}{c}\frac{\partial \mathbf{B}}{\partial t}; \tag{1.3}$$

$$\nabla \times \mathbf{H} = \frac{4\pi}{c}\mathbf{j} + \frac{1}{c}\frac{\partial \mathbf{E}}{\partial t}; \tag{1.4}$$

$$\nabla \cdot \mathbf{E} = 4\pi\rho \; ; \tag{1.5}$$

$$\nabla \cdot \mathbf{B} = 0 \,, \tag{1.6}$$

where ρ is a charge density $\rho = \sum_{\alpha} e_{\alpha}n_{\alpha}$ and $\mathbf{j}$ is a current density $\mathbf{j} = \sum_{\alpha} e_{\alpha}n_{\alpha}\mathbf{v}_{\alpha}$, $\mathbf{H} = (\mu\mu_0)^{-1}\mathbf{B}$, μ_0 is the magnetic permittivity of vacuum ($\mu_0 = 1$ in Gaussian system of units), μ is the magnetic permittivity of media. Here the index α corresponds to a fluid of particles of sort α, usually electrons ($\alpha = e$) and ions

$(\alpha = i)$. Correspondingly, e_α is the charge of particles of the sort α, n_α is the density of these particles, and $\mathbf{v}_\alpha$ is the flow velocity of the fluid of sort α. The charge and current densities should be expressed in terms of electric and magnetic fields $\mathbf{E}$ and $\mathbf{B}$, and plasma-related quantities, in order to make the system of equations closed. The simplest way to close the system of equations is to use the so-called hydrodynamic approximation. In this approximation, the charge and current densities are expressed in terms of $\mathbf{E}$ and $\mathbf{B}$ using hydrodynamic equation of motion:

$$\frac{\partial \mathbf{v}_\alpha}{\partial t} + (\mathbf{v}_\alpha \cdot \nabla)\,\mathbf{v}_\alpha = \frac{e_\alpha}{m_\alpha}\left(\mathbf{E} + \frac{1}{c}\mathbf{v}_\alpha \times \mathbf{B}\right) - \frac{\nabla p_\alpha}{m_\alpha n_\alpha} - \nu_\alpha \mathbf{v}_\alpha\,, \qquad (1.7)$$

and equation of continuity of the conducting fluid of sort α without sources and sinks:

$$\frac{\partial n_\alpha}{\partial t} + \nabla \cdot (n_\alpha \mathbf{v}_\alpha) = 0\,. \qquad (1.8)$$

In the equation of motion (1.7) p_α is the pressure of the fluid of sort α, ν_α is the effective frequency of collisions of particles of sort α with other particles, c is the speed of light in vacuum. All terms in the right-hand side of (1.7) correspond to forces acting on the element of fluid of sort α: the first term corresponds to the forces exerted by the electromagnetic field on the conducting fluid, the second term corresponds to the force due to pressure gradient in the fluid (hydrostatic force), and the third term corresponds to the friction due to interparticle collisions.

Our system (1.3-1.8) needs one more equation in order to be closed; this is an equation of state, which relates the pressure p_α and the fluid density n_α and temperature T_α. If we assume the adiabatic change of the state of plasma components (fluids of sort α), the equation of state is

$$p_\alpha = \gamma_0 T_\alpha n_\alpha = (\gamma_0/2) m_\alpha v_{T\alpha}^2 n_\alpha\,, \qquad (1.9)$$

where $v_{T\alpha} = (2T_\alpha/m_\alpha)^{1/2}$ is an average thermal velocity of particles of sort α, γ_0 is the adiabatic index.

The hydrodynamic approximation, however, has some limitations, for example, it is invalid if the plasma particle mean free path (the length of particle's path between collisions) v_{Te}/ν_e, or the distance that a particle travels during a period of field oscillations v_{Te}/ω, exceeds a characteristic length of plasma or field inhomogeneity. In such cases a more rigorous and general, yet more complicated, kinetic treatment is needed. It is based on the concept of a distribution function $f_\alpha(t, \mathbf{r}, \mathbf{v})$ of particles of sort α. The distribution function is a statistical description of ensemble of plasma particles. The quantity $f_\alpha(t, \mathbf{r}, \mathbf{v})\, d\mathbf{r}\, d\mathbf{v}$ is a probability to locate a particle of sort α, which has velocity in the range $[\mathbf{v}, \mathbf{v}+d\mathbf{v}]$, in position with coordinates in the range $[\mathbf{r}, \mathbf{r}+d\mathbf{r}]$, at the time instant t. The equation governing the behavior of the distribution function is the Boltzmann equation:

$$\frac{\partial f_\alpha}{\partial t} + \mathbf{v} \cdot \frac{\partial f_\alpha}{\partial \mathbf{r}} + \frac{1}{m_\alpha} \mathbf{F}_\alpha \cdot \frac{\partial f_\alpha}{\partial \mathbf{v}} = \hat{S}\left(f_\alpha\right), \tag{1.10}$$

where $\mathbf{F}_\alpha$ is the total force acting on a particle of sort α, $\hat{S}\left(f_\alpha\right)$ is the collisional operator which describes the evolution of the distribution function due to collisions of all kinds between a particle of the sort α and all other particles. In our consideration of electromagnetic wave penetration into plasma the total force $\mathbf{F}_\alpha$ is

$$\mathbf{F}_\alpha = e_\alpha \left(\mathbf{E} + \frac{1}{c} \mathbf{v} \times \mathbf{B} \right). \tag{1.11}$$

Note that this is the force acting on a particle, while in the hydrodynamic equation of motion (1.7) the forces act on a fluid element.

The charge density ρ and the current density $\mathbf{j}$ are expressed in terms of the distribution function f_α in the following fashion:

$$\rho = \sum_\alpha e_\alpha \int_{\mathbf{v}} f_\alpha \, d\mathbf{v}, \tag{1.12}$$

$$\mathbf{j} = \sum_\alpha e_\alpha \int_{\mathbf{v}} \mathbf{v} \, f_\alpha \, d\mathbf{v}. \tag{1.13}$$

Here the integration is performed over the whole velocity space. The distribution function f_α is expressed in terms of the fields $\mathbf{E}$ and $\mathbf{B}$ through (1.10).
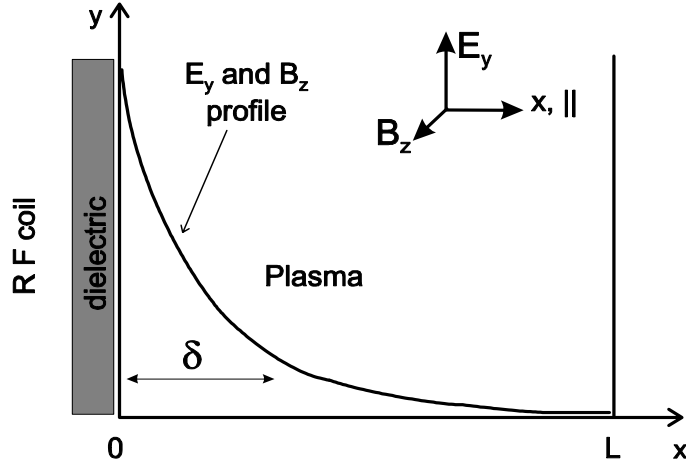
Figure 1.3: The idealized model of ICP of length L. The coordinate system and typical RF field variation. The RF coil is to the left of $x = 0$.

Now that we have the system of equations describing the electromagnetic field in plasma in either hydrodynamic or kinetic approximation, let us consider the idealized model of either planar coil or cylindrical coil ICP, which is a model of plasma slab [7] sketched on Fig. 1.3. In the case of planar coil configuration, x corresponds to the axial coordinate of the cylindrical ICP, and z corresponds to the radial coordinate, whereas in the case of cylindrical coil configuration, x corresponds to the radial coordinate of the cylindrical ICP, and z corresponds to the axial coordinate. In both cases, y represents the azimuthal coordinate (azimuthal is the direction of the electric field in either configuration). The electromagnetic field in the system can be represented as the field of a linearly polarized electromagnetic wave with the field components E_y, B_z (TE-wave), incident on plasma from the region $x < 0$ (where the antenna coil is located) at a direct (90°) angle. The electromagnetic field spatially decays with a characteristic decay length δ, in the x-direction away from the position of the antenna coil.

The idealization of this model is in assuming of strictly azimuthal symmetry of the fields, while this is not exactly so in the real ICPs. Nevertheless,

9

this idealized discharge model is applicable to describing real discharges if the azimuthal asymmetry is not too large. Although the real discharge is cylindrical, we can use the idealized model of a planar plasma slab if the cylinder radius is not small, i.e. $R > \delta$. Typically, R is of the order of 10 cm, while δ is of the order of 1 cm, therefore the idealized model is well applicable for describing cylindrical plasma discharge.

The incident wave will partially reflect from plasma, and partially will penetrate into plasma; the amplitudes of the reflected and penetrated waves are determined from the boundary conditions for the electric and magnetic fields, which should be satisfied at any point of the plasma boundary at any moment of time. Therefore, if the dependence of fields of the incident wave on time t is defined by $\exp(-i\omega t)$, the same time dependence should hold for the fields of both reflected and penetrated waves, in linear theory and if the plasma is stationary.

Let us derive an equation for the electric field of the wave in plasma and in vacuum. Taking the curl of the first Maxwell's equation (1.3) we get:

$$\nabla \times \nabla \times \mathbf{E} = -\frac{1}{c}\frac{\partial}{\partial t}\nabla \times \mathbf{B}\,, \tag{1.14}$$

and, using the second Maxwell's equation (1.4), we have

$$\nabla \times \nabla \times \mathbf{E} = -\frac{4\pi}{c^2}\frac{\partial \mathbf{j}}{\partial t} - \frac{1}{c^2}\frac{\partial^2 \mathbf{E}}{\partial t^2}. \tag{1.15}$$

Using identity $\nabla \times \nabla \times \mathbf{E} = \boldsymbol{\nabla}(\nabla \cdot \mathbf{E}) - \nabla^2\mathbf{E}$ and the third Maxwell's equation (1.5), we get for the left hand side $\nabla \times \nabla \times \mathbf{E} = \boldsymbol{\nabla}(4\pi\rho) - \nabla^2\mathbf{E}$. Since the electromagnetic wave is transverse, and the electric field E_y is directed along the plasma boundary, there is no charge separation in plasma due to this field, and therefore $\boldsymbol{\nabla}(4\pi\rho) = 0$. Finally, taking into account the time dependence of the fields $\exp(-i\omega t)$ and replacing $\partial/\partial t$ with $-i\omega$, we obtain a wave equation for the electric field in plasma:

$$\nabla^2\mathbf{E} + \frac{\omega^2}{c^2}\mathbf{E} = -\frac{4\pi i\omega}{c^2}\mathbf{j}, \tag{1.16}$$

10

and in vacuum:

$$\nabla^2 \mathbf{E} + \frac{\omega^2}{c^2} \mathbf{E} = 0. \tag{1.17}$$

The magnetic fields in plasma and in vacuum are defined from the electric field using (1.3).

Now it is easy to write down the fields of the incident and reflected waves in vacuum, using (1.17). For the incident wave $E_{yi} = E_0 \exp\left(i\left(\omega/c\right)x\right)$, $B_{zi} = E_{yi}$, and for the reflected wave $E_{yr} = RE_0 \exp\left(-i\left(\omega/c\right)x\right)$, $B_{zr} = -E_{yr}$, where E_0 is the amplitude of the incident wave, R is the reflection coefficient (here we dropped the common multiplier $\exp\left(-i\omega t\right)$). The fields of the penetrated wave in plasma are defined by the Eq. (1.16). The reflection coefficient R and the amplitude of the penetrated wave in plasma $E(0)$, $B(0)$ are determined by the condition of continuity of tangential components of electric and magnetic fields at the plasma boundary $x = 0$:

$$A_i(0) + A_r(0) = A(0); \quad A = E_y \text{ or } B_z. \tag{1.18}$$

Here A_i, A_r are the amplitudes of incident and reflected wave, respectively, and $A(0)$ is the amplitude of the fields in plasma (penetrated wave). Equation (1.16) needs to be closed by an equation that relates the current density $\mathbf{j}$ with the electric field $\mathbf{E}$ in plasma (Ohm's law). This relation between $\mathbf{j}$ and $\mathbf{E}$ depends on plasma properties, and it defines how the electromagnetic field penetrates into plasma. Below we will review briefly the penetration of electromagnetic wave into cold plasma (classical skin effect) and into warm plasma (anomalous skin effect).

1.2.1 Skin Effect

Classical Skin Effect

First let us consider penetration of the electromagnetic wave into cold plasma consisting of two sorts of charged particles, electrons and ions, and neutral gas atoms. "Cold" means that both the electron mean free path v_{Te}/ν_e

11

(here v_{Te} is the electron mean thermal velocity, and ν_e is the frequency of collisions of the electron with all other particles) and the distance that a thermal electron travels during the period of fields oscillations v_{Te}/ω is small compared to the characteristic length δ of fields inhomogeneity in plasma, $v_{Te}/\delta << \omega, \nu_e$. The ions are assumed to be cold and immobile. The case of cold plasma can be treated within the hydrodynamic approximation (1.7-1.8). Since the ions are immobile, the only meaningful fluid equations are the equations of motion and of continuity for the cold electron component of the plasma:

$$\frac{\partial \mathbf{v}_e}{\partial t} + (\mathbf{v}_e \cdot \nabla) \mathbf{v}_e = -\frac{e}{m_e} \left(\mathbf{E} + \frac{1}{c} \mathbf{v}_e \times \mathbf{B} \right) - \nu_e \mathbf{v}_e , \qquad (1.19)$$

$$\frac{\partial n_e}{\partial t} + \nabla \cdot (n_e \mathbf{v}_e) = 0 . \qquad (1.20)$$

Let us consider weak fields; the electron fluid velocity and density can then be represented as $\mathbf{v}_e = \mathbf{v}_{0e} + \tilde{\mathbf{v}}_e$ and $n_e = n_{0e} + \tilde{n}_e$ respectively, where $\mathbf{v}_{0e}$ and n_{0e} are the equilibrium values, and $\tilde{\mathbf{v}}_e$ and $\tilde{n}_e$ are the small perturbed values due to the weak fields, $\tilde{\mathbf{v}}_e << \mathbf{v}_{0e}$, $\tilde{n}_e << n_{0e}$. This separation allows us to simplify the problem by linearizing the Eq. (1.19), yielding

$$\frac{\partial \tilde{\mathbf{v}}_e}{\partial t} = -\frac{e}{m_e} \left(\mathbf{E} + \frac{1}{c} \mathbf{v}_{0e} \times \mathbf{B} \right) - \nu_e \tilde{\mathbf{v}}_e . \qquad (1.21)$$

As the plasma is stationary, the time dependence of $\tilde{\mathbf{v}}_e$ is the same as that of $\mathbf{E} \sim \exp(-i\omega t)$. Replacing the time derivative with $-i\omega$, we get for the electron fluid velocity perturbation due to the electric field:

$$\tilde{\mathbf{v}}_e = -\frac{e}{m_e} \frac{i}{\omega + i\nu_e} \mathbf{E}. \qquad (1.22)$$

The electric current density is $\mathbf{j} \equiv -e n_e \mathbf{v}_e$. Neglecting the term proportional to E^3, which is small, we get for the current density

$$\mathbf{j} = -e n_{0e} \tilde{\mathbf{v}}_e = \frac{e^2 n_{0e}}{m_e} \frac{i}{\omega + i\nu_e} \mathbf{E}, \qquad (1.23)$$

which represents the Ohm's law for cold plasma, $\mathbf{j} = \sigma \mathbf{E}$, where $\sigma = (i/4\pi) \times \times \omega_{pe}^2/(\omega + i\nu_e)$ is the conductivity of the cold plasma, and $\omega_{pe} = \sqrt{4\pi e^2 n_{0e}/m_e}$

is the electron plasma frequency. Using (1.23), the equation (1.16) for the electric field $E_y(x,t)$ in plasma becomes

$$\frac{\partial^2 E_y}{\partial x^2}+\frac{\omega^2}{c^2}E_y = -\frac{\omega_{pe}^2}{c^2}\frac{\omega}{\omega + i\nu_e}E_y. \tag{1.24}$$

From (1.24) it is now possible to write down the fields in plasma as $E_y(x) = E_y(0)\exp(ikx)$, $B_z(x) = (ck/\omega)\,E_y(x)$, where the wavenumber k is defined as

$$k^2 = \frac{\omega^2}{c^2} + \frac{\omega_{pe}^2}{c^2}\frac{\omega}{\omega + i\nu_e}. \tag{1.25}$$

If k is an imaginary or complex number, then the fields in plasma exponentially decay away from the plasma boundary, $E_y(x) = E_y(0)\exp(-\operatorname{Im}(k)x + i\operatorname{Re}(k)x)$ (note that, in order to rule out the exponentially growing solution, we take $\operatorname{Im}(k) > 0$ for k defined from (1.25) in semi-infinite plasma). This fast spatial decay of the electromagnetic field in plasma is called a *skin effect*. In the case of high frequencies ω the collisions can be neglected, and for $\nu_e << \omega < \omega_{pe}$ we have a collisionless skin effect (k is purely imaginary). For the case $\omega > \omega_{pe} >> \nu_e$ the electromagnetic wave propagates in plasma without decaying (k is real), i.e. there is no skin effect. In a general case, k is a complex number.

We can introduce the characteristic depth of penetration of the electromagnetic wave into plasma, $\delta = (\operatorname{Im}(k))^{-1}$, which is also called a *skin depth*. This is the depth at which the amplitude of the decaying fields of the wave is reduced by a factor of $e = 2.71...$ The skin depth is defined from (1.25) as

$$\delta = \frac{c}{\omega_{pe}}\left(1 + \frac{\nu_e^2}{\omega^2}\right)^{1/4}\frac{1}{\cos\left(\phi/2\right)}, \tag{1.26}$$

where $\phi = \arctan\left(\nu_e/\omega\right)$ [2] (the term ω^2/c^2, corresponding to the displacement current $(1/c)\,\partial\mathbf{E}/\partial t$, has been neglected in derivation of (1.26). This can be done for relatively low frequencies, such as RF). In the case of high frequencies $\nu_e << \omega < \omega_{pe}$ the skin depth does not depend on the wave frequency, $\delta = c/\omega_{pe}$ (collisionless limit). In a low frequency limit or in a highly collisional plasma, $\nu_e >> \omega$, $\omega_{pe}^2 >> \nu_e\omega$, the skin depth is $\delta = c/\omega_{pe}\left(2\nu_e/\omega\right)^{1/2}$.

The skin effect in cold plasma considered here is called the *classical skin effect*, and (1.26) defines the *classical skin depth*. The regime of classical skin effect is also called the *local regime* [3]. This name comes from the form of the Ohm's law in cold plasma (1.23): the relation between the electric field and current in plasma is "local", i.e. the current at some location in plasma depends only on the electric field at the very same location. However, this is true only in a cold plasma, when $v_{Te}/\delta << \omega, \nu_e$; if the electrons are not cold, the Ohm's law does not have the simple local form (1.23) anymore, and the skin effect is much more complex than the classical skin effect.

Anomalous Skin Effect

Let us now consider the penetration of the electromagnetic wave into plasma with the electrons that are not cold anymore; the ions are still assumed to be cold and immobile. With the electrons being "warm" the condition for the classical skin effect is violated, so that $\omega, \nu_e \lesssim v_{Te}/\delta$. With the characteristic wavenumber of the electromagnetic wave $k \sim 1/\delta$ this condition implies that the electron mean thermal velocity is of the order of, or larger than, the wave phase velocity, and the mean free path of an electron v_{Te}/ν_e is larger than the characteristic scale of the field inhomogeneity. The shape of the electromagnetic field in plasma, as well as the characteristic depth of its penetration into plasma, depends critically on the form of Ohm's law, which does not have the simple form (1.23) for warm electrons $\omega, \nu_e \lesssim v_{Te}/\delta$. As an electron travels a significant distance between collisions, it is affected by the electromagnetic field along its whole path (the electron "samples" the field), before a next collision randomizes its velocity. Therefore, the velocity of a thermal electron depends not only on the electromagnetic field at the electron's current location, as in the case of cold electrons, but also on the field along the whole path of the electron. The relation between the electron current and

the electric field has a "nonlocal" form:

$$\mathbf{j}(x) = \int \sigma(x, x') \mathbf{E}(x') \, dx', \qquad (1.27)$$

where $\sigma(x, x')$ is the "nonlocal conductivity", and the integration is generally performed over the entire volume of plasma. The derivation of (1.27) requires the kinetic approach; this will be discussed in more details in Chapter 2.

Substituting $\mathbf{j}(x)$ into (1.16) we get the integro-differential equation for the electric field E_y in plasma:

$$\frac{\partial^2 E_y}{\partial x^2} + \frac{\omega^2}{c^2} E_y = -\frac{4\pi i \omega}{c^2} \int \sigma(x, x') E_y(x') \, dx'. \qquad (1.28)$$

The solution of this equation will be discussed in Chapter 2; however, it is almost evident now that the solution for the electric field in plasma does not have the simple exponential shape, as in the case of classical skin effect. As we will see in Chapter 2, the spatial profile of the electromagnetic field in plasma in the case of warm electrons is rather complicated and nonmonotonic. However, it is possible to derive a qualitatively correct expression for the skin depth in the case of warm electrons, using the expression for the classical skin depth. The qualitative scheme of doing this is as follows. Since the electron mean free path is of the order of, or larger than, the characteristic scale of the field inhomogeneity, i.e. the skin depth, the collisions are rare within the region where the electromagnetic field is significant (the skin region), i.e. the plasma is in nearly collisionless regime. The collisions that become important are the reflections of electrons in the skin region (of the width δ) from the plasma boundary; the effective frequency of such collisions is v_{Te}/δ. Replacing ν_e with v_{Te}/δ [5, 8] in the expression for the classical skin depth $\delta = c/\omega_{pe}(2\nu_e/\omega)^{1/2}$, we obtain the equation

$$\delta = \frac{c}{\omega_{pe}} \left(\frac{2v_{Te}}{\omega\delta} \right)^{1/2}, \qquad (1.29)$$

which yields a qualitatively correct expression for the skin depth δ_a in nearly collisionless plasma with warm electrons:

$$\delta_a = \left(\frac{2c^2 v_{Te}}{\omega_{pe}^2 \omega} \right)^{1/3}. \qquad (1.30)$$

15

Comparing δ_a to the classical skin depth $\delta = c/\omega_{pe} \left(2\nu_e/\omega\right)^{1/2}$, we see, first of all, that the dependence on the wave frequency is quite different. This "anomalous" frequency dependence, together with other "abnormalities" of the skin effect in a warm plasma, gave the skin effect in plasma with warm electrons a name – *anomalous skin effect*. The index a in (1.30) implies that δ_a is the anomalous skin depth. A regime of the anomalous skin effect takes place for $\omega, \nu_e \lesssim v_{Te}/\delta_a$, and it is also called a *nonlocal regime* [2, 3, 4, 5, 6], due to the nonlocal form of the Ohm's law (1.27).

1.2.2   Wave Power Absorption/Plasma Heating

Acceleration of plasma electrons by the field of electromagnetic wave leads to the transfer of energy from the wave to plasma electrons. The electron velocities are randomized due to intraspecies (electron-electron) and interspecies (electron-other particles) collisions, and collisions of electrons with the walls confining the plasma. As a result, the mean kinetic energy of the electrons is increased, causing the heating of plasma electrons by the electromagnetic wave. This is the process that sustains plasma, as the heated electrons ionize gas atoms when colliding with them. As the electron temperature increases, the process of electron heating is compensated by the process of electron cooling due to their inelastic collisions with other particles (ionization), and therefore the equilibrium state of plasma with certain degree of ionization is established.

To find the power transferred from the electromagnetic wave to plasma electrons, we calculate the work performed by the electromagnetic field on one plasma electron: $dA_1 = -e\mathbf{E} \cdot d\mathbf{r}$, where $d\mathbf{r}$ is the displacement of the electron (note that the magnetic field does not perform work). Therefore the power transferred from the electromagnetic field to the electron is $w_1 = dA_1/dt = -e\mathbf{E} \cdot \mathbf{v}$, where $\mathbf{v}$ is the electron velocity. Averaging over all electrons, we find the density of power transferred from the electromagnetic wave to the plasma as $w = -en\mathbf{E} \cdot \langle \mathbf{v} \rangle = \mathbf{E} \cdot \mathbf{j}$, where $\mathbf{j}$ is the electron current density in plasma.

To better understand the process of wave power transfer to plasma, let us

consider two different types of power absorption (plasma heating). First type is the absorption due to collisions of electrons with other particles, called a *collisional absorption*, or *collisional heating*. Let us consider the wave power absorption in cold collisional plasma in hydrodynamic approximation. The Ohm's law is local and is given by (1.23). The time averaged power transferred from the wave field to plasma electrons, also called the absorbed power, $w = \langle \mathbf{E} \cdot \mathbf{j} \rangle = 1/2\,\mathrm{Re}\,(\mathbf{E} \cdot \mathbf{j}^*)$, where $\mathbf{j}^*$ is a complex conjugate of $\mathbf{j}$, is

$$w = \frac{\omega_{pe}^2}{8\pi} \left| \mathbf{E} \right|^2 \frac{\nu_e}{\nu_e^2 + \omega^2}. \qquad (1.31)$$

It is seen that the collisional absorption (1.31) diminishes when collision frequency is reduced. In a case of no collisions the current density in cold plasma becomes $\mathbf{j} = \omega_{pe}^2/\left(8\pi\omega\right) i\mathbf{E}$, i.e. the current and the electric field are out of phase by $\pi/2$, and therefore there is no power transfer from the field to plasma. If collisions are present, the phase difference between the current and the electric field is different from $\pi/2$, causing the power transfer from the wave to plasma (1.31).

However, if plasma is not cold, i.e. electron thermal velocity is comparable to the wave phase velocity, then another type of heating, a *collisionless*, or *resonant* heating, occurs. This type of heating does not require collisions. The effect was first recognized by Landau in his seminal work [9] where he considered the initial value problem, yielding the temporal damping of an infinite (in space) longitudinal (Langmuir) wave, which is usually referred to as Landau damping. He also considered the boundary value problem, yielding a spatial decay of the longitudinal wave launched from the plasma boundary. The spatial decay of the transverse (electromagnetic wave) due to the wave-particle interaction (the anomalous skin effect) was studied later [2, 10, 11, 12, 13, 14].

The mechanism of collisionless heating by the electromagnetic wave is the resonant interaction of the wave with plasma electrons. This effect requires kinetic description; this will be done in detail in Chapter 3, while here we

will give a qualitative description of collisionless heating. With a Maxwellian distribution function (typical for warm plasma) there are electrons in plasma moving both faster and slower than the wave phase velocity ω/k. Electrons having a velocity close to ω/k along the direction of wave propagation are in resonance with the wave, meaning that they interact with the wave field most efficiently. These electrons, called resonant electrons, experience almost static field, being effectively accelerated by it, unlike all other electrons which experience time-varying field which provides much reduced acceleration. As a result, only the resonant electrons are being heated by the electromagnetic wave in collisionless plasma. Note that the plasma has to be warm in order to have a significant number of electrons in resonance with the wave. Since the ICP discharge typically operate in the regime where the electrons are warm, the resonant heating is expected to be important there. However, the electron collisions are also expected to be of importance. One of the expected effects of collisions on collisionless heating is the detuning of the resonance between the wave and electrons. In Chapter 3, using kinetic approach, we will discuss quantitatively the evidence of collisionless (resonant) heating in ICP, as well as the cooperative effect of electron thermal motion and collisions on plasma heating by the electromagnetic wave.

1.2.3   Ponderomotive Force

When considering the penetration of electromagnetic wave into plasma, beside the heating, we also have to consider the force exerted by the wave on plasma. This force is important because it affects the plasma density profile [7, 15, 16, 17] and the electron energy distribution function [7, 15, 18].

The electromagnetic wave incident on plasma carries momentum $\mathbf{p} = E^2/(4\pi c)\,\mathbf{n}$, where $\mathbf{n}$ is the direction of the wave propagation. The wave partially reflects from and partially penetrates into plasma. The penetrated wave loses its momentum to plasma as the wave amplitude decays inside the plasma. Both wave reflection from plasma and wave decay in plasma lead to

the momentum transfer to the plasma, i.e. a force is exerted on plasma. This force is called a *ponderomotive force*. Historically, the ponderomotive force referred to a force exerted by constant electrostatic field on dielectric, however, this term has been adopted to also refer to an average force due to high frequency electromagnetic field.

The ponderomotive force can also be viewed as a nonlinear force caused by nonuniformity of energy density of electromagnetic field in media. This force pushes electrons away from regions of strong field towards regions of weaker field. For the introduction purposes, let us derive the classical expression for the ponderomotive force exerted by electromagnetic field on cold collisional plasma [1, 19].

The momentum equation for a single electron in electromagnetic field reads

$$m_e \frac{d\mathbf{v}}{dt} = -e\left(\mathbf{E} + \frac{1}{c}\mathbf{v} \times \mathbf{B}\right) - m_e \nu_e \mathbf{v}, \tag{1.32}$$

where $\mathbf{E}$ and $\mathbf{B}$ are evaluated at the instantaneous position of the electron, therefore both terms are nonlinear. In the equivalent fluid formulation, $\mathbf{E}$ and $\mathbf{B}$ are evaluated in laboratory frame, and the convective derivative has to be added so that $d\mathbf{v}/dt = \partial\mathbf{v}/\partial t + (\mathbf{v} \cdot \nabla)\mathbf{v}$, and we also have two nonlinear terms $(\mathbf{v} \cdot \nabla)\mathbf{v}$ and $\mathbf{v} \times \mathbf{B}$.

Following Johnston [19] and Schmidt [20], we solve (1.32) by orders. In first order, let the local RF electric field be $\mathbf{E}^{(1)} = \mathbf{E}_s \exp(-i\omega t) + c.c.$, where $\mathbf{E}_s$ (which is generally a complex number) denotes spatial part of the field, and $c.c.$ denotes complex conjugate. Neglecting nonlinear terms in (1.32), we obtain for the electron velocity $\mathbf{v}^{(1)}$ and excursion $d\mathbf{r}^{(1)}$:

$$\mathbf{v}^{(1)} = -\frac{e}{m_e}\frac{\mathbf{E}_s}{i\omega}\frac{1 - i\nu_e/\omega}{1 + \nu_e^2/\omega^2}\exp(-i\omega t) + c.c., \tag{1.33}$$

$$d\mathbf{r}^{(1)} = -\frac{e}{m_e}\frac{\mathbf{E}_s}{\omega^2}\frac{1 - i\nu_e/\omega}{1 + \nu_e^2/\omega^2}\exp(-i\omega t) + c.c..$$

Faraday's law gives for the magnetic field $\mathbf{B}^{(1)}$:

$$\mathbf{B}^{(1)} = -\frac{ic}{\omega}\nabla \times \mathbf{E}_s \exp(-i\omega t) + c.c. \tag{1.34}$$

19

In second order, the term $\mathbf{v}^{(1)} \times \mathbf{B}^{(1)}$ should be retained in (1.32), and $\mathbf{E}$ must be evaluated at the position $\mathbf{r}_0 + d\mathbf{r}^{(1)}$. The second-order equation for $\mathbf{v}^{(2)}$ is

$$m_e \frac{d\mathbf{v}^{(2)}}{dt} = -e \left[\left(d\mathbf{r}^{(1)} \cdot \nabla \right) \mathbf{E}^{(1)} + \frac{1}{c} \mathbf{v}^{(1)} \times \mathbf{B}^{(1)} \right] - m_e \nu_e \mathbf{v}^{(2)}. \tag{1.35}$$

Substituting the first order terms from (1.33), and averaging over the field period $2\pi/\omega$, we obtain [19]:

$$
\begin{aligned}
\frac{d \left\langle \mathbf{v}^{(2)} \right\rangle}{dt} + \nu_e \left\langle \mathbf{v}^{(2)} \right\rangle &= -\frac{e^2}{2m_e^2\omega^2} \left(1 + \nu_e^2/\omega^2 \right)^{-1} \times \\
&\quad \times \left\{ \mathrm{Re} \left[\left(\mathbf{E}_s \cdot \nabla \right) \mathbf{E}_s^* + \mathbf{E}_s \times \nabla \times \mathbf{E}_s^* \right] + \right. \tag{1.36} \\
&\quad \left. + \frac{\nu_e}{\omega} \mathrm{Im} \left[\left(\mathbf{E}_s \cdot \nabla \right) \mathbf{E}_s^* + \mathbf{E}_s \times \nabla \times \mathbf{E}_s^* \right] \right\}
\end{aligned}
$$

Using the vector identity $\mathbf{E}_s \times \nabla \times \mathbf{E}_s^* = \mathbf{E}_s \cdot \left(\nabla \mathbf{E}_s^* \right) - \left(\mathbf{E}_s \cdot \nabla \right) \mathbf{E}_s^*$, we get

$$\left(\mathbf{E}_s \cdot \nabla \right) \mathbf{E}_s^* + \mathbf{E}_s \times \nabla \times \mathbf{E}_s^* = \mathbf{E}_s \cdot \left(\nabla \mathbf{E}_s^* \right) = E_{sj} \frac{\partial E_{sj}^*}{\partial x_i} \hat{\mathbf{e}}_i. \tag{1.37}$$

Here a summation on repeated indices is assumed, $\hat{\mathbf{e}}_i$ are unit basis vectors. Multiplying the dc part of the force in the right-hand side of (1.36) by $m_e n$ we get the dc part of ponderomotive force per unit volume:

$$\mathbf{F}_p^{dc} = -\frac{\omega_{pe}^2}{8\pi\omega^2} \left(1 + \nu_e^2/\omega^2 \right)^{-1} \left\{ \mathrm{Re}\, \mathbf{E}_s \cdot \left(\nabla \mathbf{E}_s^* \right) + \frac{\nu_e}{\omega} \mathrm{Im}\, \mathbf{E}_s \cdot \left(\nabla \mathbf{E}_s^* \right) \right\}. \tag{1.38}$$

Now, $\mathrm{Re}\, \mathbf{E}_s \cdot \left(\nabla \mathbf{E}_s^* \right) = 1/2 \left(\mathbf{E}_s \cdot \left(\nabla \mathbf{E}_s^* \right) + \mathbf{E}_s^* \cdot \left(\nabla \mathbf{E}_s \right) \right) = 1/2\nabla \left(\mathbf{E}_s \cdot \mathbf{E}_s^* \right) = 1/2\nabla \left| \mathbf{E}_s \right|^2$. If we put $\mathbf{E}_s = \left| E_{sj} \right| \exp \left(i\phi_j \right) \hat{\mathbf{e}}_j$, where $\left| E_{sj} \right|$ is the projection of $\mathbf{E}_s$ onto $\hat{\mathbf{e}}_j$, and ϕ_j is the spatial phase of E_{sj}, then we get

$$\mathrm{Im}\, \mathbf{E}_s \cdot \left(\nabla \mathbf{E}_s^* \right) = -E_{sj} E_{sj}^* \frac{\partial \phi_j}{\partial x_i} \hat{\mathbf{e}}_i, \tag{1.39}$$

and finally for $\mathbf{F}_p^{dc}$ we get [19]:

$$\mathbf{F}_p^{dc} = -\frac{\omega_{pe}^2}{8\pi\omega^2} \left(1 + \nu_e^2/\omega^2 \right)^{-1} \left[\frac{1}{2}\nabla \left| \mathbf{E}_s \right|^2 - \frac{\nu_e}{\omega} E_{sj} E_{sj}^* \frac{\partial \phi_j}{\partial x_i} \hat{\mathbf{e}}_i \right]. \tag{1.40}$$

Generally, the ponderomotive force, besides the dc term (1.40), also has second and higher harmonic terms, investigated by Godyak *et al.* [4, 21]. However, in this thesis we will be interested in a dc ponderomotive force exerted by a plane electromagnetic wave.

The first term in (1.40) is what is known as the gradient field term, and shows that there is a time-averaged acceleration of particles towards regions of electric field strength minima. This term is also referred to as Miller force [22], thus we will call it $\mathbf{F}_M$:

$$\mathbf{F}_M = -\frac{\omega_{pe}^2}{8\pi\omega^2} \frac{1}{1 + \nu_e^2/\omega^2} \nabla \left\langle \mathbf{E}^2 \right\rangle, \tag{1.41}$$

where $\langle ... \rangle$ denotes time-averaging over the wave period (note that for an oscillating field $\langle \mathbf{E}^2 \rangle = 1/2\nabla |\mathbf{E}_s|^2$).

The second term in (1.40) only exists for a propagating wave since $\partial \phi_j / \partial x_i = 0$ for a standing wave (except at nodes where $E_{sj} = 0$). Physically this term describes the wave momentum deposition into plasma due to collisions of electrons, i.e. due to "viscous drag" of the wave by electrons. This is essentially a radiation pressure on an absorber.

As it is seen from (1.40), in ICP with the electromagnetic wave propagating and decaying inward the plasma, the ponderomotive force is directed inward the plasma, thus pushing plasma away from the boundary [7].

This derivation of the ponderomotive force used an assumption of cold electrons in plasma. The case of warm or hot electrons (the case of anomalous skin effect) requires a different approach, which is based on kinetic equation (1.10). This is done in Chapter 3.

1.3   Objective and Thesis Outline

The major objective of this thesis is to study the plasma heating and ponderomotive force at the conditions of anomalous skin effect (in nonlocal regime). Our goal is to develop a theory which provides a good insight on the

basic physics of plasma heating and ponderomotive effect in nonlocal regime, and is capable of describing the main features of the experimental data. As it will be discussed below, to large extent the need for a new theoretical model was highlighted by the observed discrepancies between the experimental data and previously available theoretical predictions for the ponderomotive force.

This major objective can be divided into the following sub-objectives, outlining the structure of this thesis:

In Chapter 2 we review the theory of the anomalous skin effect. We also present the typical results of experimental measurements of electromagnetic field and electric current in plasma at conditions of anomalous skin effect, and compare them with the theoretical results for anomalous skin effect. Also, we present experimental results for plasma heating and ponderomotive effect at conditions of anomalous skin effect, and compare them with the results of classical theory. Then we review some theories of heating and ponderomotive force that account for electron thermal motion, and on the basis of this review the motivation for our theoretical work is given.

In Chapter 3 we develop our linear kinetic theory that allows to calculate both plasma heating and ponderomotive force, taking into account both electron thermal motion and collisions. Under some simplifying assumptions, we derive simple, ready-to-use expressions for plasma heating and ponderomotive force, and compare the results of our theory with typical experimental results, as well as with results of some other theories. In particular, we confirm theoretically the effect of thermal reduction of ponderomotive force in anomalous regime, that was observed experimentally. Also, from our theory, we predict a novel and rather interesting effect – the effect of reduction of total heating in anomalous regime compared to purely collisional heating, that occurs at low driving frequencies.

In Chapter 4 we develop a quasilinear theory of plasma heating in nonlocal regime, in order to study the weakly-nonlinear influence of the induced RF magnetic field on plasma heating. We show that taking into account of the

weak electromagnetic field leads to a nonlinear deviation of heating at low frequencies from the prediction of the linear theory. This nonlinear deviation occurs mainly due to the nonlinear effect of the RF magnetic field, as shown in Chapter 4.

Chapter 5 discusses Particle-In-Cell (PIC) simulation of ICP in nonlocal regime with collisions. We introduce the basic principles of PIC method, and present our 1d3v (1 spatial and 3 velocity components) PIC model with collisions, designed for simulations of plasma heating in planar ICP by externally applied electromagnetic field. The primary objectives for developing this PIC code were: a) verification of our theory in general, and, in particular, of the novel effect of reduction of heating at low frequencies, and b) investigation of nonlinear effects, such as the RF magnetic field, on plasma heating. Using the numerical code, we demonstrate the existence of collisionless heating, compare the results on heating with the predictions of our linear theory, and discuss deviations of the simulation results from the linear theory due to nonlinear effects at low driving frequencies.

Finally, in Chapter 6 we list the major conclusions of this study, and present suggestions for future research.

Chapter 2

Inductively Coupled Plasma in Nonlocal Regime

2.1 Anomalous Skin Effect

In the Introduction we gave a qualitative description of the anomalous skin effect. Now we will give its quantitative description, based on the theoretical models developed by different authors [2, 23, 24].

In 1967 Weibel [2] developed a theory of anomalous skin effect in plasma, which is similar to theories of anomalous skin effect in metals developed earlier [11, 25, 26, 27, 28]. Later, Kondratenko [23] and Shaing [24] developed virtually the same theory for the penetration of TE electromagnetic waves into plasma with warm electrons. Here we will give a brief overview of the theory of anomalous skin effect for electromagnetic waves, based on [2, 23, 24].

Let us consider the penetration of weak electromagnetic field into isotropic (no constant magnetic field) semi-infinite plasma occupying a region $0 < x < \infty$. The plasma boundary at $x = 0$ is assumed to be sharp, which is a good approximation if the width of the sheath (of the order of several Debye lengths) is much smaller than the characteristic length of plasma inhomogeneity. The plasma electrons are assumed to be warm, i.e. $\omega,\ \nu_e \lesssim v_{Te}/\delta$, which is the condition

of anomalous skin effect, as we discussed in the Introduction. In this situation we have to use the kinetic approach based on Boltzmann equation (1.10) for electrons (the ions are assumed to be immobile). We can linearize the kinetic equation (1.10) for the electron distribution function $f_e = f_{0e}(\mathbf{v}) + \tilde{f}_e(\mathbf{v}, \mathbf{r}, t)$, where f_{0e} is the electron distribution function without the field (equilibrium distribution), and $\tilde{f}_e$ is a small perturbation of the electron distribution function due to the field, $\left|\tilde{f}_e\right| \ll f_{0e}$. Neglecting the terms quadratic in small quantities, and using the Bhatnagar-Gross-Krook (BGK) [29] collision term $\hat{S}\left(f_e\right) = -\nu_e \tilde{f}_e$, we obtain the linearized equation for $\tilde{f}_e$:

$$\frac{\partial \tilde{f}_e}{\partial t} + \mathbf{v} \cdot \frac{\partial \tilde{f}_e}{\partial \mathbf{r}} - \frac{e}{m_e} \left(\mathbf{E} + \frac{1}{c}\mathbf{v} \times \mathbf{B}\right) \cdot \frac{\partial f_{0e}}{\partial \mathbf{v}} = -\nu_e \tilde{f}_e. \quad (2.1)$$

Assuming f_{0e} to be isotropic, $f_{0e} = f_{0e}(|\mathbf{v}|)$, we get $(\mathbf{v} \times \mathbf{B}) \cdot \partial f_{0e}/\partial \mathbf{v} = 0$, and finally

$$\frac{\partial \tilde{f}_e}{\partial t} + \mathbf{v} \cdot \frac{\partial \tilde{f}_e}{\partial \mathbf{r}} - \frac{e}{m_e}\mathbf{E} \cdot \frac{\partial f_{0e}}{\partial \mathbf{v}} = -\nu_e \tilde{f}_e. \quad (2.2)$$

The electric field $\mathbf{E}$ of the incident wave has the form $E_y(x) \exp(-i\omega t)\hat{y}$ (for simplicity we are considering the wave incident perpendicularly onto plasma). Here $\hat{y}$ is a unit vector along y, and y corresponds to the azimuthal direction in cylindrical geometry (see Fig. 1.3). Then the equation (2.2) reduces to

$$-i\omega \tilde{f}_e + v_x \frac{\partial \tilde{f}_e}{\partial x} - \frac{e}{m_e}E_y(x)\frac{\partial f_{0e}}{\partial v_y} = -\nu_e \tilde{f}_e. \quad (2.3)$$

The general solution of this equation has the form [24]:

$$\tilde{f}_e = \int_\infty^x dx' \frac{D}{v_x} \exp\left(\int_x^{x'} \frac{\nu_e - i\omega}{v_x}dx''\right) + g \exp\left(-\int^x \frac{\nu_e - i\omega}{v_x}dx'\right), \quad (2.4)$$

where $\partial g/\partial x = 0$, i.e. the arbitrary function g depends only on $\mathbf{v}$, and $D = e/m_e\mathbf{E} \cdot \left(\partial f_{0e}/\partial \mathbf{v}\right)$. The function $g(\mathbf{v})$ has to be determined from boundary conditions.

We need two boundary conditions to determine $\tilde{f}_e$; the first condition states that the electrons moving towards the plasma boundary (with $v_x < 0$) from $x = \infty$ are not under influence of the field $\mathbf{E}$, i.e. $\tilde{f}_e(x = \infty) = 0$ for $v_x < 0$.

25

This condition allows us to find the distribution function of electrons moving towards the plasma boundary, $\tilde{f}_e(v_x < 0)$:

$$\tilde{f}_e(v_x < 0) = \int_\infty^x dx \frac{D}{v_x} \exp\left(\int_x^{x'} \frac{\nu_e - i\omega}{v_x} dx'\right). \tag{2.5}$$

The second boundary condition is the condition of electron reflection from the sheath potential at the plasma boundary, $\tilde{f}_e(x_t, v_x > 0) = p\, \tilde{f}_e(x_t, v_x < 0)$, where x_t is the turning point for electrons (at this point the electrons are turned by the sheath potential on the plasma edge, i.e. $v_x = 0$), and p is the relative number of electrons reflecting specularly from the sheath potential at the plasma boundary. Neglecting the sheath spatial structure, we can say that the electrons simply bounce off the plasma boundary at $x = 0$. Also, if we assume that all electrons reflect specularly from the plasma boundary, i.e. $p = 1$, we get for the second boundary condition: $\tilde{f}_e(x = 0, v_x > 0) = \tilde{f}_e(x = 0, v_x < 0)$. This gives the distribution function of electrons moving away from the plasma boundary, $\tilde{f}_e(v_x > 0)$ [24]:

$$\tilde{f}_e(v_x > 0) = \int_\infty^x dx' \frac{D}{v_x} \exp\left(\int_x^{x'} \frac{\nu_e - i\omega}{v_x} dx''\right) + \exp\left(-\int_0^x \frac{\nu_e - i\omega}{v_x} dx'\right) \times$$

$$\times \left\{ \int_\infty^0 dx' \left[\left(\frac{D}{v_x}\right)_{\zeta=-1} \exp\left(\int_0^{x'} \left(\frac{\nu_e - i\omega}{v_x}\right)_{\zeta=-1} dx''\right) - \right.\right.$$

$$\left.\left. - \left(\frac{D}{v_x}\right)_{\zeta=+1} \exp\left(\int_0^{x'} \left(\frac{\nu_e - i\omega}{v_x}\right)_{\zeta=+1} dx''\right)\right]\right\}, \tag{2.6}$$

where $\zeta = v_x/|v_x|$. The subscript ζ indicates the proper sign of v_x that should be taken inside the parentheses.

With the electric field having the form $E_y(x)\exp(-i\omega t)\hat{y}$, we get for D in $\tilde{f}_e$:

$$D = -\frac{2ev_y E_y}{m_e v_{Te}^2} f_{0e}. \tag{2.7}$$

With this D the expressions for $\tilde{f}_e$ simplify to

$$\tilde{f}_e(v_x < 0) = -\frac{2ev_y}{m_e v_{Te}^2 |v_x|} f_{0e} \int_x^\infty dx' E_y(x') \exp\left(-\frac{\nu_e - i\omega}{|v_x|}(x - x')\right), \tag{2.8}$$

26

$$\tilde{f}_e(v_x > 0) = -\frac{2ev_y}{m_e v_{Te}^2 |v_x|} f_{0e} \left\{ \exp\left(-\frac{\nu_e - i\omega}{|v_x|} x\right) \left[\int_0^\infty dx' E_y(x') \times \right. \right.$$

$$\left. \left. \times \exp\left(-\frac{\nu_e - i\omega}{|v_x|} x'\right) + \int_0^x dx' E_y(x') \exp\left(\frac{\nu_e - i\omega}{|v_x|} x'\right) \right] \right\} \quad (2.9)$$

Now we can define the current density in plasma as $j_y = -e \int v_y \tilde{f}_e \, d^3 v$. To simplify the calculation of the current density and self-consistent electric field, we extend the solution from $0 < x < \infty$ to $-\infty < x < \infty$ so that $E_y(x) = E_y(-x)$. Note that although E_y defined in such a way is continuous at $x = 0$, the derivative dE_y/dx is not continuous because of the existence of the coil current at $x = 0$. The current density is [24]

$$j_y = \frac{2}{\sqrt{\pi}} \frac{n_0 e^2}{m_e v_{Te}^2} \int_{-\infty}^\infty dx' E_y(x') \Sigma_a(|x - x'|), \quad (2.10)$$

where $\Sigma_a(|x - x'|)$ is the nonlocal plasma conductivity,

$$\Sigma_a(|x - x'|) = \int_0^\infty dt \, t^3 \exp(-t^2) \int_0^{\pi/2} d\Theta \frac{\sin^3 \Theta}{\cos \Theta} \exp\left(-\frac{a}{t \cos \Theta} |x - x'|\right),$$
$$(2.11)$$

and $a = (\nu_e - i\omega)/v_{Te}$.

As we see, the current density (2.10) has the form of nonlocal Ohm's law (ref. Eq. 1.27).

The spatial profile of the electric field $E_y(x)$ is still unknown. To define it self-consistently, we use the equation (1.16), which in our case has the following form:

$$\frac{\partial^2 E_y}{\partial x^2} + \frac{\omega^2}{c^2} E_y = -i\alpha \int_{-\infty}^\infty dx' \Sigma_a(|x - x'|) E_y(x'), \quad (2.12)$$

where $\alpha = 8\sqrt{\pi} n_0 e^2 \omega / (m_e v_{Te} c^2) = 2 \left(\omega_{pe}^2/c^2\right) \left(\omega/\sqrt{\pi} v_{Te}\right)$.

Equation (2.12) can be solved by Fourier transformation. When doing Fourier transform, we should keep in mind that dE_y/dx is not continuous at $x = 0$. The Fourier transformed equation (2.12) is [24]:

$$\left(k^2 - \frac{\omega^2}{c^2} - i\alpha\sigma_a(k)\right) E_k = -2\mu, \quad (2.13)$$

where $\mu = dE_y/dx|_{x=0^+} = -dE_y/dx|_{x=0^-}$, $E_k = 2\int_0^\infty dx E_y(x) \cos(kx)$ is the Fourier image of $E_y(x)$, and $\sigma_a(k) = \int_{-\infty}^\infty dx \, \Sigma_a(|x - x'|) \exp(-ikx)$ is the

27

Fourier image of nonlocal plasma conductivity $\Sigma_a(|x - x'|)$. From (2.13) we get for E_k:

$$E_k = -\frac{2\mu}{k^2 - (\omega^2/c^2) - i\alpha\sigma_a(k)}. \tag{2.14}$$

Finally, the self-consistent electric field in plasma at conditions of anomalous skin effect is

$$E_y(x) = -\frac{2\mu}{\pi} \int_0^\infty dk \frac{\cos(kx)}{k^2 - (\omega^2/c^2) - i\alpha\sigma_a(k)}. \tag{2.15}$$

For low frequency oscillations, such as radio frequencies, the term (ω^2/c^2) is small and can be neglected in (2.14-2.15).

The self-consistent electric current in plasma can be restored from its Fourier image $j_k = \sigma_a(k)E_k$.

An important characteristic of plasma, in terms of penetration of TE electromagnetic wave into it, is the surface impedance, defined as $Z_H = E_y(0)/B_z(0)$. Following Shaing [24] (or Kondratenko [23]), we get for the surface impedance at low frequencies

$$Z_H = \frac{i\omega}{c}\frac{2}{\pi} \int_0^\infty \frac{dk}{k^2 - i\alpha\sigma_a(k)}. \tag{2.16}$$

The surface impedance defines the reflection and transition coefficients of the wave, $R = (Z_H - 1)/(Z_H + 1)$ (for the perpendicularly incident wave) and $W = 1 - |R|^2$ accordingly, which in turn define what part of the wave power gets reflected from plasma, and what part penetrates into plasma and gets absorbed. Also, the characteristic depth of penetration of the electromagnetic wave into plasma (skin depth) also depends on the surface impedance. If we define the characteristic depth of penetration of magnetic field of the electromagnetic wave into plasma as $\lambda_H = B_z^{-1}(0) \int_0^\infty B_z(x)dx$, then in terms of the surface impedance Z_H it becomes

$$\lambda_H = i\frac{c}{\omega}Z_H. \tag{2.17}$$

We can also define the characteristic depth of penetration of electric field into plasma as $\lambda_E = E_y^{-1}(0) \int_0^\infty E_y(x)dx$. In terms of Z_H it becomes [23]

$$\lambda_E = \frac{i\omega}{ck_1 Z_H}, \tag{2.18}$$

28

where k_1 is a wavenumber of the electromagnetic wave in plasma. In hydrodynamic limit λ_E and λ_H are the same, but in general they are different [23].

In the highly collisional limit $\nu_e \gg \omega$ in cold plasma ($kv_{Te}/\nu_e \ll 1$) we have $a \approx \nu_e/v_{Te}$, $k/a \ll 1$, and the Fourier image of plasma conductivity reduces to $\sigma_a(k) \approx (1/a)\sqrt{\pi}/2$. The surface impedance (2.16) reduces to [24]:

$$Z_H = \frac{\omega}{c}\frac{1+i}{\sqrt{2}}\left(\frac{\nu_e}{\omega}\right)^{1/2}\frac{c}{\omega_{pe}}, \qquad (2.19)$$

and the collisional skin depth $\delta_c = c/\omega\,|iZ_H|$ is

$$\delta_c = \frac{c}{\omega_{pe}}\sqrt{\frac{2\nu_e}{\omega}}, \qquad (2.20)$$

which coincides with the classical skin depth (1.26) in the highly collisional limit, as expected.

In the opposite collisionless limit, $\nu_e \ll \omega$ and $kv_{Te}/\nu_e \gg 1$, we have $\sigma_a(k) \approx \pi/2k$, and the surface impedance is [23, 24]:

$$Z_H \approx \frac{\omega}{c}\frac{2}{3}\left(\alpha\pi/2\right)^{-1/3}\left(\frac{1}{\sqrt{3}}+i\right), \qquad (2.21)$$

and the corresponding anomalous skin depth is

$$\delta_a = \left(\frac{v_{Te}}{\sqrt{\pi}}\frac{c^2}{\omega_{pe}^2\omega}\right)^{1/3}. \qquad (2.22)$$

As we see, the anomalous skin depth in the collisionless limit coincides with the expression (1.30) for δ_a derived using the qualitative analysis (see the Introduction, Eq. 1.30).

Thus the self-consistent theory of anomalous skin effect [2, 23, 24] provides the correct expressions for the skin depth in the limiting cases of collisional and collisionless plasma. In the intermediate regimes one has to use the complete expression for the surface impedance (2.16) to estimate the skin depth.

The equation (2.12) can also be cast in the following form [2, 3]:

$$\frac{d^2E_y}{dx^2} = i\Lambda\int_{-\infty}^{\infty}\Sigma_a\left(\varsigma\,|x-x'|\right)E_y(x')dx', \qquad (2.23)$$

where the parameters Λ and ς are defined as

$$\Lambda = \left(\frac{\omega_{pe} v_{Te}}{c}\right)^2 \frac{\omega}{(\omega^2 + \nu_e^2)^{3/2}}, \qquad (2.24)$$

$\varsigma = i \exp(-i\phi)$, $\phi = \arctan(\nu_e/\omega)$. The parameter Λ is a fundamental measure of nonlocality of electromagnetic phenomena in plasmas [3]. It is proportional to the square of a ratio of the effective mean free path $\lambda_{eff} = v_{Te}/\sqrt{\omega^2 + \nu_e^2}$ to the classical (local) skin depth, $\Lambda = (\lambda_{eff}/\delta)^2$. Therefore, the nonlocal effects are pronounced for $\Lambda > 1$, when the electron mean free path exceeds the skin depth, and they are small otherwise. It is interesting to note that $\Lambda < 1$ for both high and low driving frequencies, i.e. the skin effect is classical both at low ($\omega < \nu_e (c\nu_e/\omega_{pe} v_{Te})^2$) and high frequencies. However, this observation is valid only in planar geometry.

We see from the expression (2.15) for the electric field in plasma in nonlocal regime (the regime of anomalous skin effect) that the field profile in plasma does not have the simple exponentially decaying form as in the local regime (classical skin effect). In the nonlocal regime the field profile is strongly affected by the thermal motion of electrons. Electrons that have acquired momentum from the electric field in the skin layer carry this momentum into bulk plasma due to their thermal motion, generating the high-frequency electric current deeper inside the plasma. Because of this, the decay of both the current and electric field in plasma are governed by two characteristic scales of different order of magnitude – δ and λ (electron mean free path) [3]. The typical profiles of electric field in plasma at conditions of anomalous skin effect for different Λ (different degrees of nonlocality of electromagnetic phenomena, corresponding to different driving frequencies), are shown in Fig. 2.1. As we see, the fields in plasma exhibit complex nonmonotonic behavior; however, we should note that near the plasma boundary, where the field amplitude is the largest, and where the most plasma heating and ponderomotive effect should be expected, the spatial profile of the electromagnetic field is very close to the exponentially decaying profile, with the appropriate anomalous skin depth,
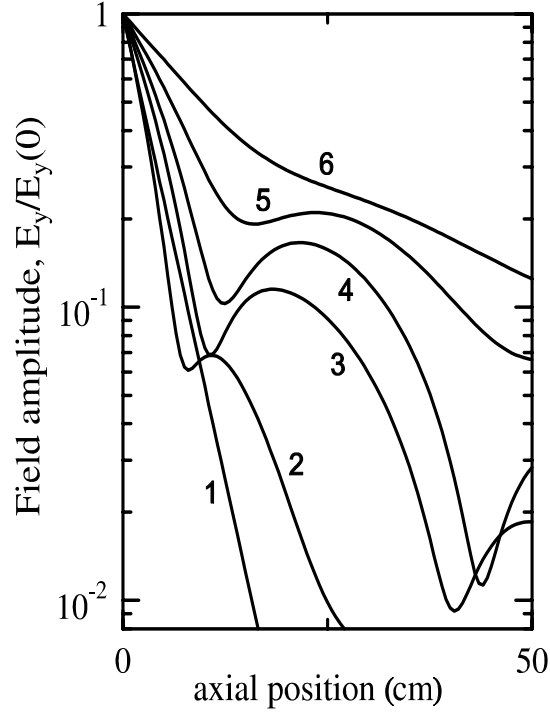
Figure 2.1: Spatial profiles of electric field amplitude for different values of the nonlocality parameter Λ, corresponding to different driving frequencies. The plasma electron temperature is 10 eV, electron-atom collision frequency $\nu_{en} \sim \nu_e = 0.15 \cdot 10^7$ s^{-1}. Parameters for lines 1-6: line 1: $\omega/2\pi = 50$ MHz ($\Lambda \approx 0.03$), line 2: $\omega/2\pi = 5$ MHz ($\Lambda \approx 2.8$), line 3: $\omega/2\pi = 1$ MHz ($\Lambda \approx 65$), line 4: $\omega/2\pi = 0.4$ MHz ($\Lambda \approx 280$), line 5: $\omega/2\pi = 0.1$ MHz ($\Lambda \approx 400$), line 6: $\omega/2\pi = 0.03$ MHz ($\Lambda \approx 152$).

which is generally greater than the classical skin depth at the same parameters. This observation is quite important and will be used for simplifying our theory of plasma heating and ponderomotive force in nonlocal regime, which we will develop in Chapter 3.

Note from Fig. 2.1 how the characteristic depth of electromagnetic field penetration increases with the decrease of ω, in accordance with the qualitative expression for the anomalous skin depth (1.30). Also we see that the nonmonotonic behavior of the field profile is most pronounced for large values of nonlocality parameter Λ, while for $\Lambda < 1$, when plasma is in local regime, the field profile is exponential (line 1 on Fig. 2.1). Note the previously mentioned transition to local regime at low frequencies as well (line 6 in Fig. 2.1 is close to the exponential profile).

Now that we reviewed the self-consistent theory of anomalous skin effect, and calculated the field and current profiles in plasma, let us consider the experimental measurements of electromagnetic field and electric current in ICP in nonlocal regime, as well as the measurements of plasma heating and ponderomotive effect in nonlocal regime of ICP.

2.2   Experimental Measurements

Recently, Godyak *et al.* [4, 30, 31, 32] conducted a series of experimental measurements of electromagnetic field and current structure in ICP operating in nonlocal regime (regime of anomalous skin effect), as well as measurements of plasma heating and ponderomotive effects in this regime. Here we will review briefly the experimental setup, discharge parameters used, and typical results.

In their experiment Godyak *et al.* used a planar coil configuration (Fig. 1.2) of argon ICP. They used the cylindrical stainless steel discharge chamber with a Pyrex glass bottom. The chamber inside diameter was 19.8 cm, its length L was 10.5 cm, and the glass thickness was 1.27 cm. A five turn planar induction

coil was mounted 1.9 cm below the bottom surface of the discharge chamber. To achieve a high degree of azimuthal symmetry, each turn of the induction coil was made concentric about the center of the discharge chamber with a radial conducting bridge between them.

A two dimensional magnetic probe was used for simultaneous measurement of the radial and axial components of the RF magnetic field magnitude and phase along the discharge axis x (corresponding to the direction of propagation of the electromagnetic wave in plasma) at a fixed radius of 4 cm, which corresponds approximately to maximum of the electromagnetic field in the cylindrical discharge (the radial dependence of electromagnetic field in a cylindrical discharge is $J_1(\mu_1 r/R)$, where J_1 is the cylindrical Bessel function of the first order, $\mu_1 \approx 3.83$ is the first root of J_1, R is the cylinder inner radius. The maximum of $J_1(\mu_1 r/R)$ with $R = 9.9$ cm corresponds to $r \approx 4.75$ cm). The measured magnetic field components were used to find the azimuthal electric field and current in plasma using Maxwell's equations in the following form: $E_\theta(x) = -i\omega \int B_r \, dx$ and $j_\theta(x) = c/(4\pi) \left(dB_r/dx - dB_x/dr \right)$ with the boundary condition $E = 0$ at the metal wall ($x = 10.5$ cm).

Also a Langmuir probe was used for measurement of plasma density n, plasma potential V and electron energy distribution function (EEDF). The collision frequency ν_e was determined from the measured EEDF using argon cross sections according to [32, 33, 34].

The measurements were made in ICP discharge operating at driving frequencies $\omega/2\pi = 0.45$, 3.39, 6.78 and 13.56 MHz with the discharge powers $P_{pl} = 25$, 50, 100 and 200 W. The discharge power P_{pl} was determined as the difference between the power transmitted to the induction coil (forward minus reflected power) and the losses in the coil and impedance matching circuit determined *a priori* (before the experiment) as a function of coil current and temperature. In what follows, the discharge power refers to the total power dissipated in the plasma. The gas pressures in the discharge chamber ranged from 0.3 to 100 mTorr, and the electron temperature in plasma was of the

order of few eV.

2.2.1 Structure of Electromagnetic field and Current

The typical results for axial distribution of electric field $|\mathbf{E}|$ and current density in plasma $|\mathbf{j}|$ (rms – root mean square, $\sqrt{\langle \mathbf{A} \cdot \mathbf{A} \rangle}$), and axial distribution of phases of the electric field and the current, relative to the phase of the electric field in vacuum, are shown on Figs. 2.2, 2.3.
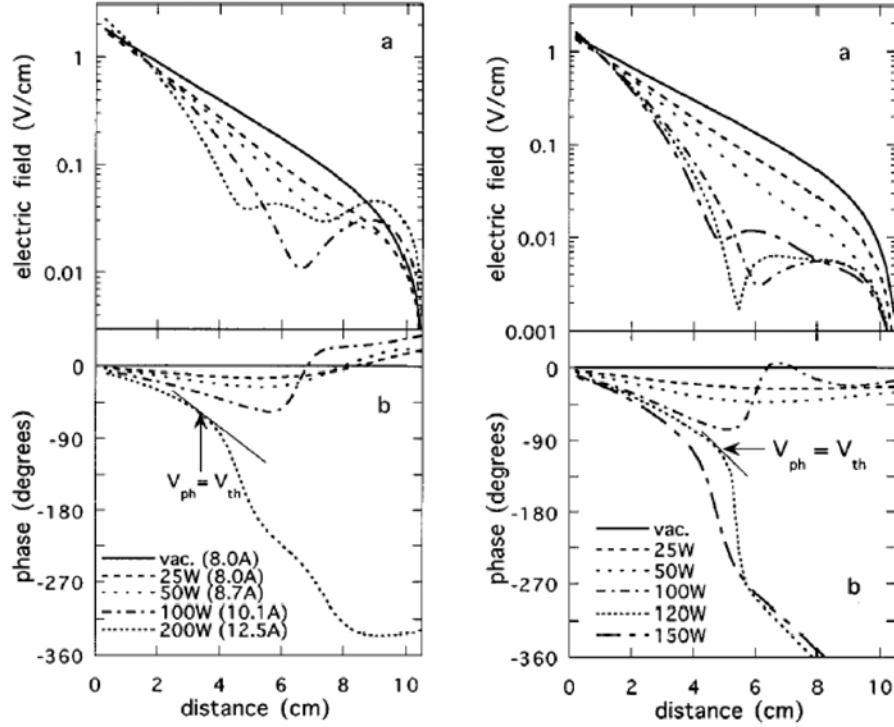
Figure 2.2: The RF electric field distribution (rms value and relative phase) for $p = 1$ mTorr (left), and $p = 10$ mTorr (right), by Godyak *et al.* [30]. The tangent line shows the slope of the phase equal to $-\omega/v_{Te}$. The numbers in parenthesis are the induction coil current values. The discharge driving frequency $\omega/2\pi = 6.78$ MHz.

As seen on Fig. 2.2, within the skin layer near the glass window, where the RF field is largest, the field amplitude decays exponentially and the field phase

decreases linearly as is found from the classical skin effect theory (see Chapter 1). However, deeper into plasma, the RF field profile becomes nonmonotonic, just as we have seen on theoretical plots of field profiles in anomalous skin effect regime in Fig. 2.1. The phase velocity of the electromagnetic wave $v_{ph} = -\omega \left(d\phi/dx \right)^{-1}$ (ϕ is the relative field phase) becomes equal to the electron thermal velocity at some point within the skin layer, which suggests that the resonant heating of electrons by the electromagnetic wave is important.
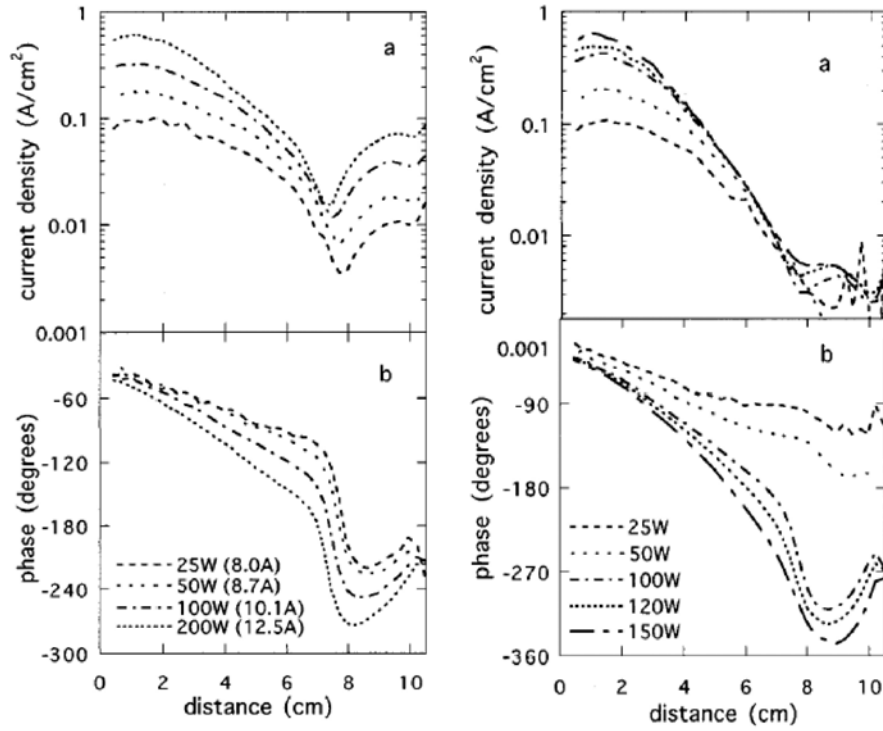
Figure 2.3: The RF current density distribution (rms value and relative phase) for $p = 1$ mTorr (left) and $p = 10$ mTorr (right), by Godyak *et al.* [30]. The discharge driving frequency $\omega/2\pi = 6.78$ MHz.

The RF current density and its phase distribution (Fig. 2.3) demonstrate the effect of RF current transport out of the skin layer, leading to formation of a second current layer (with current that is opposite in direction to that in the skin layer) near the right (metal) wall of the chamber [30]. The peak current

35

density in the second current layer for $p = 1$ mTorr at $x \approx 9$ cm is just ten times less than that in the first (skin) layer at $x \approx 1$ cm, while the RF electric field at these points differs by a factor of 50. The phase difference of the RF current at these points agrees well with the estimate for the phase of the current transferred by thermal electrons, $\Delta\phi \sim \omega\Delta x/v_{Te} \approx 240°$. This suggests that the current is being transported from the skin layer into bulk plasma by thermal electrons. A similar pattern is seen for $p = 10$ mTorr, however, as the pressure increases, the second current layer becomes less pronounced, since the electron mean free path becomes significantly reduced, and thus the current thermal transport in plasma is reduced.

These results demonstrate the nonlocal properties of typical ICP discharges. They also demonstrate the agreement with the theory of anomalous skin effect, at least in what concerns the complicated, nonmonotonic shape of the electromagnetic field and electric current in plasma. We also observe in Fig. 2.2 that, just as in Fig. 2.1, the electric field and current density near the plasma boundary decay almost exponentially, as in the case of classical skin effect. We will use this observation later.

2.2.2   Plasma Heating

Since the electrons in ICP plasma are warm and the electromagnetic wave phase velocity becomes equal to v_{Te} (as we have seen from Fig. 2.2), the resonant (collisionless) heating of electrons by the wave should be important, and this has been well recognized [35]. However, until recently, there was no direct experimental evidence of collisionless heating. In 1998, Godyak *et al.* [32] measured the plasma heating in ICP (using the experimental setup described above) and compared it to the purely collisional heating. The density of absorbed power (plasma heating) was calculated from the measured current density and electric field in plasma as

$$w(x) = E(x)\,j(x)\cos\left[\phi_E(x) - \phi_j(x)\right],\qquad(2.25)$$

where $E(x)$ and $j(x)$ are the rms magnitudes of azimuthal field and current density, $\phi_E(x)$ and $\phi_j(x)$ are the field and current phases, respectively. The total power absorption by the plasma can be characterized by the total absorbed power flux into plasma

$$S(x) = \int_0^x w(x')dx'. \tag{2.26}$$

Evidence of Collisionless Heating in Nonlocal Regime

The absorbed power flux is shown in Fig. 2.4 for 1.0 and 0.3 mTorr. For both pressures, the driving frequency was 6.78 MHz, and the discharge power was 100 W. For comparison, the purely collisional absorbed power flux, calculated from a cold plasma theory (using Eqs. 1.31 and 2.26) is also shown in Fig. 2.4. It is seen that the measured absorbed power flux significantly exceeds the purely collisional one. This implies that the collisionless heating is quite important and should be taken into account to correctly evaluate the heating of typical ICP. Thus the experimental evidence of collisionless heating in ICP in nonlocal regime has been provided by Godyak *et al.*

It should be noted that in calculating the purely collisional part of the absorbed power flux (2.26) with (1.31) in Fig. 2.4, the same collision frequency ν_e should be used in (1.31) as that measured in the warm ICP discharge. More detailed comments on how to calculate the purely collisional part of power absorption can be found in [32].

A plasma pressure dependence of the ratio of the measured absorbed power flux to the purely collisional value is shown in Fig. 2.5, for the driving frequencies of 3.39, 6.78 and 13.56 MHz. It is seen that at low gas pressures $p < 10$ mTorr the measured power absorption significantly exceeds the purely collisional one, while at higher pressures from 10 to 100 mTorr the measured power absorption almost coincides with the purely collisional value, implying that the collisional heating dominates over the collisionless (resonant) heating at high pressures, when the collisions of electrons with gas atoms become frequent, $\nu_e > v_{Te}/\delta$.

37
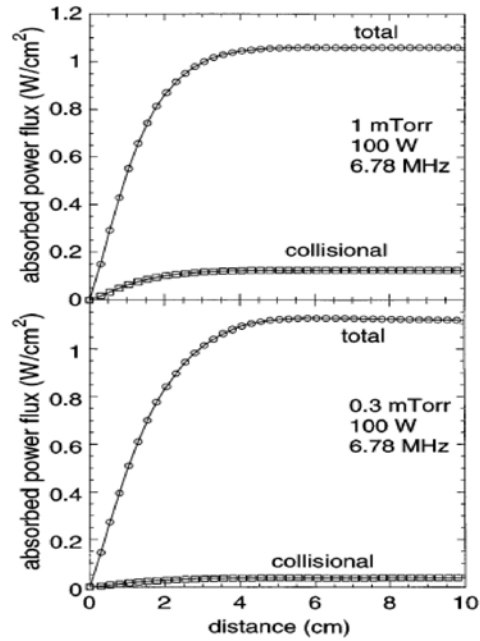
Figure 2.4: Absorbed power flux (2.26) for $p = 0.3$ and 1.0 mTorr, by Godyak *et al.* [32]. The purely collisional power flux is shown by squares.
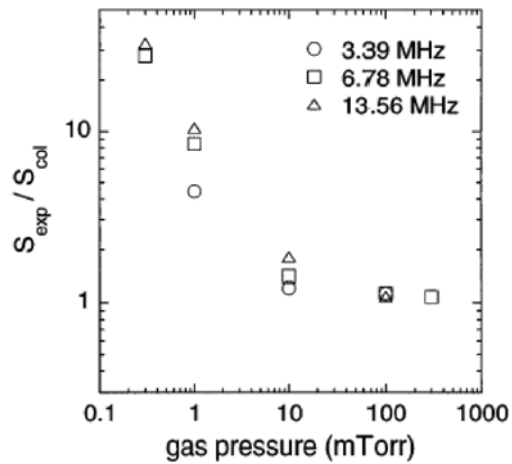
Figure 2.5: The ratio of the total measured to purely collisional absorbed power flux as a function of argon pressure, by Godyak *et al.* [32].

Negative Power Absorption in Nonlocal Regime

The spatial profiles of the measured absorbed power density (2.25) for different driving frequencies [31] are shown on Fig. 2.6. These profiles reveal another interesting feature of bounded plasma in nonlocal regime – the existence of regions of negative power absorption in plasma (denoted by the "-" sign on Fig. 2.6). In these regions the power is transferred from plasma electrons back to the electromagnetic wave. As it is seen from Fig. 2.6, the number
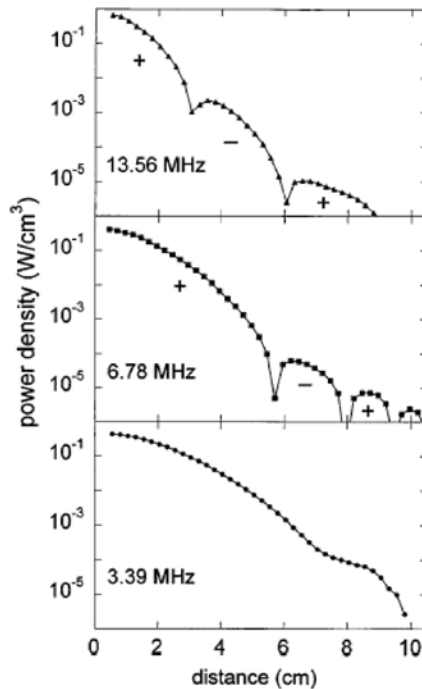
Figure 2.6: Experimental power absorption profiles for different driving frequencies, by Godyak *et.al.* [31]. Signs denote regions of positive (+) and negative (-) power absorption.

of regions with negative power absorption depends on the driving frequency, and there is no negative power absorption for $\omega/2\pi = 3.39$ MHz. The distance between the maximum in the RF current density and first zero crossing point in the absorbed power density profile is inversely proportional to the driving frequency. This suggests that the reason for these regions of negative power

39

absorption is the thermal diffusion of current from the skin layer deeper into plasma, as we have discussed above. Indeed, the absorbed power density is proportional to $\cos\left[\phi_E(x) - \phi_j(x)\right]$ (ref. Eq. 2.25), therefore, if the phase difference between the current and the field increases by 180°, then the power absorption becomes negative. The current is formed mainly in the skin layer, where the electric field is large, and is transferred by thermal electrons deeper into plasma with mean velocity v_{Te}, preserving its phase. While the current is transferred, the electric field changes its phase (due to its time oscillations), and after a time period π/ω its phase inverts, making the phase difference between the field and the current change by 180°. During this time of inversion of the phase of the electric field, the current gets transferred into plasma to a distance of the order of $v_{Te}\pi/\omega$. Therefore, the power absorption should inverse its sign (become negative) at the distance $v_{Te}\pi/\omega$ from the skin layer. For $\omega = 2\pi \cdot 13.56$ MHz, $v_{Te} = 1.06 \cdot 10^8$ cm/s (the value in the experiment of Godyak *et al.*) our qualitative analysis gives the position of the region of negative power absorption at approximately 3.9 cm from the plasma boundary, which agrees very well with the actual position of negative power absorption region (see Fig. 2.6).

As we have seen from the theory of anomalous skin effect, the degree of nonlocality of plasma is described by a fundamental parameter of nonlocality [3, 12]:

$$\Lambda = \left(\frac{\lambda_{eff}}{\delta}\right)^2 = \left(\frac{\omega_{pe}v_{Te}}{c}\right)^2 \frac{\omega}{(\omega^2 + \nu_e^2)^{3/2}}. \tag{2.27}$$

This expression for Λ is valid for planar plasma. Here λ_{eff} is the electron effective mean free path, δ is the classical skin depth. For $\Lambda > 1$ plasma is in nonlocal regime (anomalous skin effect), for $\Lambda < 1$ plasma is in local regime (classical skin effect). In this experiment, $\Lambda \approx 1$, therefore, both collisions and electron thermal motion are important.

As the negative power absorption is caused by the electron thermal motion, it is a purely nonlocal effect, and it is expected to be more pronounced at lower

frequencies, when Λ is large. However, as we see from Fig. 2.6, at 3.39 MHz there is no negative power absorption. While the nonlocal effects are more important at 3.39 MHz than at 6.78 and 13.56 MHz, the position of the first region of negative power absorption $v_{Te}\pi/\omega$, being inversely proportional to the driving frequency, simply is not within the discharge chamber (the estimate $v_{Te}\pi/\omega$ gives the position of negative absorption at ≈ 15 cm from the plasma boundary, while the length of discharge chamber is only 10.5 cm), and thus the negative power absorption is not seen at 3.39 MHz.

In Chapter 3 we will develop a kinetic model of ICP in nonlocal regime which, besides all, predicts the negative power absorption very similar to that observed experimentally by Godyak *et al.*

2.2.3 Ponderomotive Effect

In modern ICP sources there is a trend towards lower driving frequencies. At low frequencies, the RF Lorentz force $\mathbf{F}_L = -e/c\,(\mathbf{v} \times \mathbf{B})$ becomes significant, therefore a significant ponderomotive effect is expected. The ponderomotive force in cold collisional plasma is given by the Miller formula (1.41), which has the form of a potential force $F_M = -\nabla U_M$ with the potential $U_M = \varepsilon = m_e \langle \mathbf{v} \rangle^2 /2$, where ε is the average electron oscillatory energy, $\langle \mathbf{v} \rangle = e/(\sqrt{2}m_e)E_\theta/\sqrt{\omega^2 + \nu_e^2}$. A noticeable ponderomotive effect on plasma density profile is expected when the ponderomotive force is comparable to, or larger than the competing pressure gradient force in plasma [17]:

$$\nabla \left(m_e \langle \mathbf{v} \rangle^2 /2 \right) \gtrsim eT_e \frac{\nabla n}{n}, \quad \text{or} \quad \varepsilon/T_e \gtrsim \delta/2d, \tag{2.28}$$

where T_e is the electron temperature in eV, n is the plasma density, δ is the electromagnetic field skin depth, and d is the characteristic length of the plasma density variation. Attempts over the last 30 years to observe the ponderomotive effect in collisional weakly ionized gas discharge plasma have failed because in such plasmas the ratio ε/T_e is small, and the ponderomotive effect is too weak to be observed.

Recently, Godyak *et al.* were the first to measure the ponderomotive effect in ICP. This was made possible due to the extremely low gas pressures at which the modern ICP sources are maintained, which makes the electron average oscillatory energy comparable to the electron temperature. However, under such low pressures (few mTorr) and high electron temperatures (few eV) the plasma is in nonlocal regime, and the Miller formula for the ponderomotive force, as well as the condition (2.28), may no longer be valid.

Godyak *et al.* measured the basic plasma parameters (plasma density n, electron temperature T_e, dc plasma potential V) along the axial direction x with a Langmuir probe moved along the discharge axis. As in the experiments on defining the structure of electromagnetic field and current in plasma, the measurements were performed at two radial positions: $r = 4$ cm (position of maximum electromagnetic field amplitude), and $r = 0$ (position where there is no electromagnetic field). The axial profiles of plasma density and dc potential at these two radial positions for the driving frequencies of 0.45 and 6.78 MHz are shown on Fig. 2.7. At 6.78 MHz, at both radial positions, the measured $n(x)$ and $V(x)$ are rather symmetrical about the discharge mid-plane and have a Boltzmann distribution $n(x)/n_{\max} = \exp\left(-eV(x)/T_e\right)$ [17]. This distribution of plasma density is typical for discharges where the ponderomotive effect is insignificant. However, at 0.45 MHz we see a significant asymmetry in the measured profiles of $n(x)$ and $V(x)$. Moreover, at $r = 4$ cm there is a clear shift between the maximum of $n(x)$ and a minimum of $V(x)$, while at $r = 0$ the maximum of $n(x)$ coincides with the minimum of $V(x)$. This shift, occurring at the position of the strongest electromagnetic field, and not occurring at the position of zero electromagnetic field, and the asymmetry in $n(x)$ and $V(x)$, are signatures of the ponderomotive effect which causes both the shift and the asymmetry. To calculate the ponderomotive potential from the measured spatial profiles of plasma density and potential, we write down the equation of plasma equilibrium, following Godyak *et al.* [17]:

$$T_e \nabla n + n \nabla V + n \nabla U = 0, \qquad (2.29)$$
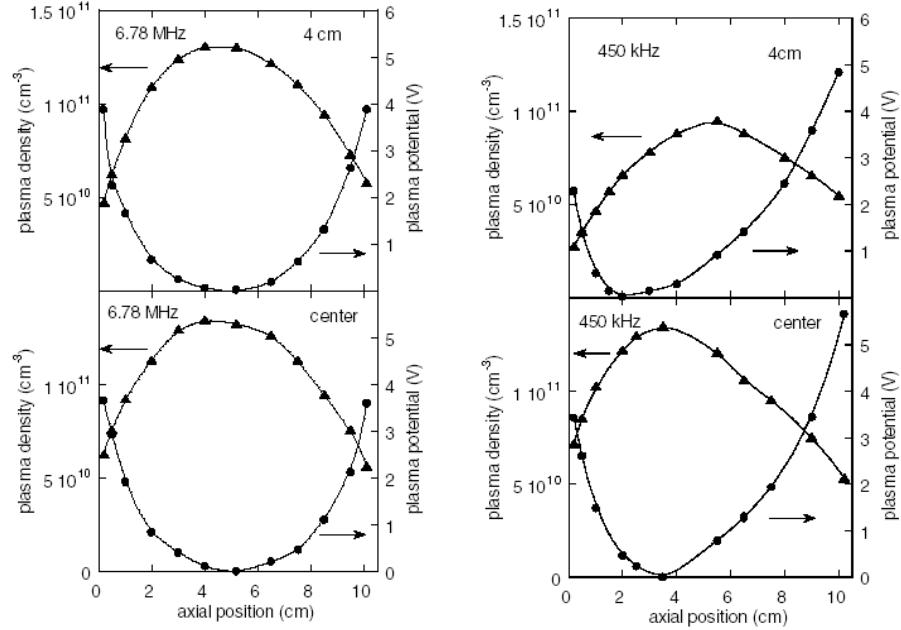
Figure 2.7: Measured plasma density and potential distribution at driving frequencies 6.78 MHz (left) and 0.45 MHz (right), by Godyak *et al.* [17].

with three forces canceling each other: the force due to pressure gradient $eT_e n^{-1} \nabla n$, the force due to ambipolar potential gradient $e\nabla V$, and the ponderomotive force $e\nabla U$, where U is the ponderomotive potential that we need to find. The solution of (2.29) has the following form: $n/n_0 = \exp\left(-\left(V + U\right)/T_e\right)$. This can be rewritten as $T_p \equiv V + U = T_e \ln\left(n_0/n\right)$. Having measured n, V and T_e, we can plot the plasma thermal potential $T_p = V + U$ together with V (see the plot in Fig. 2.8), and define U from their difference. As we see in Fig. 2.8, at $r = 0$ there is no difference between T_p and V, i.e. $U = 0$ in the discharge center, where there is no electromagnetic field. At $r = 4$ there is a significant difference between T_p and V, due to a significant ponderomotive potential U. Now we can define the ponderomotive potential U from Fig. 2.8.
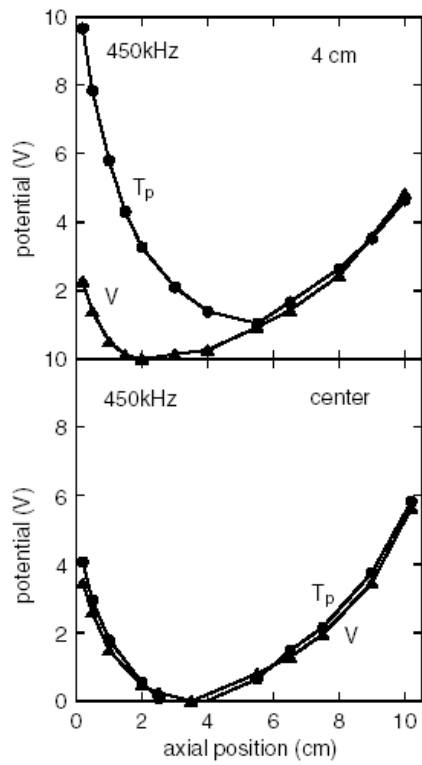
Figure 2.8: Plasma thermal T_p and electrical V potential distributions at 0.45 MHz, by Godyak *et al.* [17].
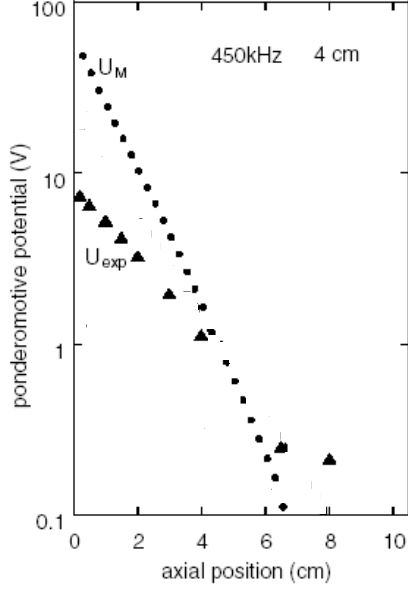
Figure 2.9: Measured ponderomotive potential U_{exp} spatial profile, together with the Miller potential U_M, by Godyak *et al.* [17].

Discrepancy with Prediction of Classical Theory

The experimentally defined ponderomotive potential U_{exp}, found in the way described in the previous paragraph, is plotted in Fig. 2.9 together with the Miller potential U_M for comparison (U_M is defined from the Miller force F_M (1.41) as $U_M(x) = -\int_\infty^x F_M(x')dx'$). We see that there is a significant discrepancy between the measured ponderomotive potential and that predicted by the classical theory of ponderomotive effect in cold collisional plasma. Namely, we see that the measured ponderomotive potential is almost 10 times less than that predicted by the Miller formula (1.41). In this experiment plasma was in the regime of strongly anomalous skin effect (strongly nonlocal regime) at the driving frequency 0.45 MHz [17]. Thus, the Miller formula for ponderomotive force is proven to be inadequate for describing the ponderomotive force in ICP in the nonlocal regime.

2.3 Motivation for Theoretical Work

As we review the results of experimental measurements of plasma heating and ponderomotive effect in modern ICP operating in the regime of anomalous skin effect, we continuously encounter discrepancies with the predictions of classical theory of heating and ponderomotive force in cold collisional plasma. Even the skin effect itself is quite different from the classical skin effect. We have many strong clues that the major factor that should be responsible for all these discrepancies is the electron thermal motion, which is not taken into account in classical theory. Thermal motion appears to be quite important in the typical experimental regimes of modern ICP discharges. Therefore in order to correctly describe the plasma heating and ponderomotive force in nonlocal regime, we need a theory that accounts for electron thermal motion, as well as for collisions. This theory should be developed on a basis of kinetic equation (1.10), as the hydrodynamic equation (1.7) is not applicable for plasmas with $\omega, \nu_e < v_{Te}/\delta$.

As for the theories of plasma heating in nonlocal regime, there exist two different approaches. One is based on the calculation of the surface impedance of plasma in nonlocal regime (2.16) and using it for finding the absorbed power of the wave as [24]

$$\left\langle \int dV \, \mathbf{j} \cdot \mathbf{E} \right\rangle = \frac{1}{2} \int dS \, (\text{Re} \, Z_H) \, B_z^2, \tag{2.30}$$

where $\langle ... \rangle$ denote a time average, V is the plasma volume, S is the plasma surface area, and B_z is the magnetic field driven by the antenna coil. This approach can be referred to as the surface impedance method. The major advantage of this method is that it uses the self-consistent electromagnetic field in plasma to calculate the surface impedance, and thus to find the power absorption. However, this advantage turns into a disadvantage when we realize that the electromagnetic field and the surface impedance can only be calculated numerically, and the expressions for plasma heating derived by this approach, yet being rigorous, are not very insightful.

Another approach to calculating the power absorption in nonlocal regime is usually referred to as the stochastic method [35, 36]. It is based on calculation of the gain of energy by a single particle (electron) traveling through the skin region in the prescribed electromagnetic field. This method, while being much less rigorous than the surface impedance method, is more physically intuitive. It adopts a few assumptions that greatly simplify the analysis, among which is an assumption of exponentially decaying profile of the electromagnetic field in plasma. This assumption is based on the observation that we made earlier from the theoretical and experimental profiles of the electromagnetic field in plasma in nonlocal regime: within the skin layer the field profile is quite close to exponential. Another assumption made in this approach is that the magnetic field is weak and does not influence the electron trajectory in the skin layer. As we will see later, this assumption is invalid at low driving frequencies. With this assumption, the model is linear. Vahedi *et al.* [36] consider an electron moving through the skin layer and being bounced back from the plasma boundary. The idea is that, "if the electron transit time through the power absorption region is shorter than the RF period, $\tau = \delta/v_x < 2\pi/\omega$, then the electron is nonadiabatically heated, i.e., the electron acquires a net velocity change in the direction transverse to x." [36] (we should note, however, that if the magnetic field is not neglected, the direction of electron's velocity change is along x for any magnetic field [7, 15]). In the absence of collisions, the magnitude of this velocity change is found as [36]

$$\Delta u_{e\,y} = -\frac{e}{m_e} \int_{t_1}^{t_2} E_y dt, \qquad (2.31)$$

where t_1, t_2 is the interval of time during which the electron experiences the electric field E_y. Assume the electric field in the exponentially decaying form $E_y(x,t) = E_0 \exp\left(-x/\delta\right) \sin \omega t$ (in cylindrical geometry there is also a radial dependence of the azimuthal electric field as $J_1(\mu_1 r/R)$, $\mu_1 \approx 3.83$, R is the cylinder radius; therefore, to make the result of this planar calculation applicable to cylindrical geometry, one has to multiply the electric field by $J_1(\mu_1 r/R)$).

Therefore the skin depth enters the model as a given parameter. If the electron initial position is x_0, then we can find $t_1 = -x_0/v_x$, $t_2 = x_0/v_x$. With the exponentially decaying electric field we can set $x_0 = \infty$, and finally we get for the electron velocity change after the full round trip through the skin region [36]:

$$\Delta u_{ey} = -\frac{e}{m_e} E_0 \int_{-\infty}^{\infty} \exp\left(-\left|t\right|/\tau\right) \sin\left(\omega t + \phi_0\right) \, dt, \qquad (2.32)$$

where $\tau = \delta/v_x$, and ϕ_0 is the phase of the incoming electron relative to the electric field. Performing the integration, we obtain

$$\Delta u_{ey} = -\frac{e}{m_e} E_0 \frac{2\tau \sin \phi_0}{1 + (\tau\omega)^2}. \qquad (2.33)$$

Averaging over all possible phases ϕ_0 we calculate the average energy gained per single electron over the round trip through the skin region as [36]

$$\langle \Delta \varepsilon_{st} \rangle = \frac{e^2 E_0^2}{m_e} \frac{\tau^2}{\left[1 + (\tau\omega)^2\right]^2}. \qquad (2.34)$$

In order to find the total power deposited into all plasma electrons, we have to average the energy gain per single electron over all electrons in plasma. Assuming that nearly all electrons are reflected by the sheath, we get for the power per unit area

$$S_{st} = \int_0^{\infty} dv_x \, \langle \Delta \varepsilon_{st} \rangle \, v_x \, f_{e0}(v_x), \qquad (2.35)$$

where f_{e0} is the electron velocity distribution function. Taking f_{e0} to be Maxwellian, we finally get for the collisionless power absorption per unit area [36]

$$S_{st} = \frac{e^2 E_0^2}{4m_e} \frac{\delta}{\bar{v}_e} \frac{4\delta}{}\, \Im\left(\beta\right) n_0, \qquad (2.36)$$

where $\bar{v}_e = \sqrt{8T_e/\pi m_e}$,

$$\Im\left(\beta\right) = \frac{1}{\pi} \int_0^{\infty} dx \frac{x \exp(-x)}{(x+\beta)^2} = \frac{1}{\pi} \left[e^\beta \left(1+\beta\right) \operatorname{Ei}(1,\beta) - 1\right], \qquad (2.37)$$

with $\beta = \left(4\delta^2\omega^2\right)/\left(\pi\bar{v}_e^2\right)$, and $\operatorname{Ei}(1,\beta) = \int_\beta^{\infty} dy \exp(-y)/y$.

Expression (2.36) is a simple practical expression for the collisionless heating of plasma. It is an approximate expression, valid as long as the assumptions made in its derivation are valid. It reduces to the well known results for collisionless heating in strongly nonlocal and in local regimes (see [36] for details).

However, as in typical discharges the electron collision frequency is of the same order of magnitude as the wave driving frequency, $\nu_e \sim \omega \lesssim v_{Te}/\delta$, the collisions can play an important role in plasma heating. But if the collisions are included into the stochastic model of Vahedi *et al.*, then we do not get such simple expression for the power absorption as the expression for collisionless power absorption (2.36). The analysis analogous to the previous collisionless analysis, only with collisions included, yields for the energy gained per one electron [36]:

$$
\begin{aligned}
\langle \Delta \varepsilon_{1e} \rangle &= \frac{e^2 E_0^2}{4 m_e} \left[\left(\frac{\nu_e + 1/\tau}{(\nu_e + 1/\tau)^2 + \omega^2} + \frac{\nu_e - 1/\tau}{(\nu_e - 1/\tau)^2 + \omega^2} \right) \tau + \right. \\
&\quad + \left(\frac{\nu_e + 1/\tau}{(\nu_e + 1/\tau)^2 + \omega^2} - \frac{\nu_e - 1/\tau}{(\nu_e - 1/\tau)^2 + \omega^2} \right) \frac{2 (\nu_e + 1/\tau)}{(\nu_e + 1/\tau)^2 + \omega^2} - \\
&\quad \left. - \left(\frac{1}{(\nu_e + 1/\tau)^2 + \omega^2} - \frac{1}{(\nu_e - 1/\tau)^2 + \omega^2} \right) \frac{2 \omega^2}{(\nu_e + 1/\tau)^2 + \omega^2} \right].
\end{aligned}
\tag{2.38}
$$

The power per unit area is again

$$
S_e = \frac{e^2 E_0^2}{4 m_e} \frac{\delta}{\delta} \frac{\Im}{\delta} n_0,
\tag{2.39}
$$

where $\Im$ is now the integral of Eq. (2.38) over the electron velocity distribution. The final expression for the total absorbed power with account for collisions is not given in the paper of Vahedi *et al.* [36]. It is also unknown how well it describes the heating in nonlocal regime with collisions, as the authors did not compare their theoretical model with experimental data.

One of our objectives was to develop a theoretical model that would yield relatively simple, easy to calculate expressions for the power absorption in nonlocal regime with collisions. We will develop such a model in Chapter 3, combining, in a sense, the two methods (surface impedance method and stochastic method) – we will use the Boltzmann equation to describe the electrons and

the technique of its solution, as in the surface impedance method, and the simplifying assumption of the exponentially decaying electric field profile, as in the stochastic method.

As for the theory of ponderomotive force in nonlocal regime, there is even more diversity in approaches comparing to the two principal approaches in theories of plasma heating. There are almost as many different ways of treating the ponderomotive force as there are authors on the subject (see [37]). Here we will review briefly the theory of ponderomotive force exerted by high frequency electromagnetic wave onto plasma in nonlocal regime, which accounts for resonant interaction between the wave and plasma electrons (Landau interaction). This theory was developed by Akama and Nambu [38]. They considered the force per unit volume exerted by electromagnetic waves on plasma as (the Fourier component of the force):

$$\mathbf{F}(k) = \frac{1}{4} \left[\rho^*(\mathbf{k}, \omega) \mathbf{E} + c.c. \right] + \frac{1}{4} \left[\mathbf{j}^*(\mathbf{k}, \omega) \times \mathbf{B} + c.c. \right], \qquad (2.40)$$

where $\rho(\mathbf{k}, \omega)$ and $\mathbf{j}(\mathbf{k}, \omega)$ are the induced charge and current densities, the asterisk implies the operation of complex conjugate, c.c. stands for complex conjugate of the first term in the brackets, and $\mathbf{E}$ and $\mathbf{B}$ are the amplitudes of the electric and magnetic fields cast in the form $\mathbf{E}(\mathbf{r}, t) = \mathbf{E} \exp\left[i\left(\mathbf{k} \cdot \mathbf{r} - \omega t\right)\right]$, $\mathbf{B}(\mathbf{r}, t) = \mathbf{B} \exp\left[i\left(\mathbf{k} \cdot \mathbf{r} - \omega t\right)\right]$. For the electromagnetic waves the induced charge density is zero, $\rho(\mathbf{k}, \omega) = 0$, and the force exerted on plasma by the electromagnetic wave (ponderomotive force) is just

$$\mathbf{F}(k) = \frac{1}{4} \left[\mathbf{j}^*(\mathbf{k}, \omega) \times \mathbf{B} + c.c. \right], \qquad (2.41)$$

and, after introducing the vector potential as $\mathbf{A}(\mathbf{r}, t) = \mathbf{A} \exp\left[i\left(\mathbf{k} \cdot \mathbf{r} - \omega t\right)\right]$ and defining the plasma conductivity Fourier image $\sigma(\mathbf{k}, \omega)$ from $\mathbf{j}(\mathbf{k}, \omega) = \sigma(\mathbf{k}, \omega)\mathbf{E}$, they got for the α-th component of the force:

$$F_\alpha(k) = \frac{1}{4} \left[A_\beta^* P^*(\mathbf{k}, \omega) A_\beta + c.c. \right], \qquad (2.42)$$

where $P^*(\mathbf{k}, \omega) = k_\alpha \omega \sigma^*(\mathbf{k}, \omega)$, and the summation over the repeated indices is assumed. The plasma conductivity is defined from the linearized kinetic

equation as [38]

$$\sigma(\mathbf{k}, \omega) = \frac{ine^2}{m_e} \int \frac{f_0(\mathbf{v})}{\omega - \mathbf{k} \cdot \mathbf{v} + i\nu_e} d\mathbf{v}, \tag{2.43}$$

therefore taking into account the resonant interaction of electrons (having velocities close to the wave phase velocity ω/k) with the wave. Defining the transverse dielectric function as $K(\mathbf{k}, \omega) = 1 + 4\pi i \sigma(\mathbf{k}, \omega)/\omega$, we can reduce $P^*(\mathbf{k}, \omega)$ to

$$P^*(\mathbf{k}, \omega) = (i/4\pi) k_\alpha \omega^2 \left[K^*(\mathbf{k}, \omega) - 1 \right]. \tag{2.44}$$

Changing to the amplitudes of the wave weakly depending on $\mathbf{r}$ and t, $\mathbf{A} = \mathbf{A}(\mathbf{r}, t) \exp \left[i \left(\mathbf{k} \cdot \mathbf{r} - \omega t \right) \right]$, Akama and Nambu replace $P^*(\mathbf{k}, \omega)$ in (2.42) with $P^* (\mathbf{k} - i\nabla, \omega - i\partial_t)$. Expanding P^* into Taylor series and neglecting higher order terms (i.e. retaining only the effects of weak spatial inhomogeneity and temporal dependence of field amplitude), they finally derive the expression for the Fourier image of α-th component of the ponderomotive force exerted by electromagnetic wave on plasma in nonlocal regime as

$$
\begin{aligned}
F_\alpha(k) & = \frac{1}{8\pi} k_\alpha \operatorname{Im}(K(\mathbf{k}, \omega)) \, |\mathbf{E}|^2 + \frac{1}{16\pi} \left(\operatorname{Re}(K(\mathbf{k}, \omega)) - 1 \right) \frac{\partial}{\partial x_\alpha} |\mathbf{E}|^2 + \\
& \quad + \frac{1}{16\pi} k_\alpha \frac{\partial \operatorname{Re}(K(\mathbf{k}, \omega))}{\partial k_\beta} \frac{\partial}{\partial x_\beta} |\mathbf{E}|^2 + \frac{\partial g_\alpha}{\partial t},
\end{aligned} \tag{2.45}
$$

where

$$g_\alpha = \frac{1}{16\pi} k_\alpha \frac{1}{\omega^2} \frac{\partial}{\partial \omega} \left[\omega^2 \left(\operatorname{Re}(K(\mathbf{k}, \omega)) - 1 \right) \right] |\mathbf{E}|^2. \tag{2.46}$$

The physical meaning of the terms in the expression for the force (2.45) is as follows [38]. The first term on the right-hand side of (2.45) represents the density of force exerted on resonant particles when they absorb the wave, i.e. the force due to Landau damping. The second term is the usual ponderomotive force (similar to the Miller force), it does not have an explicit dependence on k. The third term contains the effects of high temperature (spatial dispersion). The fourth term is the time rate of change of momentum of the nonresonant particles.

While the expression for the ponderomotive force derived by Akama and Nambu (2.45) accounts for thermal effects, it is derived for the case of weakly

inhomogeneous field amplitude. Therefore our case of strongly inhomogeneous fields in ICP cannot be adequately described by the model of Akama and Nambu [38] or other similar models (see [39, 40, 41, 42, 43] and the extensive list of references in [37]). We were able to develop an adequate description of ponderomotive force based on the linear kinetic model of plasma electron dynamics, which will be presented in Chapter 3. As we will see, this model predicts the thermal reduction of the ponderomotive force similar to that observed in the experiment (see Fig. 2.9). Another advantage of our model, as we will see later, is a relative simplicity of its final expressions for the ponderomotive force and plasma heating.

Chapter 3

Linear Kinetic Theory of Heating and Ponderomotive Force in Nonlocal Regime

3.1 Preliminary Discussion. Formulation of the Problem

As we have seen, the experimental results on measuring plasma heating and ponderomotive force in typical ICP discharge prove the classical theory of heating and ponderomotive force (Miller force) to be inadequate in nonlocal regime, when the electron thermal motion is significant. Our task here is to develop a theoretical model that explains the discrepancy between the observed experimental value of the ponderomotive potential and the existing theoretical results, as well as describes other features of nonlocal ICP, e.g. negative power absorption and collisionless plasma heating.

This model should account for electron thermal motion and collisions, therefore we will be using the kinetic approach based on the Boltzmann equation (1.10) for the electron distribution function (ions are assumed to be cold and immobile). Once we know the electron distribution function which de-

fines the electron response to the electromagnetic field of the driving wave, we can calculate the heating rate of electrons (plasma heating) and ponderomotive force exerted on plasma (i.e. on plasma electrons) by the electromagnetic wave.

However, in order to make the problem solvable, we have to make some simplifying assumptions. First of all, we will be considering the idealized model of planar ICP (ref. Fig. 1.3), representing the cylindrical discharge with planar coil configuration, just as Shaing [24] or Vahedi *et al.* [36] did. Let us consider a TE electromagnetic wave with the electric field having the only component along y (corresponds to azimuthal field in cylindrical discharge) and the magnetic field along z (corresponds to radial field in cylindrical discharge) incident on our semi-infinite plasma. Plasma is in nonlocal regime (anomalous skin effect regime), therefore the spatial profile of the electromagnetic field in plasma is nonmonotonic (see Figs. 2.1, 2.2). However, as we noted in the previous chapter, in the skin layer where the field is the largest the spatial profile is very close to the exponentially decaying profile. We will use this observation to make an important assumption of exponentially decaying fields in nonlocal regime, which will greatly simplify our model, as we will not have to solve for the self-consistent field, like in surface impedance method. This assumption has also been made in [36]. As it was shown by Haas [44], this assumption works quite well in description of plasma heating (and therefore the ponderomotive force) in nonlocal regime. Thus the electric field in plasma is assumed to be of the form $E_y(x,t) = E_0 \exp(-\gamma x) \exp(-i\omega t)$, where $\gamma = 1/\delta - i\,\kappa$ is a complex wave vector, δ is the skin depth in the nonlocal regime (δ enters the theory as an input parameter), and κ defines the absorbed power (Poynting flux).

Other assumptions that we use in our theoretical model are:

- All quantities are assumed to be independent on y. In real cylindrical discharge this assumption corresponds to the assumption that the plasma and therefore all quantities are azimuthally symmetric, i.e. $\partial/\partial\theta = 0$.

- The plasma boundary is assumed to be sharp. This is a good assumption if the sheath width in plasma, which is of the order of few Debye lengths λ_{De}, is much smaller than the typical length scale of plasma density gradient and of the field gradient (skin depth).

- The bulk plasma is assumed to be quasineutral in the absence of fields (in equilibrium), and homogeneous, i.e. $n_i = n_e = n_0$.

- Ions are assumed to be cold and immobile.

- The density of neutral atoms is assumed to be uniform in space, therefore the electron-neutral collision frequency is the same at any position.

3.2 Linearized Kinetic Equation

The electron distribution function can be separated into two parts: $f_e = f_{0e}(\mathbf{v}) + \tilde{f}(\mathbf{v}, \mathbf{r}, t)$, where f_{0e} is the equilibrium distribution function of electrons (in the absence of fields), and $\tilde{f}$ describes the response of electrons to the field. We will be considering weak fields, when $\left|\tilde{f}\right| \ll f_{0e}$. The linearized Boltzmann equation for electrons is

$$\frac{\partial \tilde{f}}{\partial t} + v_x \frac{\partial \tilde{f}}{\partial x} = \frac{e}{m_e} \left(\mathbf{E} + \frac{1}{c} \mathbf{v} \times \mathbf{B} \right) \cdot \frac{\partial f_{0e}}{\partial \mathbf{v}} + \hat{S}(\tilde{f}). \qquad (3.1)$$

We approximate the collision term as $\hat{S}(\tilde{f}) = -\nu_e \tilde{f}$ (BGK collision term [29]). Since plasma in ICP discharges is weakly ionized, the primary collisions in such plasma are the collisions between electrons and neutral gas atoms, $\nu_e \simeq \nu_{en}$. If the equilibrium distribution function $f_{0e} = f_{0e}(\varepsilon)$, where ε is electron kinetic energy, then $(\mathbf{v} \times \mathbf{B}) \cdot \partial f_{0e}/\partial \mathbf{v} = 0$. Assuming that $\tilde{f}$ has the same time dependence as E_y, we reduce the equation for $\tilde{f}$ to obtain

$$\frac{\partial \tilde{f}}{\partial x} - i\alpha \tilde{f} - \frac{e}{v_x} \mathbf{v} \cdot \mathbf{E} \, \frac{\partial f_0}{\partial \varepsilon} = 0 \,. \qquad (3.2)$$

Here $\alpha = \tilde{\omega}/v_x$, $\tilde{\omega} = \omega + i\nu_{en}$. The general solution of equation (3.2) is

$$\tilde{f} = \left[C(\mathbf{v}) + \frac{e}{v_x} \int_0^x \mathbf{v} \cdot \mathbf{E} \; \partial f_0/\partial \varepsilon \exp(-i\alpha x') \, dx' \right] \exp(i\alpha x). \qquad (3.3)$$

Here $C(\mathbf{v})$ depends only on electron velocity, not on coordinate. It is convenient to write the distribution function $\tilde{f}$ as a sum of two distribution functions, $\tilde{f} = f^{(+)}(v_x, x) + f^{(-)}(-v_x, x)$, $v_x > 0$, where $f^{(+)}$ is the distribution function of electrons moving away from the boundary $x = 0$, and $f^{(-)}$ is the distribution function of electrons moving towards the boundary. After this separation, we can easily specify the boundary conditions for $\tilde{f}$ to determine $C(\mathbf{v})$, similar to the boundary conditions in the theory of anomalous skin effect [23, 24]. The first boundary condition is for specular reflection of electrons from the boundary by the sheath (we ignore the spatial structure of the sheath potential):

$$f^{(+)}(v_x, x) = f^{(-)}(-v_x, x) \quad \text{at} \;\; x = 0. \qquad (3.4)$$

The second boundary condition states that $f^{(-)}$ should vanish at infinity (since the electrons coming from infinity towards the boundary are not influenced by the field):

$$f^{(-)}(-v_x, \, x) = 0 \;\; \text{at} \;\; x = \infty. \qquad (3.5)$$

Using (3.4) and (3.5), and assuming that the equilibrium electron distribution is Maxwellian, we obtain for $f^{(+)}$ and $f^{(-)}$:

$$f^{(+)} = \frac{2ev_y}{m_e v_{Te}^2} E_0 f_M \exp(-i\omega t) \left[\frac{\exp(-\gamma x)}{i\tilde{\omega} + \gamma v_x} - 2\frac{\exp(i\tilde{\omega}x/v_x) \, \gamma v_x}{(\gamma v_x)^2 + \tilde{\omega}^2} \right], (3.6)$$

$$f^{(-)} = \frac{2ev_y}{m_e v_{Te}^2} E_0 f_M \exp(-i\omega t) \frac{\exp(-\gamma x)}{i\tilde{\omega} - \gamma v_x}, \;\; v_x > 0. \qquad (3.7)$$

Here $f_M = n_0 \exp(-v^2/v_{Te}^2)/v_{Te}^3 \pi^{3/2}$ is the Maxwellian distribution function, $v_{Te}^2 = 2T_e/m_e$. By assuming $f_{0e} = f_M$ we automatically made an assumption of a uniform plasma in the absence of fields, with the density n_0.

3.3 Nonlocal Electric Current in Plasma. Non-locality Parameter

The density of current in plasma induced by the electric field is then $j_y = -e \int v_y \left(f^{(+)} + f^{(-)} \right) d^3v$, and after integration it becomes

$$j_y = \frac{e^2 n_0}{m_e} \frac{1}{\gamma v_{Te}} E_0 \exp(-i\omega t) \left(G(x) - \exp(-\gamma x) Z(-is) \right) , \qquad (3.8)$$

where $Z(p) = 1/\sqrt{\pi} \int_{-\infty}^{\infty} dt \exp(-t^2)/ (t-p)$ is the plasma dispersion function, $s = \tilde{\omega}/\gamma v_{Te}$ and $G(x)$ is a complex function of x,

$$G(x) = \frac{2}{\sqrt{\pi}} \int_0^{\infty} \frac{t \exp(i\gamma s \, x \, / \, t - t^2)}{t^2 + s^2} dt . \qquad (3.9)$$

Note that j_y is a nonlocal function of $E_y \sim \exp(-\gamma x)$.

The parameter $s = (\omega + i\nu_{en})/\gamma v_{Te}$ describes the degree of nonlocality of the plasma. The condition $|s| = 1$ separates local ($|s| > 1$) and nonlocal ($|s| < 1$) regimes of the ICP. The absolute value of s is an analog of plane-geometry parameter of nonlocality Λ (see Eq. 2.24 and [2, 3, 12]). In the plane geometry case $|s| = 1/\sqrt{\Lambda}$, and $|s|$ becomes large (i.e. plasma is in local regime) both for low and high driving frequencies. In the cylindrical geometry the situation is different. In the latter case, the complex wave vector γ_{cyl} is defined by [45]

$$\gamma_{cyl}^2 = \left(\frac{\mu_1}{R} \right)^2 + \gamma_{plane}^2 , \qquad (3.10)$$

where $\gamma_{plane} \approx 1/\delta$, $\mu_1 \approx 3.83$, and R is the cylindrical gas chamber radius. Then one gets for $|s|$ in the cylindrical case:

$$|s| = \frac{\sqrt{\nu_{en}^2 + \omega^2}}{v_{Te}} \left\{ \left(\frac{\mu_1}{R} \right)^4 + \frac{\omega_{pe}^2}{c^2} \left(1 + \frac{\nu_{en}^2}{\omega^2} \right)^{-1} \left[2 \left(\frac{\mu_1}{R} \right)^2 + \frac{\omega_{pe}^2}{c^2} \right] \right\}^{-1/4} . \qquad (3.11)$$

At high frequencies ($\omega \gg \nu_{en}$) $|s|$ is proportional to ω and thus the plasma is in local regime similar to the plane geometry case. The difference between cylindrical and plane cases appears at low frequencies ($\omega \ll \nu_{en}$), when (3.11)

becomes $|s| = (R/\mu_1)/(v_{Te}/\nu_{en})$, which is small if $R\nu_{en}/v_{Te} < 1$, and thus in cylindrical geometry plasma with warm electrons can remain in nonlocal regime even at very low frequencies contrary to the plane geometry case in which plasma returns into local regime for low ω.

3.4   Power Absorption (Heating)

Now that we know the electric current density in plasma, we can calculate the power absorption spatial profile $w(x) = 1/2\,\mathrm{Re}(j_y E_y^*)$, where E_y^* is a complex conjugate of E_y. Thus we obtain for $w(x)$ [45]

$$w(x) = \frac{e^2 n_0}{2 m_e} E_0^2 \,\mathrm{Re}\left[\frac{1}{\gamma v_{Te}}\left(G(x)\exp(-\gamma^* x) - \exp(-\frac{2x}{\delta})Z(-is)\right)\right] . \quad (3.12)$$

Total power flux of absorption of wave by discharge plasma in nonlocal regime is

$$S_{tot} = \int_0^\infty w(x)\,dx ,$$

and after integration

$$S_{tot} = \frac{e^2 n_0}{2 m_e} E_0^2 \,\mathrm{Re}\left[\frac{1}{\gamma v_{Te}}\left(\frac{2}{\sqrt{\pi}}\int_0^\infty \frac{t^2 \exp(-t^2)}{t^2 + s^2}\frac{1}{\gamma^* t - i\gamma s}dt - \frac{\delta}{2}Z(-is)\right)\right] .$$
$$(3.13)$$

The general expressions (3.12) and (3.13) describe spatial profile of absorbed power density and total absorbed power of the electromagnetic wave taking into account both collisional and nonlocal effects due to electron thermal motion. These expressions are relatively simple to calculate.

In the limit of cold collisional plasma (local regime) the dependence between j_y and E_y becomes local:

$$j_y(x) = i\frac{e^2 n_0}{m_e \tilde{\omega}} E_y(x) , \quad (3.14)$$

and the total power absorption in (3.13) reduces to the well-known expression for the purely collisional heating (ref. Eq. 1.31),

$$S_{coll} = \frac{e^2 n_0}{2 m_e}\frac{\delta}{2}E_0^2\frac{\nu_{en}}{\omega^2 + \nu_{en}^2} . \quad (3.15)$$

58

Here we neglected $\kappa \ll 1/\delta$.

In the case of nonlocal collisionless regime, when $\nu_{en} = 0$ and electron thermal motion is significant, the total power absorption (3.13) reduces to

$$S_{tot} = \frac{e^2 n_0}{m_e} E_0^2 \delta \frac{\delta}{\bar{v}_e} \Im(\beta) , \qquad (3.16)$$

where $\beta = 4\delta^2 \omega^2 / (\pi \bar{v}_e^2)$, $\bar{v}_e^2 = 8T_e / \pi m_e$, and

$$\Im(\beta) = \frac{1}{\pi} \int_0^\infty dx \frac{x \exp(-x)}{(x + \beta)^2} = \frac{1}{\pi} \left[\exp(\beta) \, (1 + \beta) \, \mathrm{Ei}(1, \beta) - 1 \right] . \qquad (3.17)$$

This result corresponds to that obtained by Vahedi et $al.$ [36] for collisionless power absorption in nonlocal regime (Eq. 2.36) using the stochastic method.

Since the skin depth δ and the imaginary part κ of the wave vector $\gamma = 1/\delta - i\,\kappa$ enter our model as input parameters, a few words should be said about what δ and κ one should use when calculating the power absorption (3.12, 3.13). One way to estimate δ and κ is to calculate Z_H from (2.16) and then use $\delta^{-1} = (\omega/c) \, \mathrm{Im}\left(Z_H^{-1} \right)$, $\kappa = \omega/c \, \mathrm{Re}\left(Z_H^{-1} \right)$. However, in this way we come across the calculational challenges associated with numerical evaluation of Z_H. Another, faster way to estimate the skin depth in nonlocal regime was suggested by Vahedi et $al.$ [36]. We define the effective collision frequency ν_{eff} for electrons by equating the total heating in nonlocal regime (3.13) to an $ansatz$ of purely collisional heating (3.15) with $\nu_{en} = \nu_{eff}$. Then we get

$$\mathrm{Re}\left[\frac{1}{\gamma v_{Te}} \left(\frac{2}{\sqrt{\pi}} \int_0^\infty \frac{t^2 \exp(-t^2)}{t^2 + s^2} \frac{1}{\gamma^* t - i\gamma s} dt - \frac{\delta}{2} Z(-is) \right) \right] = \frac{\delta}{2} \frac{\nu_{eff}}{\omega^2 + \nu_{eff}^2}, \qquad (3.18)$$

The skin depth δ in (3.18) is now obtained from the classical formula (1.26) with $\nu_e = \nu_{eff}$

$$\delta = \frac{c}{\omega_{pe}} \left(1 + \frac{\nu_{eff}^2}{\omega^2} \right)^{1/4} \frac{1}{\cos(\phi/2)}, \qquad (3.19)$$

with $\phi = \arctan(\nu_{eff}/\omega)$. Equations (3.18-3.19) can be solved simultaneously (by iterative method, for example) to define ν_{eff} and δ. The anomalous skin depth δ, defined in such a way, is in very good agreement with experimentally

observed skin depth in nonlocal regime and with the skin depth calculated from the surface impedance (2.16), while the calculation itself is much simpler and faster than that of the surface impedance Z_H. It is interesting to note that the resulting δ found from Eqs. (3.18-3.19) is not very sensitive on the value of κ used in Eq. (3.18): the result varies only by approximately 25% of its value when κ is changed from 0 to δ^{-1}. Therefore, for simplicity, we can put $\kappa = 0$ (really $\kappa \ll \delta^{-1}$, see Appendix A) when calculating the anomalous skin depth δ from Eqs. (3.18-3.19). This weak sensitivity on κ is also observed for the heating rate (3.13).

3.4.1   Resonant Absorption. Influence of Collisions

Let us write down the absorbed power density $w = \langle j_y E_y \rangle = 1/2\,\mathrm{Re}\left(j_y E_y^*\right)$ as

$$w = \frac{1}{2}\,\mathrm{Re}\iint dk\,dk'\exp\left[i\left(k-k'\right)x\right]j_k\,E_{k'}^*, \tag{3.20}$$

where j_k and $E_{k'}$ are the Fourier images of the electric current and electric field in plasma, respectively. Averaging w over all phases and using $j_k = -e\int v_y\,\tilde{f}_k d^3v$, we get

$$\bar{w} = -\frac{e}{2}\int dk\,\mathrm{Re}\left[E_k^*\int v_y\,\tilde{f}_k d^3v\right], \tag{3.21}$$

where

$$\tilde{f}_k = \frac{e}{m_e}\frac{1}{\nu_e - i\left(\omega - kv_x\right)}E_k\frac{\partial f_{0e}}{\partial v_y}. \tag{3.22}$$

Thus we get for the absorbed power spectral density:

$$w_k = -\frac{e^2}{2m_e}\left|E_k\right|^2\int d^3v\frac{\nu_e}{\nu_e^2 + \left(\omega - kv_x\right)^2}v_y\frac{\partial f_{0e}}{\partial v_y}. \tag{3.23}$$

In the collisionless limit, when $\nu_e \to 0$, we get $\nu_e/\left(\nu_e^2 + \left(\omega - kv_x\right)^2\right) \to \pi\delta\left(\omega - kv_x\right)$, where $\delta\left(\omega - kv_x\right)$ is the Dirac delta function, and then

$$w_k\big|_{\nu_e\to 0} = -\frac{e^2}{2m_e}\left|E_k\right|^2\frac{\pi}{k}\left(\iint dv_y dv_z v_y\frac{\partial f_{0e}}{\partial v_y}\right)_{v_x=\omega/k}, \tag{3.24}$$

60

which implies that in the absence of collisions only the electrons whose velocities are in resonance with the wave, $v_x = \omega/k$, are heated by the wave. Indeed, these electrons, moving in phase with the wave, experience an electric field of constant phase, i.e. a constant electric field, and therefore are being effectively accelerated by this field. This is the resonant (collisionless) heating.

The collisions between the electrons and other species "detune" this resonance, making the Dirac delta function to "spread". This is illustrated in
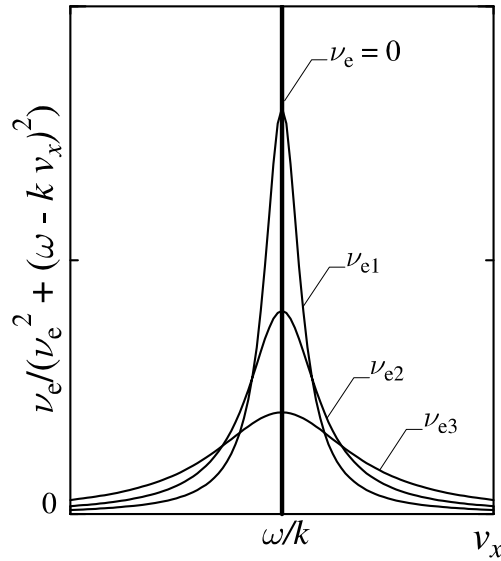
Figure 3.1: The kernel $\nu_e/\left(\nu_e^2 + (\omega - kv_x)^2\right)$ of the integral in (3.23) as a function of electron velocity v_x along the direction of the wave propagation, for different ν_e. Here $\nu_{e1} < \nu_{e2} < \nu_{e3}$; the transition to $\delta\left(\omega - kv_x\right)$ for $\nu_e \to 0$ is seen.

Fig. 3.1, where the kernel of the integral in (3.23) $\nu_e/\left(\nu_e^2 + (\omega - kv_x)^2\right)$ is plotted for different values of ν_e. It is seen that as the collision frequency increases, more electrons in wider velocity range contribute to the integral in (3.23), while the contribution of the resonant electrons (with $v_x = \omega/k$) diminishes. Therefore in warm plasma with collisions more electrons are being heated "resonantly" by the wave than in the collisionless case, but they are also "detuned" from the resonance by collisions.

Generally, if $\nu_e > 0$, the value of the integral in (3.23) is smaller than the value of the integral in (3.24). This implies that collisions, detuning resonance of electrons with the wave, reduce the heating compared to the heating in collisionless plasma.

3.4.2 Negative Power Absorption due to Electron Thermal Motion

Let us now compare the theoretical profiles of absorbed power density (3.12) plotted in Fig. 3.2 with the experimentally measured profiles plotted in Fig. 2.6 on page 39. The spatial profiles of power absorption in Fig. 3.2
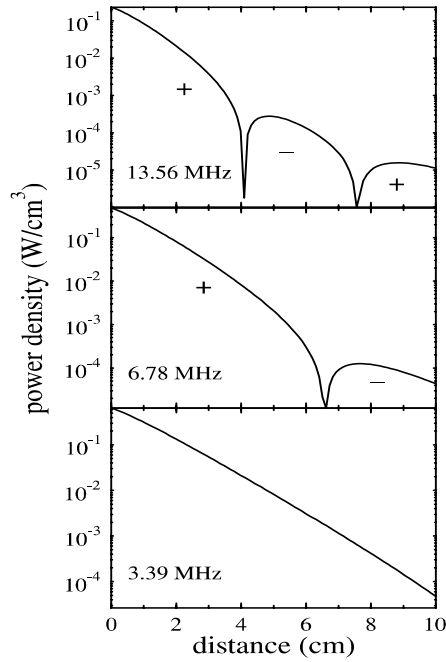
Figure 3.2: Theoretical power absorption profiles (3.12) for different driving frequencies. Signs denote regions of positive (+) and negative (-) power absorption.

are calculated from (3.12) for different wave frequencies and for plasma density of $n_0 = 1 \times 10^{11} \, \text{cm}^{-3}$ (note that in our theoretical model we assume a

uniform plasma density profile) and electron temperature of $T_e = 3.6$ eV – the same parameters at which the experimental profiles on Fig. 2.6 were measured. The skin depth δ at each frequency was calculated according to the technique presented on page 59. We see from comparing the theoretical and experimental profiles of absorbed power that they agree rather well. Particularly, we see that our theory yields the negative power absorption at approximately the same positions as observed in the experiment. This suggests that the negative power absorption is not a consequence of nonmonotonic behavior of the electromagnetic field in plasma, as our theory assumes the exponential, monotonic field profiles. Thus the only possible reason for the negative power absorption is the thermal transfer of electric current from the skin layer into bulk plasma, as was discussed in Chapter 2. The phase difference $\phi_j(x) - \phi_E(x)$ between the electric current (3.8) and the electric field in plasma $(\phi_j(x) = \arctan[\operatorname{Im} j_y(x)/\operatorname{Re} j_y(x)], \ \phi_E(x) = \kappa x - \omega t)$ is changed by $\pi/2$ at the approximate distances of $v_{Te}\pi N/\omega$ $(N = 1, 2, ...)$ from the plasma boundary, i.e. the power absorption which is proportional to $\cos\left[\phi_j(x) - \phi_E(x)\right]$ becomes negative at these distances. At $\omega/2\pi = 3.39$ MHz, when the nonlocal effects are most pronounced compared to the two other frequencies of 6.78 and 13.56 MHz, there is no negative absorption seen simply because the first region of negative absorption is beyond 10.5 cm – the size of the discharge.

3.4.3 Effect of Electron Thermal Motion on Plasma Heating

As we have already seen, the electron thermal motion has a significant effect on plasma heating. In order to investigate *how* the electron thermal motion influences the heating, let us compare the total heating S_{tot} (3.13) with the purely collisional heating S_{coll} (3.15) using the parameter $\eta = S_{tot}/S_{coll}$, as it was done by Godyak *et al.* in their experimental work [32]. When calculating η, we have to use the same electron collision frequency ν_{en} in (3.15) as that

used in (3.13). In other words, the parameter η compares the actual heating in nonlocal regime to the heating that would have occurred if only the collisional mechanism of power absorption was active, with all other conditions being the same.

Enhancement of Heating by Resonant Absorption

It is interesting to investigate the dependence of $\eta = S_{tot}/S_{coll}$ on the driving frequency, $\eta(\omega)$. One can expect that the resonant power absorption is most pronounced at $\omega \sim v_{Te}/\delta$ (without collisions), when the electromagnetic wave is in resonance with a significant number of electrons.

In Fig. 3.3 we plot $\eta(\omega)$ for two values of electron-atom collision frequency $\nu_{en} = 0.15 \times 10^7 \ s^{-1}$ and $\nu_{en} = 0.46 \times 10^7 \ s^{-1}$, corresponding to the experimental discharges at the neutral gas pressures of 0.3 and 1.0 mTorr, and compare it to the experimental results from Godyak *et al.* [32]. We see that indeed there is a significant enhancement of heating, with the maximum heating at $|s| = 1$, i.e. when $\sqrt{\omega^2 + \nu_{en}^2} = v_{Te}/\delta$. If we now set $\nu_{en} = 0$, then we get the resonance at $\omega \sim v_{Te}/\delta$, as we expected for collisionless case.

As the driving frequency increases, plasma gradually transfers into local regime ($|s|$ becomes large), and $\eta(\omega)$ gradually goes to unity (see Fig. 3.3), as expected. Quite unexpectedly though, we see that as frequency becomes low, $\omega < \nu_{en}$, the ratio $\eta(\omega)$ becomes less than unity, i.e. the total heating becomes less than the purely collisional value. This interesting effect will be discussed in detail shortly.

There is a reasonable agreement between the theoretical results for $\eta(\omega)$ and experimental results for the same parameters (shown in Fig. 3.3 by diamonds and circles, respectively). The remaining discrepancy between theory and experiment could be associated with the approximate nature of our theoretical model, however, as we will see later, our model gives results that are in very good agreement with the results of the self-consistent theory [23, 24], and both models have the same discrepancy with the experimental data. Thus most
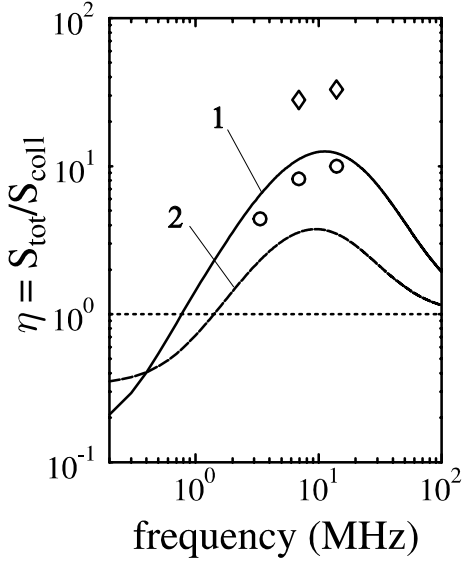
Figure 3.3: Ratio of the total heating in nonlocal regime (3.13) to the purely collisional heating (3.15). Lines represent the theory, symbols represent the experiment. Line 1 and diamonds are for $\nu_{en} = 0.15 \times 10^7\, s^{-1}$, line 2 and circles are for $\nu_{en} = 0.46 \times 10^7\, s^{-1}$.

probably this discrepancy is due to the use of the energy independent collision frequency ν_{en} in the theoretical model, as well as due to the assumption of a uniform plasma density.

Reduction of Heating at Low Frequencies due to Electron Thermal Motion

As we have just seen from Fig. 3.3, at low frequencies the total heating in nonlocal regime can become smaller than the purely collisional heating for the same parameters (including same ν_{en}). In other words, the heating due to both collisional and collisionless mechanisms, acting simultaneously, becomes smaller than it would have been if only the collisional mechanism was active. This is a quite surprising effect. Let us investigate it more closely.

First of all, let us do a qualitative analysis of a possibility of such effect.

65

Let us again consider the spectral density of the absorbed power (3.23)

$$w_k = -\frac{e^2}{2m_e} |E_k|^2 \int d^3v \frac{\nu_e}{\nu_e^2 + (\omega - kv_x)^2} \frac{\partial f_{0e}}{\partial v_y}. \qquad (3.25)$$

As the wave field decays with the skin depth δ, the characteristic value of k in (3.25) is $k \simeq 1/\delta$. One can see that for low frequency, $\omega < \nu_{en}$, $\omega < v_{Te}/\delta$, the absorbed power spectral density $w_k \sim \nu_{en}/(\nu_{en}^2 + v_{Te}^2/\delta^2)$ is indeed reduced by the effect of the thermal motion compared to the cold plasma expression $w_{k\,collisional} \sim \nu_{en}/(\nu_{en}^2 + \omega^2)$. On the other hand, for relatively high frequencies approaching the resonant condition $\omega \simeq v_{Te}/\delta$, the heating is enhanced due to the wave-particle interaction, as we have already seen. For even larger frequencies, in the local regime when $\omega > v_{Te}/\delta$, thermal effects can be neglected. This analysis is also applicable to the case of $\omega = 0$. Note that the expression for $\mathrm{Re}(\sigma)$ implicitly assumes a finite spatial localization of the electric field with a characteristic inhomogeneity scale δ, so that the thermal modification of a dc ($\omega = 0$) electric conductivity can be detected only in a situation with strongly inhomogeneous electric field, $\delta < v_{Te}/\nu_{en}$.

Now that we have a qualitative reasoning for the effective reduction of heating compared to the purely collisional value (we will further call this effect simply as effective reduction of heating), let us do a quantitative analysis of this effect.

Let us calculate the ratio $\eta = S_{tot}/S_{coll}$ (recall that S_{tot} is the total heating in nonlocal regime (3.13), S_{coll} is the purely collisional heating for the same parameters (3.15)) at low driving frequencies $\omega < \nu_{en}$. Since typically $\kappa \ll \delta^{-1}$ (see Appendix A), we can simplify the calculation by neglecting κ, which makes the nonlocality parameter s purely imaginary, $s = i\delta\nu_{en}/v_{Te}$. After some algebra, we get for η [46]

$$\eta = \frac{2}{\sqrt{\pi}} |s| \left(-1 + \sqrt{\pi} |s| + \left(1 - |s|^2\right) \left\{ \pi\, \mathrm{erfi}\,(|s|) + \mathrm{Re}\left[\mathrm{Ei}(1, -|s|^2)\right] \right\} e^{-|s|^2} \right). \qquad (3.26)$$

Here $\mathrm{erfi}\,(|s|) = -i\,\mathrm{erf}(i\,|s|)$ is the imaginary error function, $\mathrm{erf}(x)$ is the error function $\mathrm{erf}(x) = 2/\sqrt{\pi} \int_0^x \exp(-t^2)dt$, $\mathrm{Ei}(n, x) = \int_1^\infty dt \exp(-xt)/t^n$ is the
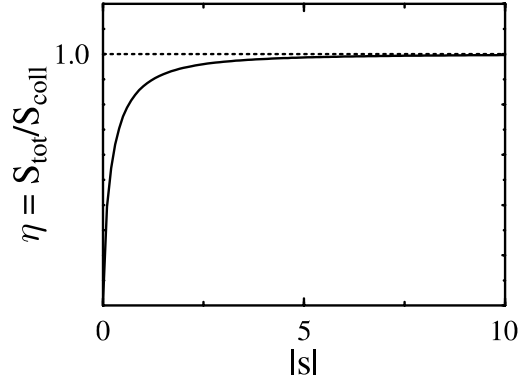
Figure 3.4: Dependence of $\eta = S_{tot}/S_{coll}$ on the nonlocality parameter $|s|$ at low frequencies $\omega < \nu_{en}$, from (3.26).

exponential integral.

The dependence of η on $|s|$ is shown on Fig. 3.4. As it is seen, for low frequencies η is always smaller than unity for arbitrary values of $|s|$. For higher collisionality, $|s| \geq 1$, the parameter η approaches unity, which corresponds to the transition into the collisional regime.

Finally, let us extend the plots in Fig. 3.3 to low frequencies. Also, let us compare our approximate theory with the more rigorous self-consistent theory [2, 23, 24] by plotting the relative heating calculated from both theories on the same Fig. 3.5. As we see from Fig. 3.5, both theories agree quite well on heating, thus we have shown that the assumption of exponentially decaying fields in nonlocal regime works quite well, and the theory that uses this assumption (our theory) is a simple, relatively clear and accurate tool for description of plasma heating. Also we see that both of them yield the effective reduction of heating at low frequencies. At moderate frequencies the total heating can significantly (almost an order of magnitude) exceed the purely collisional heating, just as it was observed experimentally (ref. Figs. 2.4, 2.5). As the frequency is further increased, the ratio η of total to collisional heating tends to unity as plasma gradually transfers into local regime $\omega > v_{Te}/\delta$.

The qualitative and quantitative analyses given here both show existence
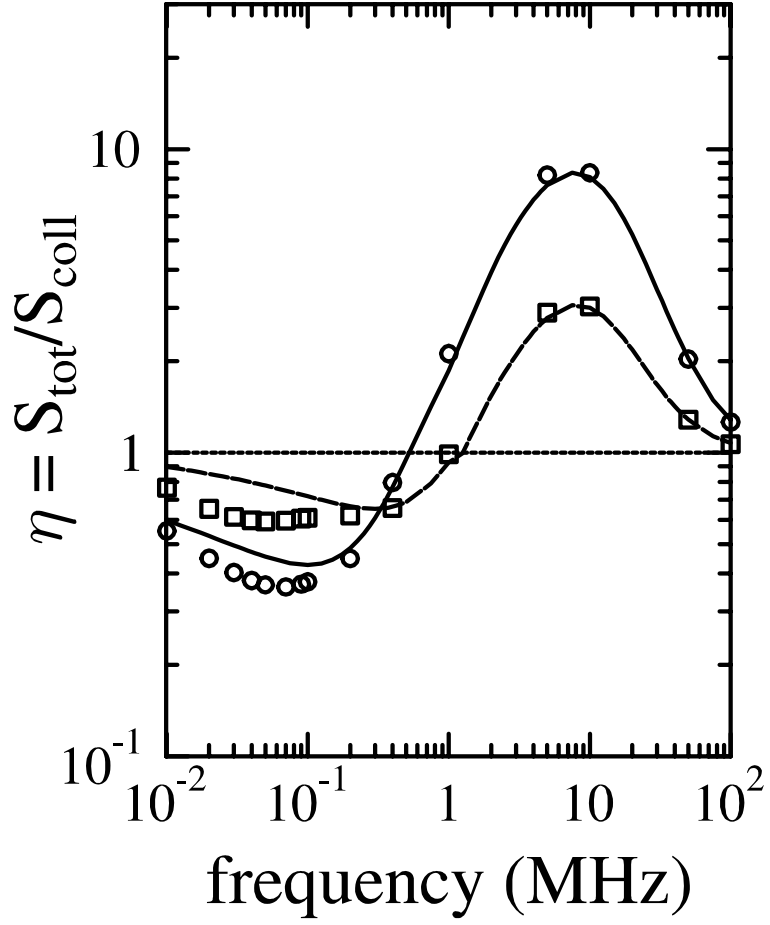
Figure 3.5: Ratio of the total heating in nonlocal regime to the purely collisional heating. Lines represent our theory (3.13) (solid line is for $\nu_{en} = 0.15 \times 10^7 \, s^{-1}$, dashed line is for $\nu_{en} = 0.46 \times 10^7 \, s^{-1}$), symbols represent the self-consistent theory [24] (circles are for $\nu_{en} = 0.15 \times 10^7 \, s^{-1}$, squares are for $\nu_{en} = 0.46 \times 10^7 \, s^{-1}$).

of the effective reduction of heating. There is no experimental evidence available in support of this effect, therefore we will conduct an idealized numerical experiment by means of Particle-In-Cell simulations to support this effect in particular and our theoretical model in general. This numerical experiment will be discussed in Chapter 5.

3.5 Ponderomotive Force

As we have discussed before, the experiments on measuring the ponderomotive effect in nonlocal regime of ICP revealed a significant discrepancy between the actually measured ponderomotive effect and the one predicted by classical theory (see Fig. 2.9). The reason for such a discrepancy is the electron thermal motion, which should be accounted for in theoretical model of ponderomotive force in nonlocal regime. Our kinetic model of electron dynamics described above accounts for both electron thermal motion and electron collisions, therefore being capable to adequately describe the ponderomotive effect in the nonlocal regime. Below we derive the expression for the ponderomotive force in nonlocal regime of ICP, using our kinetic model.

In planar plasma the ponderomotive force consists of two terms – the nonlinear term $m_e \left(\mathbf{v} \cdot \nabla \right) \mathbf{v}$ (which is a part of the convective derivative $d\mathbf{v}/dt$ in the fluid equation of motion of electrons), and the nonlinear term $1/c \left(\mathbf{j} \times \mathbf{B} \right)$, which is the Lorentz force acting on plasma in magnetic field. In the planar geometry the term $\left(\mathbf{v} \cdot \nabla \right) \mathbf{v}$ vanishes, and the time-averaged ponderomotive force is simply $\mathbf{F}_p = 1/c \left\langle \mathbf{j} \times \mathbf{B} \right\rangle$ (here $\left\langle ... \right\rangle$ denotes time averaging over the period of field oscillations $2\pi/\omega$). As $\mathbf{j} = j_y \hat{\mathbf{y}}$, $\mathbf{B} = B_z \hat{\mathbf{z}}$, the ponderomotive force is directed along x inwards the plasma:

$$F_p = \frac{1}{c} \left\langle \mathbf{j} \times \mathbf{B} \right\rangle = \frac{1}{2c} \operatorname{Re} \left(j_y B_z^* \right). \tag{3.27}$$

Using the expression for the nonlocal current j_y (3.8), we get for the pon-

deromotive force in nonlocal regime [47]:

$$F_p = \frac{\omega_{pe}^2}{8\pi\omega} E_0^2 \exp(-\frac{2x}{\delta}) \operatorname{Re}\left[i\frac{\gamma^*}{\gamma v_{Te}}\left(Z(-is) - \exp(\gamma x)G(x)\right)\right]. \qquad (3.28)$$

Here we use the same notations as in (3.8).

In the limit of cold collisional plasma, when $|s|$ is large, $G(x)$ is small, $Z(-is) \simeq 1/is$, and Eq. (3.28) reduces to

$$F_{p\,cold} = \frac{\omega_{pe}^2}{8\pi\omega}\frac{E_0^2}{\delta}\exp(-2x/\delta)\left[\frac{\omega}{\omega^2 + \nu_{en}^2} + \frac{\nu_{en}\kappa\delta}{\omega^2 + \nu_{en}^2}\right]. \qquad (3.29)$$

This expression corresponds to the classical expression for ponderomotive force in cold collisional plasma (1.40). The first term of $F_{p\,cold}$ is the Miller force (1.41), and it appears due to the momentum transfer from the reflected part of the wave. The second term in (3.29) describes the wave momentum deposition in plasma due to a finite κ (momentum of the decaying penetrated wave) [19, 48, 49]. Thus our expression for the ponderomotive force in nonlocal regime (3.28) is validated by its cold plasma limit (1.40).

3.5.1 Reduction of the Ponderomotive Force by Electron Thermal Motion

Let us now evaluate the ponderomotive force in a strongly nonlocal regime, when $|s| \ll 1$. For simplicity we will evaluate the ponderomotive force at the plasma boundary $x = 0$ (where it is maximal). First we evaluate the ponderomotive force in collisionless nonlocal regime, assuming $\nu_{en} \to 0$. Then we obtain

$$\begin{aligned} F_p(x \quad = \quad 0) &= -\frac{\omega_{pe}^2}{8\pi\omega}\frac{E_0^2}{\sqrt{\pi}}\operatorname{Re}\left[i\frac{\gamma^*}{\gamma v_{Te}}\left(\operatorname{Ei}(1, s^2)\exp(s^2) + i\pi\operatorname{erfc}(s)\right)\right] \\ &\simeq \frac{\omega_{pe}^2}{8\pi\omega^2}E_0^2\frac{\sqrt{\pi}\omega}{v_{Te}}\left(\operatorname{erfc}(s) + \frac{2\kappa\delta}{\pi}\operatorname{Ei}(1, s^2)\exp(s^2)\right), \qquad (3.30) \end{aligned}$$

where $\operatorname{erfc}(s)$ is the complementary error function $\operatorname{erfc}(s) = 1 - \operatorname{erf}(s)$, and $\operatorname{Ei}(1, s^2)$ is the exponential integral. Similar to the force in local regime (3.29),

the net ponderomotive force (3.30) consists of two physically different parts. The first part represents the pressure of the reflected electromagnetic field, while the second part, proportional to $\kappa\delta$, is due to the resonant absorption of the penetrated wave momentum by the plasma. In the local regime, the wave momentum absorption is collisional [see Eq. (3.29)], while in the nonlocal regime it is due to the Landau wave damping.

In the strongly nonlocal regime $|s| \ll 1$, expression (3.30) can be simplified leading to

$$F_p \simeq \frac{\omega_{pe}^2}{8\pi\omega^2}E_0^2\frac{\sqrt{\pi}\omega}{v_{Te}}\left(1 + \frac{2\kappa\delta}{\pi}\left[-c - \ln(s^2) - \left(-c - \ln(s^2) - 1\right)s^2\right]\right), \quad (3.31)$$

where $c \simeq 0.916$ is a Catalan constant. We retain the second order terms in s^2 in combination with diverging $\ln s^2$. Expansion (3.31) works reasonably well for $|s| \leq 0.5$. For typical ICP, the wave damping is weak, $\kappa\delta < 1$ (see Appendix A), so that the second term in (3.31) can be neglected giving

$$F_p = \frac{\omega_{pe}^2}{8\pi\omega^2}E_0^2\frac{\sqrt{\pi}\omega}{v_{Te}}. \quad (3.32)$$

This is the expression for the ponderomotive force in the strongly nonlocal collisionless regime.

It is interesting to note that the expression for the ponderomotive force in the nonlocal regime can be cast in a form similar to that of the local case, i.e. $F_p \simeq \omega_{pe}^2/(8\pi\omega^2)E_0^2/\delta$, where the characteristic gradient length of the electric field (skin depth) δ is replaced with the characteristic length of the electron excursion over the wave period, $\delta \rightarrow v_{th}/\omega$. This gives a reasoning for the thermal reduction of the ponderomotive force observed experimentally [17]. Indeed, the electron thermal velocity v_{Te} in the denominator in (3.32) makes the force to diminish as the electron temperature is increased. In other words, thermal electrons "smooth" the effect of steep gradients of electromagnetic field energy, thus reducing the ponderomotive force due to these gradients.

The ponderomotive force spatial profiles (3.28) at different electron temperatures are shown in Fig. 3.6. We clearly see the thermal reduction of the ponderomotive force from Fig. 3.6.
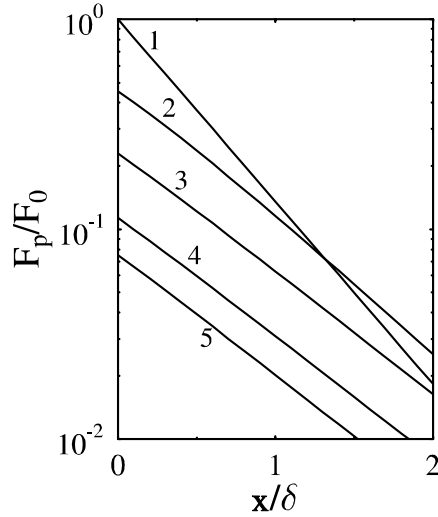
Figure 3.6: The normalized ponderomotive force $F_p/F_p(x = 0)$ as a function of normalized distance x/δ, for different electron temperatures: line 1 is for $T_e = 0$ (local regime), line 2 is for $T_e = 0.1$ eV, line 3 is for $T_e = 1$ eV, line 4 is for $T_e = 7$ eV, line 5 is for $T_e = 20$ eV. Other parameters are taken from the experiment [17]: $\omega/2\pi = 0.45$ MHz, $\nu_{en} = 4 \cdot 10^6$ s^{-1}, $\delta = 2.24$ cm, $\kappa\delta = 0.1$.

3.5.2   Comparison with Experimental Data

The expression for the ponderomotive force in nonlocal regime (3.28) is relatively simple to calculate and compare with the experimental data. As we have the experimental results for the ponderomotive potential $U_p(x)$ (see Fig. 2.9), we will compare theoretical ponderomotive potential calculated from (3.28) as $U_p(x) = -\int_\infty^x F_p(x')dx'$. The comparison of the theoretical ponderomotive potential in nonlocal regime with the experimentally measured ponderomotive potential for the same plasma parameters is shown in Fig. 3.7. For a reference, we also plotted the ponderomotive potential calculated from the Miller force (1.41) in cold plasma. We see that there is a reasonable (within an error of measurement of the ponderomotive potential itself) agreement between the theoretical values for the ponderomotive potential in nonlocal regime and the experimental data. The reason for the small overestimate of the ponderomotive effect in our theory, seen in Fig. 3.7, comes from assuming the
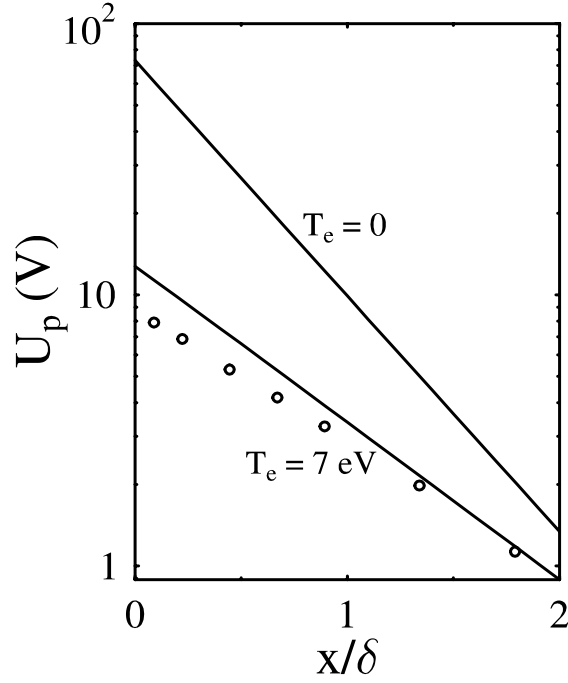
Figure 3.7: Absolute value of the ponderomotive potential $U_p(x) = -\int_{\infty}^{x} F_p dx'$ calculated from (3.28) as a function of normalized distance x/δ, in nonlocal ($T_e = 7$ eV) and local ($T_e = 0$) regimes. The experimentally measured [17] ponderomotive potential in plasma with $T_e = 7$ eV is shown by circles. Other parameters are $\nu_{en} = 4 \cdot 10^6$ s^{-1}, $\delta = 2.24$ cm, $\kappa\delta = 0.1$, $E_0 = 1.87$ V/cm.

homogeneous plasma, while in the real discharges the plasma density is rather inhomogeneous and depleted near the boundary (see, for example, Fig. 2.7), thus reducing the actual ponderomotive force acting on plasma.

3.6 Summary

In this chapter we have developed the linear kinetic theory describing the plasma heating and ponderomotive force in nonlocal regime for any degree of plasma collisionality. The theory assumes the exponentially decaying electromagnetic field profile; this assumption greatly simplifies the analysis and allows to obtain the relatively simple expressions for the absorbed power density profile, the total power absorption (plasma heating) and the ponderomotive force in nonlocal regime. These expressions are in rather good agreement with the experimental results and with the results of more rigorous and more complicated theory that uses the self-consistent field profiles. In local regime the expressions for plasma heating and ponderomotive force reduce to the corresponding "classical" expressions for cold plasma. Also, the expression for the ponderomotive force in strongly nonlocal regime provides a clear evidence for the thermal reduction of ponderomotive force observed experimentally by Godyak *et al.* [17]. In the case of collisionless plasma in nonlocal regime our expression for plasma heating reduces to the result by Vahedi *et al.* [36], while in the case of plasma in nonlocal regime with collisions our expression is much simpler than the corresponding expression that one *would* obtain from the stochastic model of Vahedi *et al.* (this expression has not been obtained in [36]).

We have also discussed the evidence of resonant (collisionless, or Landau) heating of plasma electrons by the electromagnetic wave, and discussed how collisions affect this process.

The detailed comparison of the results of our theory with the experimental data has shown that our theory explains and predicts the following effects (in

order of their importance and novelty).

1. **Thermal reduction of ponderomotive force in nonlocal regime as compared to the classical Miller expression in cold plasma.** Our theory gives the same order of magnitude for the reduction of ponderomotive force as that observed in the experiment.

2. **Effective reduction of heating at low driving frequencies**, i.e. the reduction of total plasma heating as compared to the purely collisional heating for the same parameters. This surprising effect basically means that at low driving frequencies the plasma heating due to both collisional and collisionless mechanisms becomes *smaller* than it would have been if only the collisional mechanism was in effect, i.e. the two mechanisms of plasma heating do not simply add up. The qualitative and quantitative reasoning for this resonant enhancement is given. Also a comparison with the self-consistent model [23, 24] is given, showing a good agreement between our simple model and the self-consistent, relatively more complicated model. Both theories yield the effective reduction of heating at low frequencies.

3. **Resonant enhancement of the total plasma heating as compared to the purely collisional heating** (see Fig. 3.3). The same effect has been observed experimentally (see Figs. 2.4, 2.5 and experimental points in Fig. 3.3). The qualitative and quantitative reasoning for this resonant enhancement is given.

4. **Negative power absorption.** We have shown that this effect is a consequence of thermal transfer of electric current in plasma rather than of the nonmonotonic behavior of electromagnetic field in plasma. The theoretical positions of negative power absorption regions match quite well with the actual positions observed in the experiment (compare Fig. 2.6 and Fig. 3.2).

The overall agreement between the theory and experiment is quite good; the reasons for the remaining discrepancies between the theory and experiment are discussed.

Chapter 4

Quasilinear Kinetic Theory of Heating in Nonlocal Regime. Effect of Induced RF Magnetic Field

In the linear kinetic theory developed in the previous chapter, the effect of the induced RF magnetic field $\mathbf{B} = -ic/\omega \nabla \times \mathbf{E}$ disappears for an isotropic electron distribution function $f_{0e} = f_{0e}(\varepsilon)$ (ε is electron kinetic energy), since for such distribution function the term $(\mathbf{v} \times \mathbf{B}) \cdot \partial f_{0e}/\partial \mathbf{v}$ in the kinetic equation (3.1) vanishes: $(\mathbf{v} \times \mathbf{B}) \cdot \partial f_{0e}/\partial \mathbf{v} = 0$. Thus in the linear theory the magnetic field does not affect plasma heating. The assumption of the isotropic electron distribution function is equivalent to assuming the "straight" trajectories of electrons in the electromagnetic field of the wave, when there is no acceleration in x-direction due to the Lorentz force. Other theoretical models [2, 23, 24] also neglect the effect of RF magnetic field, making the same assumption. However, at low frequencies that are of interest here, the Lorentz force can become significant, leading to anisotropization of the electron distribution function in the skin layer. In this case the electron dynamics and therefore the plasma

heating is affected by the RF magnetic field, as the term $(\mathbf{v} \times \mathbf{B}) \cdot \partial f_{0e}/\partial \mathbf{v}$ does not vanish anymore from the Eq. (3.1). In this chapter we develop a quasilinear kinetic theory allowing us to calculate a nonlinear perturbation of the electron distribution function due to weak electromagnetic field, and calculate a nonlinear correction to the plasma heating. We show how the RF magnetic field affects plasma heating by comparing the nonlinear correction to plasma heating calculated with and without the RF magnetic field.

4.1 Separation of Timescales of Electron Dynamics. Hierarchy of Kinetic Equations

Suppose the electromagnetic field has the form $\{\mathbf{E}, \mathbf{B}\} = 1/2\{\mathbf{E}(\mathbf{r}), \mathbf{B}(\mathbf{r})\}e^{-i\omega t} +$ $c.c.$, where $c.c.$ stands for complex conjugate. We can separate the timescales of electron dynamics in this oscillating electromagnetic field by expanding the electron distribution function (EDF) f_e with respect to the harmonics of the fundamental wave [39] as

$$f_e(\mathbf{r}, t) = f_{0e}(\mathbf{r}, t_{slow}) + \sum_{n=1}^{\infty} f_n(\mathbf{r}, t_{slow})e^{-in\omega t} + c.c., \qquad (4.1)$$

where f_{0e} is now the EDF averaged over field oscillation, $f_{0e} = \langle f_e \rangle$, also called the "slow" electron distribution function since it describes the electron dynamics on a timescale large compared to the field oscillation period. This "slow" EDF, as well as the amplitudes of the "fast" EDFs f_n, can have weak dependence on time, which is implied by the subscript "slow" in the time dependencies of f_{0e} and f_n in (4.1). However, we will neglect this slow time dependence in further consideration, assuming it to be weak. The expansion of the EDF with respect to the fundamental frequency ω allows us to build a hierarchy of kinetic equations for the EDFs at each timescale from the general

kinetic equation (1.10) for electrons:

$$\mathbf{v} \cdot \frac{\partial f_{0e}}{\partial \mathbf{r}} - \hat{S}(f_{0e}) = \frac{e}{m_e} \left\langle \left(\mathbf{E}(\mathbf{r},t) + \frac{1}{c}\mathbf{v} \times \mathbf{B}(\mathbf{r},t) \right) \cdot \frac{\partial \tilde{f}_1(\mathbf{r},t)}{\partial \mathbf{v}} \right\rangle, \qquad (4.2)$$

$$-in\omega f_n + \mathbf{v} \cdot \frac{\partial f_n}{\partial \mathbf{r}} - \hat{S}(f_n) = \frac{e}{m_e} \left[\left(\mathbf{E}(\mathbf{r}) + \frac{1}{c}\mathbf{v} \times \mathbf{B}(\mathbf{r}) \right) \cdot \frac{\partial f_{n-1}}{\partial \mathbf{v}} + \qquad (4.3) \right.$$

$$\left. + \left(\mathbf{E}(\mathbf{r}) + \frac{1}{c}\mathbf{v} \times \mathbf{B}(\mathbf{r}) \right)^* \cdot \frac{\partial f_{n+1}}{\partial \mathbf{v}} \right]. \quad (n \geqslant 1)$$

Here $\langle ... \rangle$ means the time averaging over the period of fundamental wave $2\pi/\omega$, asterisk denotes complex conjugate, $\tilde{f}_1(\mathbf{r},t) = f_1(\mathbf{r})e^{-i\omega t}$, and the collisional term $\hat{S}(f)$ describes the evolution of electron distribution function f due to collisions. This infinite hierarchy of kinetic equations is equivalent to the general kinetic equation (1.10). Note that the equations (4.2-4.3) are all coupled: an equation for f_n contains both f_{n-1} and f_{n+1}. There is no analytic solution for the EDF f_e for arbitrary electromagnetic field magnitude. However, the observation that $f_n \sim O(E^n)$, which follows from (4.2-4.3), allows us to truncate this hierarchy of equations for weak fields.

4.2 Quasilinear Kinetic Equation for the "Slow" Electron Distribution Function

Neglecting higher order terms with respect to the field amplitude E in (4.3), we get the linearized equation for $\tilde{f}_1 = f_1 e^{-i\omega t}$ (in our one-dimensional case) as

$$-i\omega \tilde{f}_1 + v_x \frac{\partial \tilde{f}_1}{\partial x} - \frac{e}{m_e} \left(\mathbf{E}(\mathbf{r}) + \frac{1}{c}\mathbf{v} \times \mathbf{B}(\mathbf{r}) \right) \cdot \frac{\partial f_{0e}}{\partial \mathbf{v}} = \hat{S}(\tilde{f}_1), \qquad (4.4)$$

and the "slow" EDF f_{0e} is defined from the Eq. (4.2) cast in the following form:

$$v_x \frac{\partial f_{0e}}{\partial x} = \hat{S}_{ql}(f_{0e}) + \hat{S}(f_{0e}), \quad \text{where} \qquad (4.5)$$

$$\hat{S}_{ql}(f_{0e}) = \frac{e}{m_e} \left\langle \left(\mathbf{E}(\mathbf{r},t) + \frac{1}{c}\mathbf{v} \times \mathbf{B}(\mathbf{r},t) \right) \cdot \frac{\partial \tilde{f}_1(\mathbf{r},t)}{\partial \mathbf{v}} \right\rangle. \qquad (4.6)$$

The term $\hat{S}_{ql}(f_{0e})$ describes the interaction of plasma electrons with the electromagnetic wave. This term is sometimes called the quasilinear collisional integral. The equation (4.5) describes the slow-time evolution of plasma electrons in response to the fast-oscillating weak electromagnetic field.

It is interesting to write the quasilinear operator $\hat{S}_{ql}(f_{0e})$ in (4.5) in the form which follows from Eqs. (4.4-4.5):

$$\hat{S}_{ql}(f_{0e}) = \frac{\partial}{\partial v_i} \langle D_{ij} \rangle \frac{\partial f_{0e}}{\partial v_j}, \tag{4.7}$$

where

$$D_{ij} = \frac{e^2}{m_e^2} \left(\mathbf{E}(\mathbf{r},t) + \frac{1}{c} \mathbf{v} \times \mathbf{B}(\mathbf{r},t) \right)_i \int_{-\infty}^{\infty} dk\, e^{ikx} \left(\mathbf{E}(k) + \frac{1}{c} \mathbf{v} \times \mathbf{B}(k) \right)_j \Delta, \tag{4.8}$$

with $\Delta = 1/\left(\nu_e + i\left(kv_x - \omega \right) \right)$ (here we used the BGK-type collision operator in Eq. (4.4), $\hat{S}(\tilde{f}_1) = -\nu_e \tilde{f}_1$ [29]), and a summation on repeated indices i, j is implied). With this form of the quasilinear operator the equation (4.5) for f_{0e} has the form of a diffusion equation in velocity space, with the diffusion tensor D_{ij}. In other words, the evolution of f_{0e} in velocity space is governed both by diffusion in velocity space and collisions,

$$v_x \frac{\partial f_{0e}}{\partial x} = \frac{\partial}{\partial v_i} \langle D_{ij} \rangle \frac{\partial f_{0e}}{\partial v_j} + \hat{S}(f_{0e}). \tag{4.9}$$

Here the collisional term $\hat{S}(f_{0e})$ consists of three parts: $\hat{S}_{ee}(f_{0e})$ for electron-electron collisions, $\hat{S}_{ei}(f_{0e})$ for electron-ion collisions, and $\hat{S}_{en}(f_{0e})$ for electron-atom collisions.

The system of equations (4.4-4.5), or the equivalent equation of diffusion in velocity space (4.9), describes the nonlinear response of plasma to a weak electromagnetic field, and can be solved analytically in some cases. This reduction of the system of equations (4.2-4.3) to the truncated system (4.4-4.5) for weak fields is called the *quasilinear approximation* [39, 50, 51, 52].

4.3 Nonlinear Perturbation of the "Slow" Electron Distribution Function

The equation for the "slow" distribution function (4.9) is much simpler than the original kinetic equation (1.10), however, it is still too complicated to be solved analytically. It can be further simplified by linearizing it about a homogeneous, isotropic, quasineutral background state F_0 by casting the electron distribution function in the form $f_{0e} = F_0 + \delta F$, $\delta F \ll F_0$.

The problem of calculating the electron distribution function from (4.9) has been widely discussed, and in some cases analytical or numerical solutions were obtained (see [51, 52, 53, 54, 55] and the extensive references in these papers). The solution of (4.9) depends on the relative importance of all terms in the right-hand side. In case of weak electromagnetic field the collision term dominates over the quasilinear term, and therefore we can neglect $\hat{S}_{ql}(f_{0e})$ in the equation for the background state, which then becomes (noting that $\delta F \ll F_0$):

$$0 = \hat{S}_{ee}(F_0) + \hat{S}_{ei}(F_0) + \hat{S}_{en}(F_0), \tag{4.10}$$

where the term $v_x \partial F_0 / \partial x$ is also neglected assuming the homogeneous background state F_0 (the only reason for inhomogeneity of F_0 here is the quasi-linear term, which is neglected). We will be assuming that elastic collisions in (4.10) are dominant, neglecting the inelastic processes such as ionization and recombination. Let us consider the terms $\hat{S}_{ei}(F_0)$ and $\hat{S}_{en}(F_0)$ in (4.10) in the approximation of infinitely heavy ions and atoms (compared to electrons), $m_e/m_i = m_e/m_n = 0$, where m_i, m_n are the masses of ions and neutral atoms, respectively. Since F_0 is isotropic in velocity phase space, $F_0 = F_0(v)$, it is not changed by the elastic collisions of electrons with infinitely heavy ions and atoms, as these collisions simply change direction of electron velocities without changing electron energies. Therefore the terms $\hat{S}_{ei}(F_0)$ and $\hat{S}_{en}(F_0)$ vanish from (4.10). We finally get, in the approximation of the weak heating

field, the equation for F_0 as

$$0 = \hat{S}_{ee}(F_0). \tag{4.11}$$

The solution of this equation is the Maxwellian distribution f_M with undefined electron temperature. Physically the electron temperature is defined by the balance of heating, which was neglected here (the term $\hat{S}_{ql}(f_{0e})$), and energy losses. Here we simply assume that the electron temperature is given externally, i.e. from the experimental measurements.

Generally, in the RF plasma discharges, especially those where the heating field is not weak, the background distribution F_0 is not Maxwellian [51, 52, 53, 54, 55, 56], although it is often quite close to it. For the sake of simplicity of the further analysis, in what follows we will be assuming F_0 to be homogeneous Maxwellian, noting the discussion above. However, our further analysis can be generalized for more realistic distributions F_0, if necessary.

Thus, with $f_{0e} = F_0 + \delta F$, $\delta F \ll F_0$, F_0 satisfying the equation (4.11), the quasilinear equation (4.9) reduces to the equation for the small nonlinear perturbation δF of the "slow" distribution function:

$$v_x \frac{\partial \delta F}{\partial x} = \hat{S}_{ql}(F_0) + \hat{S}(\delta F), \tag{4.12}$$

$$\text{with } \hat{S}_{ql}(F_0) = \frac{\partial}{\partial v_i} \langle D_{ij} \rangle \frac{\partial F_0}{\partial v_j},$$

and D_{ij} defined by (4.8).

The perturbation δF of the "slow" distribution function, occurring due to the heating field, generally consists of two parts: an isotropic (in velocity phase space) part $\overline{\delta F}$, and an anisotropic part $\widehat{\delta F}$. In (4.12) we will only be considering electron-atom collisions, which are the primary collisions in ICP discharges, again assuming the mass ratio of electron and atom to be zero, $m_e/m_n = 0$; in this approximation the electron-atom collisions do not change the isotropic part $\overline{\delta F}$ of the distribution perturbation, and thus the collisional operator $\hat{S}(\delta F)$ in (4.12), acting on the anisotropic part $\widehat{\delta F}$ only, can be cast in the BGK form $\hat{S}(\delta F) = -\nu_{en}(v)\left(\delta F - \overline{\delta F}\right) = -\nu_{en}(v)\widehat{\delta F}$, where $\nu_{en}(v)$ is the transport frequency of electron-atom collisions.

Now we can write down the isotropic and anisotropic parts of (4.12):

$$\overline{v_x \frac{\partial \widehat{\delta F}}{\partial x}} = \overline{\hat{S}_{ql}(F_0)} \qquad \text{(isotropic)}, \tag{4.13}$$

$$v_x \frac{\partial \overline{\delta F}}{\partial x} + \left(v_x \frac{\partial \widehat{\delta F}}{\partial x} - \overline{v_x \frac{\partial \widehat{\delta F}}{\partial x}} \right) = \hat{S}_{ql}^a(F_0) - \nu_{en}(v)\widehat{\delta F} \qquad \text{(anisotropic)}. \tag{4.14}$$

Here $\overline{A}$ denotes averaging over all directions in velocity phase space, defined as $\overline{A}(v) \equiv 1/4\pi \int_0^{2\pi} d\varphi \int_0^\pi d\theta \sin\theta \, A(v, \theta, \varphi)$, and $\hat{S}_{ql}^a(F_0) \equiv \hat{S}_{ql}(F_0) - \overline{\hat{S}_{ql}}(F_0)$ is the anisotropic part of $\hat{S}_{ql}(F_0)$ $(\overline{\hat{S}_{ql}^a}(F_0) = 0)$.

Equations (4.13-4.14) define the small nonlinear perturbation $\delta F \equiv \overline{\delta F} + \widehat{\delta F} = O\left(E^2\right) \ll F_0$ in case of weak field. This perturbation can be easily found in the approximation of cold collisional plasma, $\nu_{en} > v_{Te}/\delta$. Neglecting in (4.14) the combination $\left(v_x \partial \widehat{\delta F}/\partial x - \overline{v_x \partial \widehat{\delta F}/\partial x} \right)$ compared to the collisional term $\nu_{en}(v)\widehat{\delta F}$, we have for the anisotropic part of the perturbation:

$$\widehat{\delta F} = \frac{1}{\nu_{en}(v)} \hat{S}_{ql}^a(F_0) - \frac{v_x}{\nu_{en}(v)} \frac{\partial \overline{\delta F}}{\partial x}. \tag{4.15}$$

Then the equation for the isotropic part of the perturbation (4.13) becomes

$$-\frac{v^2}{3\nu_{en}(v)} \frac{\partial^2 \overline{\delta F}}{\partial x^2} = \overline{\hat{S}_{ql}}(F_0) - \frac{1}{\nu_{en}(v)} \frac{\partial}{\partial x} \overline{v_x \hat{S}_{ql}^a(F_0)}. \tag{4.16}$$

For the Maxwellian background distribution $F_0 = f_M$ the isotropic and anisotropic parts of the quasilinear operator $\hat{S}_{ql}(F_0)$ can be easily found using (4.4) in the cold plasma approximation as

$$\overline{\hat{S}_{ql}}(F_0) = -\frac{e^2}{m_e^2} \left(1 - \frac{2}{3} \frac{v^2}{v_{Te}^2} \right) \frac{f_M}{v_{Te}^2} |E_y|^2 \frac{\nu_{en}(v)}{\nu_{en}^2(v) + \omega^2}, \tag{4.17}$$

$$\hat{S}_{ql}^a(F_0) = \frac{e^2}{m_e^2} \left[\frac{v_x}{\nu_{en}(v)\delta} - \frac{2}{v_{Te}^2} \left(\frac{v^2}{3} - v_y^2 \right) \right] \frac{f_M}{v_{Te}^2} |E_y|^2 \frac{\nu_{en}(v)}{\nu_{en}^2(v) + \omega^2}. \tag{4.18}$$

Using these expressions, we can solve (4.16) and (4.15), finding the isotropic and anisotropic parts of the nonlinear perturbation of the "slow" electron distribution function as

$$\overline{\delta F} = \frac{e^2}{m_e^2} \frac{3\nu_{en}(v)}{v^2} \frac{f_M}{v_{Te}^2} \frac{\delta^2}{4} |E_y|^2 \frac{\nu_{en}(v)}{\nu_{en}^2(v) + \omega^2} \left[1 - \frac{2}{3} \left(\frac{v^2}{v_{Te}^2} + \frac{v^2}{\delta^2 \nu_{en}^2(v)} \right) \right], \tag{4.19}$$

$$\widehat{\delta F} = \frac{e^2}{m_e^2} \frac{f_M}{v_{Te}^2} |E_y|^2 \frac{1}{\nu_{en}^2(v) + \omega^2} \left\{ \frac{v_x}{\nu_{en}(v)\delta} - \frac{2}{v_{Te}^2} \left(\frac{v^2}{3} - v_y^2 \right) - \right. \quad (4.20)$$
$$\left. - \frac{3}{2} \frac{\delta\nu_{en}(v)}{v} \frac{v_x}{v} \left[\frac{2}{3} \left(\frac{v^2}{v_{Te}^2} + \frac{v^2}{\delta^2 \nu_{en}^2(v)} \right) - 1 \right] \right\}.$$

The criterion of validity of our solution for the isotropic and anisotropic parts of the nonlinear perturbation δF follows from the assumption we made: $\delta F \ll F_0$, i.e. the perturbation of the distribution function is small compared to the background distribution. From $\overline{\delta F} \ll F_0$ and $\widehat{\delta F} \ll F_0$, using (4.19-4.20), we get roughly:

$$\frac{v_E}{v_{Te}} \ll \frac{v_{Te}}{\nu_{en}\delta}, \text{ and} \quad (4.21)$$
$$v_E^2 \ll v_{Te}\nu_{en}\delta, \quad (4.22)$$

where $v_E = e/m_e E_0 \left(\nu_{en}^2 + \omega^2\right)^{-1/2}$ is a characteristic velocity of electron oscillations in the heating field (oscillatory velocity). Since in cold collisional plasma $\nu_{en}\delta > v_{Te}$, (4.21-4.22) are replaced by

$$v_E \ll v_{Te}. \quad (4.23)$$

4.4 Nonlinear Modification of Plasma Heating. Effect of RF Magnetic Field

The plasma heating can be calculated by taking a moment of the form $m_e/2 \int v^2 ... d^3v$ of Eq. (4.5). The resulting equation is an equation of energy balance, with the energy source, or heating, on the right-hand side:

$$Q = \frac{m_e}{2} \int v^2 \hat{S}_{ql}(f_{0e}) d^3v, \quad (4.24)$$

with $\hat{S}_{ql}(f_{0e})$ defined in (4.6). One can easily show that $\int v^2 (\mathbf{v} \times \mathbf{B}) \cdot \partial f / \partial \mathbf{v} \, d^3v = 0$ for any f which vanishes for large $\mathbf{v}$, therefore the equation for heating is reduced to

$$Q = \frac{e}{2} \int v^2 \left\langle \mathbf{E} \cdot \frac{\partial \tilde{f}_1}{\partial \mathbf{v}} \right\rangle d^3v. \quad (4.25)$$

For $f_{0e} = F_0$ we get a "linear" heating from (4.25), $Q_L \sim E_0^2$, which was calculated in Chapter 3. To find a nonlinear modification of plasma heating $\delta Q \sim E_0^4$ using (4.25), we calculate $\tilde{f}_1 = f_1 e^{-i\omega t}$ from (4.3) with $f_{0e} = F_0 + \delta F$ (where $\delta F \sim E_0^2$), keeping the terms of the orders up to E_0^3. The resulting equation for f_1 is [ref. Eq. (4.3)]

$$-i\omega f_1 + v_x \frac{\partial f_1}{\partial x} + \nu_{en} f_1 = \frac{e}{m_e} \left(\mathbf{E}(x) + \frac{1}{c} \mathbf{v} \times \mathbf{B}(x) \right) \cdot \frac{\partial (F_0 + \delta F)}{\partial \mathbf{v}}$$
$$+ \frac{e}{m_e} \left(\mathbf{E}(x) + \frac{1}{c} \mathbf{v} \times \mathbf{B}(x) \right)^* \cdot \frac{\partial f_2}{\partial \mathbf{v}}, \quad (4.26)$$

where f_2 is defined from (4.3) with terms of the orders higher than E_0^2 neglected:

$$-2i\omega f_2 + v_x \frac{\partial f_2}{\partial x} + \nu_{en} f_2 = \frac{e}{m_e} \left(\mathbf{E}(x) + \frac{1}{c} \mathbf{v} \times \mathbf{B}(x) \right) \cdot \frac{\partial f_1^{(0)}}{\partial \mathbf{v}} \sim E_0^2. \quad (4.27)$$

In (4.27) $f_1^{(0)}$ is defined from Eq. (4.4) with $f_{0e} = F_0$.

Finding f_1 from (4.26-4.27) up to the order of E_0^3, we calculate the heating in the form $Q = Q_L (E_0^2) + \delta Q (E_0^4)$ from (4.25). We will restrict ourselves to calculating the nonlinear heating in case of cold collisional plasma, for which it can be done relatively easy. We will also demonstrate how the RF magnetic field affects the nonlinear heating by comparing δQ calculated with account for both electric and magnetic components of the heating field, with $\delta Q_{B=0}$ calculated assuming zero magnetic field.

In the approximation of cold collisional plasma we can neglect the terms $v_x \partial / \partial x$ in (4.26-4.27). Then, using (4.19-4.20), we obtain simple solutions for f_2 and hence for f_1 (we are not showing them here). Substituting f_1 into (4.25), we get for the total heating:

$$Q = Q_L + \delta Q^{\overline{\delta F}} + \delta Q^{\widehat{\delta F}} + \delta Q^{f_2}, \quad (4.28)$$

where

$$Q_L = \frac{e^2}{4m_e} |E_y|^2 \int v^2 \frac{\nu_{en}(v)}{\nu_{en}^2(v) + \omega^2} \frac{\partial^2 f_M}{\partial v_y^2} d^3 v \quad (4.29)$$

is the linear heating (Ohmic heating, see Chapter 3),

$$\delta Q^{\overline{\delta F}} = \frac{e^2}{4m_e} \left|E_y\right|^2 \int v^2 \frac{\nu_{en}(v)}{\nu_{en}^2(v) + \omega^2} \frac{\partial^2 \overline{\delta F}}{\partial v_y^2} d^3 v \qquad (4.30)$$

with $\overline{\delta F}$ from (4.19),

$$\delta Q^{\widehat{\delta F}} = \frac{e^2}{4m_e} \left|E_y\right|^2 \int v^2 \frac{\partial}{\partial v_y} \left[-\frac{v_y \delta^{-1}}{\nu_{en}^2(v) + \omega^2} \frac{\partial \widehat{\delta F}}{\partial v_x} + \frac{\nu_{en}(v) + v_x \delta^{-1}}{\nu_{en}^2(v) + \omega^2} \frac{\partial \widehat{\delta F}}{\partial v_y} \right] d^3 v \qquad (4.31)$$

with $\widehat{\delta F}$ from (4.20), and

$$\delta Q^{f_2} = \frac{e^2}{4m_e} \int v^2 \frac{\partial}{\partial v_y} \left(R_1 + R_2 \right) d^3 v, \qquad (4.32)$$

where

$$\begin{aligned}
R_1 &= \frac{e^2}{m_e^2} \left|E_y\right|^2 \left|B_z\right|^2 \frac{v_y^2}{c^2} \frac{\nu_{en} \left(\nu_{en}^2 - 5\omega^2\right)}{\left(\nu_{en}^2 + \omega^2\right)^2 \left(\nu_{en}^2 + 4\omega^2\right)} \left(\frac{\partial^3 f_M}{\partial v_x^2 \partial v_y} - \frac{1}{v_y} \frac{\partial^2 f_M}{\partial v_y^2} \right) \\
&\quad + \frac{e^2}{m_e^2} \left|E_y\right|^2 \frac{v_y}{c} \frac{\partial^3 f_M}{\partial v_x \partial v_y^2} \operatorname{Re} \left[\frac{iB_z \left(E_y^* - v_x/cB_z^*\right)}{\left(\omega - i\nu_{en}\right)^2 \left(2\omega - i\nu_{en}\right)} \right], \qquad (4.33)
\end{aligned}$$

$$\begin{aligned}
R_2 &= \frac{e^2}{m_e^2 c} \left|E_y\right|^2 \operatorname{Re} \left[\frac{iB_z^* \left(E_y - v_x/cB_z\right)}{\left(\omega - i\nu_{en}\right)^2 \left(2\omega - i\nu_{en}\right)} \right] \left(\frac{\partial^2 f_M}{\partial v_x \partial v_y} + v_y \frac{\partial^3 f_M}{\partial v_x \partial v_y^2} \right) \\
&\quad + \frac{e^2}{m_e^2} \left|E_y\right|^2 \left|E_y - \frac{v_x}{c} B_z\right|^2 \frac{\partial^3 f_M}{\partial v_y^3} \frac{\nu_{en} \left(\nu_{en}^2 - 5\omega^2\right)}{\left(\nu_{en}^2 + \omega^2\right)^2 \left(\nu_{en}^2 + 4\omega^2\right)}. \qquad (4.34)
\end{aligned}$$

We see that the RF magnetic field B_z enters all three terms of nonlinear correction to plasma heating (4.30-4.32). In order to see how the magnetic field affects the nonlinear heating, we will compare the nonlinear heating, calculated with account for both electric and magnetic components of the electromagnetic field, with the nonlinear heating calculated neglecting the RF magnetic field. For the case of zero magnetic field we get for the isotropic and anisotropic parts of the nonlinear perturbation of the electron distribution function $\delta F_{B=0}$:

$$\overline{\delta F}_{B=0} = \frac{e^2}{m_e^2} \frac{3\nu_{en}(v)}{v^2} \frac{f_M}{v_{Te}^2} \frac{\delta^2}{4} \left|E_y\right|^2 \frac{\nu_{en}(v)}{\nu_{en}^2(v) + \omega^2} \left[1 - \frac{2}{3} \frac{v^2}{v_{Te}^2} \right], \qquad (4.35)$$

$$\widehat{\delta F}_{B=0} = \frac{e^2}{m_e^2} \frac{f_M}{v_{Te}^2} |E_y|^2 \frac{1}{\nu_{en}^2(v) + \omega^2} \left\{ -\frac{2}{v_{Te}^2} \left(\frac{v^2}{3} - v_y^2 \right) - \right. \tag{4.36}$$
$$\left. -\frac{3}{2} \frac{\delta\nu_{en}(v)}{v} \frac{v_x}{v} \left[\frac{2}{3} \frac{v^2}{v_{Te}^2} - 1 \right] \right\}.$$

Accordingly, the total heating in the case of zero magnetic field is $Q_{B=0} = Q_L + \delta Q_{B=0}^{\overline{\delta F}} + \delta Q_{B=0}^{\widehat{\delta F}} + \delta Q_{B=0}^{f_2}$, where Q_L is the same as in Eq. (4.29), and

$$\delta Q_{B=0}^{\overline{\delta F}} = \frac{e^2}{4m_e} |E_y|^2 \int v^2 \frac{\nu_{en}(v)}{\nu_{en}^2(v) + \omega^2} \frac{\partial^2 \overline{\delta F}_{B=0}}{\partial v_y^2} d^3v, \tag{4.37}$$

$$\delta Q_{B=0}^{\widehat{\delta F}} = \frac{e^2}{4m_e} |E_y|^2 \int v^2 \frac{\nu_{en}(v)}{\nu_{en}^2(v) + \omega^2} \frac{\partial^2 \widehat{\delta F}_{B=0}}{\partial v_y^2} d^3v, \tag{4.38}$$

and

$$\delta Q_{B=0}^{f_2} = \frac{e^2}{4m_e} \int v^2 \frac{\partial}{\partial v_y} \left(R_1^{B=0} + R_2^{B=0} \right) d^3v, \tag{4.39}$$

where

$$R_1^{B=0} = 0 \tag{4.40}$$

$$R_2^{B=0} = \frac{e^2}{m_e^2} |E_y|^4 \frac{\partial^3 f_M}{\partial v_y^3} \frac{\nu_{en} \left(\nu_{en}^2 - 5\omega^2 \right)}{\left(\nu_{en}^2 + \omega^2 \right)^2 \left(\nu_{en}^2 + 4\omega^2 \right)}. \tag{4.41}$$

In order to investigate the importance of the nonlinear correction to the plasma heating, as well as to see the effect of the RF magnetic field on the nonlinear heating, let us define the parameters $\xi \equiv Q/Q_L$ and $\xi_{B=0} \equiv Q_{B=0}/Q_L$, that measure the ratio of total (nonlinear) heating $Q = Q_L + \delta Q$ to the linear heating Q_L in the cases of non-zero and zero RF magnetic field, respectively. In cold collisional plasma the expressions for ξ and $\xi_{B=0}$ are, respectively,

$$\xi = 1 + \frac{e^2}{4m_e^2} \frac{E_0^2}{\omega^2 \delta^2 v_{Te}^4} \left(\nu_{en}^4 + 5\omega^2 \nu_{en}^2 + 4\omega^4 \right)^{-1} \left(2\omega^2 \nu_{en}^4 \delta^4 - \right. \tag{4.42}$$
$$\left. -\omega^2 \nu_{en}^2 \delta^2 v_{Te}^2 + 6\nu_{en}^2 v_{Te}^4 + 8\omega^4 \nu_{en}^2 \delta^4 - 4\omega^4 \delta^2 v_{Te}^2 - 30\omega^2 v_{Te}^4 \right),$$

$$\xi_{B=0} = 1 + \frac{e^2}{2m_e^2} E_0^2 \frac{\nu_{en}^2 \delta^2}{v_{Te}^4 \left(\nu_{en}^2 + \omega^2 \right)}. \tag{4.43}$$

Note that in calculating these expressions, we assumed ν_{en} to be independent of velocity when performing velocity integrations in (4.29-4.32) and (4.37-4.39), for simplicity. In general case one has to retain the velocity dependence $\nu_{en}(v)$ in calculating ξ and $\xi_{B=0}$.
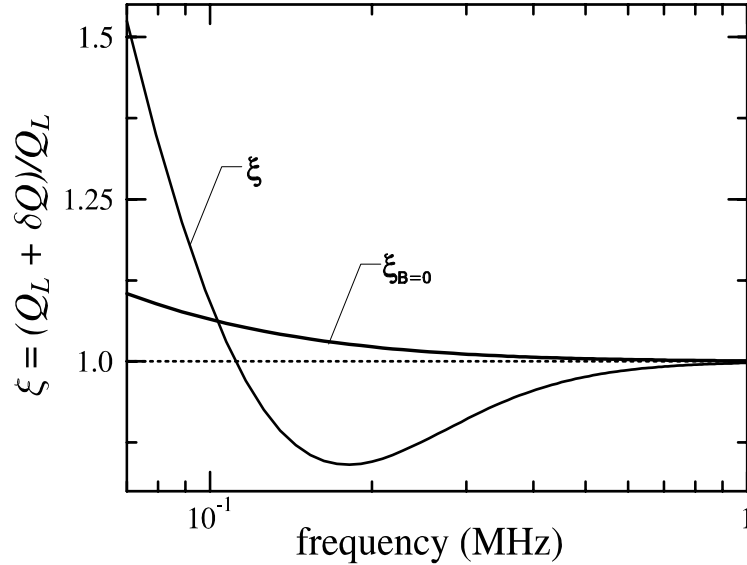
Figure 4.1: The parameters $\xi \equiv Q/Q_L$ (4.42) and $\xi_{B=0} \equiv Q_{B=0}/Q_L$ (4.43) as functions of the driving frequency, approximation of cold collisional plasma. Here $E_0 = 0.05$ V/cm, $\nu_{en} = 0.15 \cdot 10^7$ s^{-1}.

The nonlinear effects become small when $\xi, \xi_{B=0} \to 1$, i.e. when the nonlinear modification of heating vanishes. This happens at large frequencies,

$$\omega \gg \frac{e}{m_e} E_0 \frac{\nu_{en}\delta}{v_{Te}^2}, \tag{4.44}$$

as one can easily see from (4.42-4.43). At smaller frequencies the nonlinear effects become important.

A typical dependence of ξ and $\xi_{B=0}$ on the driving frequency is shown in Fig. 4.1 for cold collisional plasma. First of all, we see that in both cases of $B \neq 0$ and $B = 0$ the nonlinear effects lead to the significant deviation of plasma heating from the prediction of the linear theory (Chapter 3). This deviation is most pronounced at low frequencies, and vanishes at high frequencies $\omega \gg e/m_e E_0 \nu_{en}\delta/v_{Te}^2$ (this corresponds to $\omega/2\pi \gtrsim 0.5$ MHz for the parameters used in plotting Fig. 4.1). We also see that the nonlinear modification of plasma heating calculated considering both RF electric and magnetic fields (ξ), significantly exceeds the nonlinear modification of plasma heating calcu-

88

lated without considering the RF magnetic field ($\xi_{B=0}$). Moreover, besides the quantitative difference, there is also a qualitative difference between the cases of zero and non-zero magnetic field, as seen from Fig. 4.1: while the modification of heating in the case of zero magnetic field is positive and monotonically decreasing at increasing frequencies, the modification of heating in the case of non-zero magnetic field is nonmonotonic, starting from positive values at frequencies below 0.1 MHz, and becoming negative at higher frequencies. Therefore, we see that the nonlinear modification of plasma heating occurs mainly due to the nonlinear effect of the RF magnetic field. We should note, however, that this is true only if $\nu_{en} \lesssim \omega$; in highly collisional plasma, when $\nu_{en} \gg \omega$, the collisions render the electron distribution isotropic, and thus the nonlinear effect of the magnetic field vanishes, leaving only the nonlinear effect of the RF electric field. This can be easily seen from (4.42-4.43): ξ and $\xi_{B=0}$ become the same in highly collisional plasma, $\xi = \xi_{B=0} = e^2/2m_e^2 E_0^2 \delta^2 / v_{Te}^4$ for $\nu_{en} \gg \omega$.

The magnitude of the field used in Fig. 4.1 ($E_0 = 0.05$ V/cm) is smaller than the real experimental fields, and is dictated by the criterion of validity of the quasilinear approach (4.23).

We have calculated the nonlinear modification of heating for the case of cold collisional plasma. The case of warm plasma with collisions is more complicated, as it requires solving the Eqs. (4.13-4.14), (4.26-4.27) with all terms retained, to calculate the nonlinear heating from (4.25). However, as we will see in Chapter 5 by means of numerical experiment, the nonlinear modification of heating in *warm* plasma in case of weak heating field is similar (qualitatively) to that shown in Fig. 4.1 for the case of cold collisional plasma. We will also see in Chapter 5 how the nonlinear effects change plasma heating in case of strong heating field, when plasma is in strongly nonlinear regime for which the quasilinear approach developed here is invalid.

4.5 Summary

In this chapter we developed a quasilinear kinetic theory that accounts for the nonlinear effect of weak electromagnetic field on electron distribution function and, consequently, on plasma heating. The equations for the nonlinear perturbation of the electron distribution function and for the nonlinear modification of heating have been derived, and have been solved for the case of cold collisional plasma. The effect of the RF magnetic field has been highlighted by comparing the nonlinear modification of plasma heating calculated with and without the RF magnetic field. This comparison shows that the nonlinear modification of plasma heating occurs mainly due to the nonlinear effect of the RF magnetic field.

It has been shown that the nonlinear effect of weak electromagnetic field at low frequencies lead to some enhancement of heating compared to the linear heating. This suggests that at low driving frequencies the effective reduction of heating, predicted by our linear theory in Chapter 3, can be partially counterpart by this nonlinear enhancement of heating, in case of weak fields. At higher frequencies, the combined nonlinear effects of the electric and magnetic fields lead to some reduction of heating compared to the linear value. We will later confirm both enhancement of heating at low frequencies and reduction of heating at higher frequencies by means of numerical experiment (see Chapter 5). At high frequencies the nonlinear effects become weak, and the nonlinear modification of heating vanishes. This suggests that plasma heating is well described by the linear theory (Chapter 3) at high frequencies $\omega \gg e/m_e E_0 \nu_{en} \delta / v_{Te}^2$.

It should be noted that the description of nonlinear heating by strong fields at low frequencies is beyond the scope of this quasilinear model; it requires either a fully nonlinear treatment or a numerical experiment. The numerical experiment that we conducted to simulate plasma heating and its results are described in the next chapter.

Chapter 5

Particle-In-Cell Simulation of Heating in Nonlocal Regime

Our theoretical model described in Chapter 3 predicts a novel phenomenon of effective heating reduction at low frequencies. This phenomenon has not been mentioned in previous theoretical works on plasma heating in nonlocal regime, and it has not been observed experimentally, probably because of difficulties in measurement of plasma heating at low frequencies when this phenomenon occurs.

In order to justify our theoretical model in general, and to verify the effective reduction of heating in particular, as well as to investigate the nonlinear effect of the induced RF magnetic field on plasma heating, we undertake a numerical experiment. Recall that our linear theory does not account for the RF magnetic field, assuming the equilibrium electron velocity distribution to be isotropic and considering weak fields, and our quasilinear theory only accounts for the nonlinear effect of weak electromagnetic field. A general case of arbitrary electromagnetic field amplitude requires either a nonlinear treatment (which is a complex theoretical and computational task), or a numerical experiment.

For numerical simulation of plasma experiments, different types of simu-

lation codes could be used. For example, one could use fast hydrodynamic simulation codes to efficiently describe the long timescale evolution of plasma systems. These codes basically solve numerically the coupled system of hydrodynamic and Maxwell equations, and these codes are capable of accounting for complex geometry of plasma systems, and for sink and source terms in the hydrodynamic equations. However, hydrodynamic simulation codes have inherent limitation imposed by the limitation of the hydrodynamic approach itself in describing plasma systems. They are not suitable for simulating plasmas where electron mean free path is comparable or greater than typical length scales of gradients of plasma properties (density, temperature, etc.).

As our plasma with warm electrons requires a kinetic description, we should be using one of kinetic simulation codes. There are two types of kinetic simulation codes that are widely used: the Fokker-Planck (FP) simulation codes [57, 58], and the Particle-In-Cell (PIC) simulation codes [59]. In this work we use the PIC simulation code with collisions. We do not try to conduct realistic numerical experiment, but rather conduct an idealized numerical modeling of the ICP discharge to justify the predictions of our linear and quasilinear models for plasma heating in nonlocal regime.

Below we will describe the simulation and its main results in relation to our problem of plasma heating in nonlocal regime of ICP discharge. We will start from the basic principle of Particle-In-Cell simulation.

5.1 The Simulation Principle and Scheme

5.1.1 Particle-In-Cell Principle

The general philosophy of simulating plasma with particles is to follow the motion of all plasma particles in their self-consistent electromagnetic field. The most straightforward approach would be to simulate the motion and mutual reactions of all physical particles in plasma (electrons, ions, neutrals) in

their self-consistent field; however, this task is practically unsolvable because of extremely large number of physical particles for any type of plasma, ranging from laboratory plasmas (with densities $10^{10} - 10^{12}$ cm^{-3}) to inertial confinement fusion plasmas (with densities up to 10^{27} cm^{-3}). In simulations, a much smaller number of particles is used, typically about 10^6 particles in total. Each simulation particle represents a large number of physical particles, thus being sometimes called a "superparticle".

In standard electrostatic PIC (for a review see [59, 60]) the self-consistent electrostatic field of the ensemble of superparticles is defined from the Poisson equation (1.5), where the charge density ρ is defined from positions of particles. A force acting on i-th particle from all other particles is the sum of the contributions to the electric field from all the other particles,

$$F_i = q_i \sum_{j, i \neq j} E_{ij} \tag{5.1}$$

where q_i is the charge of the i-th particle, E_{ij} is the electric field of particle j acting on the i-th particle. This scheme of force calculation scales with the number of superparticles N as N^2, which is still too time consuming for typical numbers of simulation particles $N \sim 10^6$ necessary for simulating warm plasmas. Therefore a technique which further reduces the computational effort, while retaining important plasma phenomena, is required. This is achieved by interpolating the particle properties, such as charge density, current, kinetic energy, onto a 'coarse' grid, shown in Fig. 5.1. This grid should be fine enough to resolve the length scales of gradients of plasma quantities, but on the other hand each grid cell should contain a relatively large number of superparticles, in order to reduce the noise imposed by interpolation of particle quantities on the grid. The grid quantities (charge density, current) are used in the Maxwell equations (1.4, 1.5) which are therefore solved on the grid to determine fields at the grid points. The force acting on each superparticle is then obtained from the fields on the grid by an interpolation process inverse to that used in calculating the particle quantities on the grid. This scheme scales with the
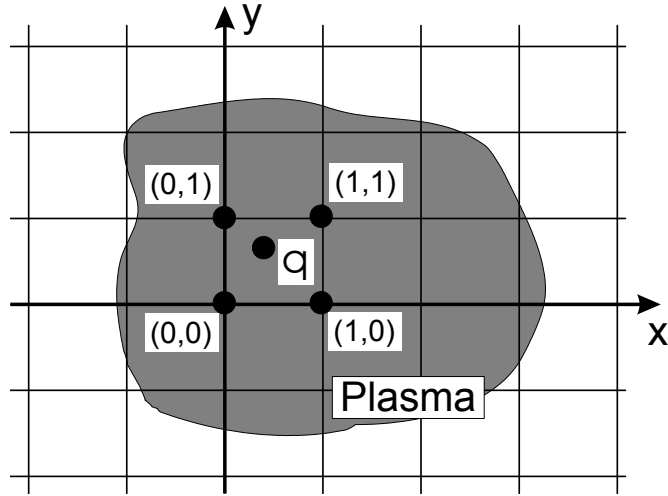
Figure 5.1: A grid is laid over the plasma region. Plasma density, current, temperature etc. are measured on the grid to obtain the electric field on the grid. Charge and velocity of a charged particle q are typically distributed among the nearby grid points $(0,0)$, $(1,0)$, $(0,1)$, $(1,1)$. The force on q is obtained from the fields at the same points.

number of particles N and the number of gridpoints Ng as $N \cdot Ng \ll N^2$, which makes it practical in simulations. This process of interpolating the particle quantities on the grid and inverse interpolating the fields on the particles afterwards gave the name to the method – Particle-In-Cell. The interpolation of particle quantities on the grid and grid quantities on the particles is also called *weighting*.

The usage of the grid smooths all phenomena in plasma over the length scale of the grid cell size, therefore we are not resolving microscopic fields in PIC method. The interaction of particles within the same grid cell is not resolved, and thus is effectively suppressed. This implies that the frequency of interparticle collisions, that mainly happen between closely located particles, is substantially reduced, and the typical PIC simulation is collisionless. If we want to have collisions, we should take a special care for them and implement them into our PIC code separately.

The time evolution of particle quantities and fields is tracked using the

temporal grid with a finite period Δt. In our code, we use the so-called leap-frog (time centered) scheme of time integration of equations (see [59] for more details). In this scheme, the particle quantities and the fields are obtained at time moments t, $t + \Delta t, t + 2\Delta t$, ..., while the particle velocities are obtained at time moments $t - \Delta t/2$, $t + \Delta t/2$, $t + 3/2\Delta t$, ..., i.e. two temporal grids, shifted by $\Delta t/2$, are used. This scheme proves to be quite accurate [59].

Obviously, by using the spatial and temporal grids we introduce some inevitable inaccuracies into the simulation. Also the effects of grid may give rise to nonphysical phenomena, such as numerical heating etc. (more on these in [59]). However, generally these nonphysical effects can be avoided; inaccuracies due to the grid usage will always be there and simply must be made small.

5.1.2 Collisions

As we have pointed out, the PIC simulation is inherently collisionless. In order to simulate collisional plasmas with PIC code, we must implement collisions 'by hand' into our code. As we want to simulate the ICP discharge and the plasma heating in nonlocal regime when both electron thermal motion and collisions are important, we have to implement two types of collisions:

1) collisions of electrons with neutral gas atoms $(e-n)$, that are the primary collisions in low temperature weakly ionized plasmas. These collisions also enter our theoretical kinetic model;

2) electron-electron collisions $(e - e)$, that are needed as the mechanism of "maxwellization" of electron distribution function. In the absence of fields and external forces the $e - e$ collisions drive the electron distribution function towards the Maxwellian distribution. In our simulation there are two mechanisms that drive the electron distribution away from Maxwellian: the electromagnetic field, which may make the electron distribution anisotropic, and the electron-atom collisions, that deplete the high-energy tail of the electron distribution. However, in real discharges

the distribution function is very close to Maxwellian [56], due to $e-e$ collisions. Thus to have a mechanism that would compete towards keeping the distribution function isotropic and close to Maxwellian, we introduce the $e-e$ collisions into our PIC code.

Electron-atom collisions

To implement the $e-n$ collisions, we use a well known Monte-Carlo method (see, for example, [61]). This method was developed during WWII for analysis of neutron moderation and transport. Here we will describe the principles of this method. The method relies on knowledge of the probability distribution function for a phenomenon of interest, to randomly select occurrences of events of this phenomenon, whose ensemble average represents the known (given) probability distribution [62]. Let us consider the method in more detail.

Suppose that some physical event has a known probability distribution function $p(x)$ which defines the probability for the event to occur at the position x. The knowledge that the event should occur somewhere gives $\int_0^\infty p(x)dx = 1$. Let us define a cumulative probability distribution function $P(x)$, which defines the probability of the event to occur prior to x, $P(x) = \int_0^x p(x')dx'$. Obviously, $P(0) = 0$, $P(\infty) = 1$. Since $p(x) > 0$, there is a one-to-one mapping of the interval $r = [0, 1]$ onto $[P(x = 0), P(x = \infty)]$. If we randomly select r (with a uniform probability distribution $p(r) = 1$ for $0 \leqslant r \leqslant 1$, $p(r) = 0$ otherwise) and solve the equation $r = P(x)$, we get the randomly selected position of the event occurrence, $x = P^{-1}(r)$. Continuing this process we will have an ensemble of random positions x of the events which, when averaged, represent the given $p(x)$.

For example, given the distribution of probability of an electron to collide at time moment Δt after a previous collision as $p(\Delta t) = \nu_{en} \exp(-\nu_e \Delta t)$, where ν_{en} is the $e-n$ collision frequency, we calculate the distribution of probability for an electron to collide before Δt, i.e. for a next collision to occur within time Δt: $P(\Delta t) = \int_0^{\Delta t} p(\Delta t') d(\Delta t') = 1 - \exp(-\nu_{en} \Delta t)$. We have $P(\Delta t = 0) = 0$,

and $P(\Delta t = \infty) = 1$. By randomly choosing $P(\Delta t) = r$ in the range $[0, 1]$, we get for the randomly selected time to a next collision:

$$\Delta t = -\frac{1}{\nu_{en}} \ln{(1 - r)}. \tag{5.2}$$

Averaging Δt over an ensemble as

$$\langle \Delta t \rangle = -\frac{1}{\nu_{en}} \int_0^1 \ln{(1 - r)}\, p(r)\, dr, \tag{5.3}$$

where $p(r)$ is the probability distribution for r ($p(r) = 1$ for $0 \leqslant r \leqslant 1$, $p(r) = 0$ otherwise), we get $\langle \Delta t \rangle = 1/\nu_{en}$, as expected.

Note that in most practical problems the calculation of the cumulative probability distribution and its inversion cannot be performed analytically and should be done numerically.

Now that we can define the random time intervals between collisions, let us consider the $e-n$ collision itself. Suppose an electron with energy ε collides with an atom with a differential cross section $\sigma(\varepsilon, \theta, \varphi)$, where θ, φ are the scattering angles defining the center of a solid angle in which the electron scatters. Typically the scattering is uniform on φ, i.e. $\sigma = \sigma(\varepsilon, \theta)$. The dependence $\sigma(\varepsilon, \theta)$ for real gas atoms can be very complicated [63]; however, in our simulation we use the simplest assumption of isotropic scattering, $\sigma(\theta) = \sigma_0$. With this assumption we can easily calculate the cumulative probability distribution $P(\theta)$ which defines the likelihood of electron scattering within the polar angles $[0, \theta]$:

$$P(\theta) = \frac{1}{2\sigma_0} \int_0^\theta \sigma_0 \sin{\theta'}\, d\theta', \tag{5.4}$$

and then we get for randomly selected scattering angle θ:

$$\theta = \arccos{(2r - 1)}, \tag{5.5}$$

where r is a random number uniformly distributed in the range $[0, 1]$. Similarly, we find for the azimuthal scattering angle $\varphi = 2\pi r$. Of course the random numbers r should be different when defining Δt, θ and φ. We will further

denote these random numbers as r_t, r_θ, r_φ respectively. Having determined the random scattering angles θ, φ and assuming elastic scattering of electrons on atoms, we can define an outcome of the collision as [62]

$$\mathbf{v}_{final} = |\mathbf{v}_{final}| \cdot \begin{pmatrix} \cos\beta\cos\alpha\sin\theta\cos\varphi + \cos\beta\sin\alpha\cos\theta - \sin\beta\sin\theta\sin\varphi \\ \sin\beta\cos\alpha\sin\theta\cos\varphi + \sin\beta\sin\alpha\cos\theta - \cos\beta\sin\theta\sin\varphi \\ -\sin\alpha\sin\theta\cos\varphi + \cos\alpha\cos\theta \end{pmatrix},$$

(5.6)

where $|\mathbf{v}_{final}|^2 = |\mathbf{v}_{initial}|^2 - 2\Delta\varepsilon/m_e$, $\Delta\varepsilon$ is the change of electron's energy due to the elastic collision with atom

$$\Delta\varepsilon = \varepsilon_{initial}\left[1 - \frac{2m_e}{M_{atom}}\left(1 - \cos\theta\right)\right],$$

and $\alpha = \arccos\left(v_z/v\right)_{initial}$, $\beta = \arctan\left(v_y/v_x\right)_{initial}$ are the Eulerian angles of $\mathbf{v}_{initial}$ in the laboratory frame.

Thus for description of $e - n$ collisions we need three random numbers: r_t, r_θ, r_φ. Note that in if we wanted to implement more realistic atom collision cross-sections, we should have calculated $P(\theta, \varepsilon)$ numerically for each ε, and also invert it numerically to obtain the random scattering angles θ.

Electron-electron collisions

The most straightforward way to implement $e - e$ collisions would be to use the Monte-Carlo technique, just as for $e - n$ collisions described above. However, the principal difference between $e - e$ and $e - n$ collisions is that the $e - e$ collisions occur already at long ranges, since the forces of interaction between electrons (Coulomb forces) are long-ranged. Any long-range collision is in fact a succession of many small-angle scatterings, and in order to represent such collisions correctly with Monte-Carlo technique, we would need to use very small timesteps. Moreover, at any given time an electron is scattering on more than one electrons, also due to long-range nature of Coulomb force. All this makes the simulation of $e - e$ collisions using the Monte-Carlo technique impractical, or at least rather computationally expensive.

An alternative approach to describe the $e - e$ collisions is to represent the Coulomb $e - e$ scattering through a Fokker-Planck equation [64, 65, 66]. However, there is no obvious way of combining a direct solution of the Fokker-Planck equation with the PIC method. Yet it is possible to construct a Langevin equation which is entirely equivalent to the Fokker-Planck equation [67], and which is easily implemented into the PIC scheme. The intraspecies collisions (electron-electron) can be effectively represented by a force $\mathbf{F}_{ee}$ acting on electrons, of the form [68]:

$$\mathbf{F}_{ee}/m_e = -\nu_e \left(\mathbf{v}_e - \langle \mathbf{v}_e \rangle \right) + \mathbf{A}, \tag{5.7}$$

where $\langle ... \rangle$ is averaging over distribution function of $(...)$, $\mathbf{A}$ is a random, isotropic vector ($\langle \mathbf{A} \rangle = 0$) which provides thermalization of electrons, and ν_e defines the dynamic friction acting on electrons. This form of the force conserves momentum, at least in a statistical sense, since obviously $\langle \mathbf{F}_{ee} \rangle = 0$. Momentum conservation means that $\langle \mathbf{v}_e \rangle$ does not change, therefore we can transform into a fluid frame moving with velocity $\langle \mathbf{v}_e \rangle$ and apply the analysis of Chandrasekhar [69] for the Langevin equation. Letting $\mathbf{v} = \mathbf{v}_e - \langle \mathbf{v}_e \rangle$ and integrating the equation of motion of electrons under the force $\mathbf{F}_{ee}$, we get [68]

$$\Delta \mathbf{v} = -\nu_e \mathbf{v} \Delta t + \mathbf{A}^*, \tag{5.8}$$

where $\mathbf{A}^* = \int_t^{t+\Delta t} \mathbf{A}(t') dt'$. Here the assumption is that the rate of velocity change (due to collisions) associated with the random vector $\mathbf{A}^*$ greatly exceeds the rate of velocity change associated with the dynamic friction ν_e, i.e. the electrons experience many small-angle scatterings. Chandrasekhar showed [69] that the Langevin equation (5.8) is equivalent to the Fokker-Planck kinetic equation describing the evolution of electron distribution function due to $e - e$ collisions. If the electron velocity is advanced according to Eq. (5.8), the electron velocity distribution approaches a Maxwellian for a proper choice of

random vector $\mathbf{A}^*$, that is if the probability distribution of $\mathbf{A}^*$ is

$$p(A^*) = \left(\frac{m_e}{4\pi \nu_e T_e \Delta t} \right)^{3/2} \exp \left(-\frac{m_e \mathbf{A}^* \cdot \mathbf{A}^*}{4\nu_e T_e \Delta t} \right), \qquad (5.9)$$

then

$$\lim_{t \to \infty} f_e(\mathbf{v}, t) = \left(\frac{m_e}{2\pi T_e} \right)^{3/2} \exp \left(-\frac{m_e v^2}{2T_e} \right). \qquad (5.10)$$

Here T_e is the final electron temperature.

The Langevin equation (5.8) can be easily implemented into PIC code by simply adding an $e - e$ collisional step which advances velocities of electrons according to (5.8), which is equivalent to adding the force (5.7) to the forces acting on electrons. Note that this additional force representing $e - e$ collisions is a grid quantity, as it depends on the grid quantities n_e, ν_e and T_e.

Using the time-centered scheme, we obtain a finite-difference equation for electron velocities from (5.8) [68]:

$$\mathbf{v}_{n+1} = \mathbf{v}_n - \frac{\nu_e \Delta t}{2} (\mathbf{v}_{n+1} + \mathbf{v}_n) + \mathbf{A}^*. \qquad (5.11)$$

The Langevin equation (5.8) and its finite-difference analog (5.11) conserve average momentum of particle ensemble automatically, since $\langle \mathbf{A}^* \rangle = 0$. A conservation of average energy is ensured for any timestep Δt, if the magnitude of the vector $\mathbf{A}^*$ is appropriately chosen according to (5.9), so that

$$\langle \mathbf{A}^* \cdot \mathbf{A}^* \rangle \equiv \int (\mathbf{A}^* \cdot \mathbf{A}^*) \, p(A^*) \, d\mathbf{A}^* = 6\nu_e \Delta t \, T_e / m_e. \qquad (5.12)$$

Indeed, one can show using Eqs. (5.12), (5.11) that

$$\frac{m_e}{2} \langle \mathbf{v}_{n+1}^2 \rangle = \frac{m_e}{2} \langle \mathbf{v}_n^2 \rangle = \frac{3}{2} T_e, \qquad (5.13)$$

i.e. that if the random vector $\mathbf{A}^*$ in (5.11) is appropriately chosen according to (5.9), the energy of the ensemble of particles, being "collided" according to (5.11), is conserved for any timestep Δt. This makes the Langevin equation much more advantageous compared to the Monte-Carlo technique in simulating the $e - e$ collisions, since one can use timesteps that are large compared to

characteristic time between $e - e$ collisions, still having the average energy conservation in the collision process.

According to Jones *et al.* [68] the dynamic friction ν_e is defined from the electron density n_e and electron temperature T_e (which are the grid quantities) as

$$\nu_e = \frac{4\sqrt{\pi}}{3} \frac{n_e e^4 \ln \Lambda_{ee}}{m_e^2 \left(T_e/m_e\right)^{3/2}}, \qquad (5.14)$$

where $\ln \Lambda_{ee}$ is a Coulomb logarithm.

The random vector $\mathbf{A}^*$ is defined as follows. The distribution function for $\mathbf{A}^*$ is given by Eq. (5.9). Let us define a vector $\mathbf{Y}$ as $\mathbf{Y} = \chi^{-1}\mathbf{A}^*$, where $\chi = \sqrt{2\nu_e \Delta t\, T_e/m_e}$. Then distribution function for the vector $\mathbf{Y}$ is defined from the equation

$$|p\left(\mathbf{A}^*\right) d\mathbf{A}^*| = |p\left(\mathbf{Y}\right) d\mathbf{Y}|, \qquad (5.15)$$

which gives a Gaussian distribution

$$p\left(\mathbf{Y}\right) = \frac{1}{(2\pi)^{3/2}} \exp\left(-\frac{\mathbf{Y} \cdot \mathbf{Y}}{2}\right), \qquad (5.16)$$

or for components of $\mathbf{Y}$

$$p\left(Y_i\right) = \frac{1}{(2\pi)^{1/2}} \exp\left(-Y_i^2/2\right). \qquad (5.17)$$

A most straightforward way to define random components of the vector $\mathbf{Y}$ and therefore of the vector $\mathbf{A}^* = \chi\mathbf{Y}$ is to define the cumulative distribution $P\left(Y_i\right) \equiv \int_{-\infty}^{Y_i} p\left(Y_i'\right) dY_i' = 1/2 \left(1 + \mathrm{erf}\left(Y_i/\sqrt{2}\right)\right)$ and find Y_i numerically from equation

$$1/2 \left(1 + \mathrm{erf}\left(Y_i/\sqrt{2}\right)\right) = r_i, \qquad (5.18)$$

where r_i is a random number distributed uniformly between 0 and 1. Note that r_i is different for each Y_i, thus we need 3 random numbers to describe the $e - e$ collision, just as one would expect. Note also that we do not define the time between successive $e - e$ collisions randomly, as for $e - n$ collisions. Instead we "collide" electrons through Langevin equation (5.11) each timestep, which can be large enough since the momentum and energy are conserved automatically.

However, solving Eq. (5.18) numerically for every electron at every timestep during the simulation is computationally expensive. Instead, we use a fast Box-Muller algorithm [70] that allows to select Y_i according to the Gaussian distribution (5.17) without solving Eq. (5.18), using only random numbers X_i distributed uniformly between 0 and 1 (see [70] for more details). Indeed, let us define the transformation between two uniformly distributed random numbers X_1, X_2 and the quantities Y_1, Y_2 as

$$Y_1 = \sqrt{-2 \ln X_1} \cos 2\pi X_2, \qquad (5.19)$$

$$Y_2 = \sqrt{-2 \ln X_1} \sin 2\pi X_2. \qquad (5.20)$$

Then equivalently we can write

$$X_1 = \exp\left[-\frac{1}{2}\left(Y_1^2 + Y_2^2\right)\right], \qquad (5.21)$$

$$X_2 = \frac{1}{2\pi} \arctan \frac{Y_2}{Y_1}. \qquad (5.22)$$

The Jacobian of this transformation is

$$\frac{\partial (X_1, X_2)}{\partial (Y_1, Y_2)} = -\left[\frac{1}{\sqrt{2\pi}} \exp\left(-Y_1^2/2\right)\right]\left[\frac{1}{\sqrt{2\pi}} \exp\left(-Y_2^2/2\right)\right]. \qquad (5.23)$$

As we see, the Jacobian of this transformation is a product of a function of Y_1 alone and a function of Y_2 alone, therefore each of Y_1 and Y_2 (5.19, 5.20) are independently distributed according to the Gaussian distribution (5.17). Having all three components of the vector $\mathbf{Y}$, we find the vector $\mathbf{A}^* = \chi\mathbf{Y}$. Apparently, this way of defining the vector $\mathbf{A}^*$ is much faster than that involving numerical solving of Eq. (5.18), as essentially we only need to evaluate Eqs. (5.19), (5.20) instead of solving Eq. (5.18). Of course, again we need 3 different random numbers to define the vector $\mathbf{A}^*$.

Now that we can select the random vector $\mathbf{A}^*$ and can calculate the $e - e$ collision frequency using Eq. (5.14), we can use the Langevin equation (5.11) to model the $e - e$ collisions.
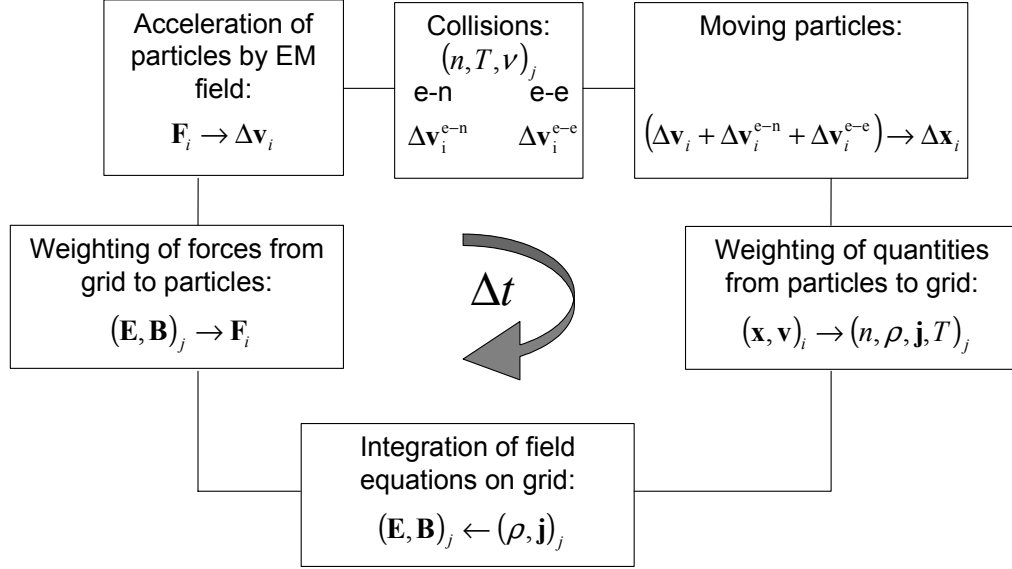
Figure 5.2: Schematic diagram of one timestep of PIC simulation with collisions.

5.1.3 Simulation Scheme

The schematic diagram of one timestep of a PIC simulation with collisions is shown on Fig. 5.2. The simulation starts at $t = 0$ with some initial conditions such as initial particle density and velocity distribution, and initial fields in the system. The simulation runs for a number of timesteps. At each timestep the simulation program performs the following operations:

- Weighting of quantities from particles to grid: from the current positions and velocities of particles $(\mathbf{x}, \mathbf{v})_i$ the program calculates particle density, charge density, current, temperature, etc. at the gridpoints $(n, \rho, \mathbf{j}, T)_j$ (hereafter the index i refers to particle quantities, and the index j refers

103

to grid quantities). For example, to calculate the charge density on the grid, the charge of each particle is distributed among the nearby gridpoints (see Fig. 5.1) according to the weighting scheme. There are different weighting schemes that could be used; the simplest is the zero-order weighting, when the charge density at the j-th gridpoint is the total charge of all particles located within the m-dimensional 'hypercube' ($m = 1, 2, 3$ for one-dimensional, two-dimensional and three-dimensional geometries respectively) with the center at the j-th gridpoint and a side of Δx (Δx is the period of the grid), divided by the volume of this hypercube Δx^m (in the one-dimensional case it is the total charge of all particles within the distance $\Delta x/2$ divided by the grid period Δx). Using the zero-order weighting scheme is equivalent to having the finite-size particles of rectangular shape [59]. The physics observed in such simulation will be that of such particles rather than that of point particles. Because close encounters between the physical particles in plasma are rare, this new physics arising from the finite size of particles does not significantly alter the effects observed in the simulation compared to the effects observed in real plasmas. However, the particle quantities collected on the grid using the zero-order weighting are rather noisy. The cause of this noise is that the grid quantities jump up and down as particles enter or leave the 'hypercube' containing the given gridpoint. Therefore the use of higher-order weighting schemes is desired to suppress the effects of the grid such as noise. For example, the usage of first-order weighting is equivalent to having triangular-shaped particles [59] rather than rectangular-shaped particles for zero-order weighting. This smooths the grid quantities and eliminates the jumps associated with particle passages through the boundaries of the grid cells. In this scheme the charge assigned to the j-th gridpoint (in one-dimensional

case) is calculated from the charge of the particle q_p as

$$q_j = q_p \frac{\Delta x - (x_i - X_j)}{\Delta x} = q_p \frac{X_{j+1} - x_i}{\Delta x}, \qquad (5.24)$$

and the charge assigned to the $(j+1)$-th gridpoint is calculated as

$$q_{j+1} = q_p \frac{x_i - X_j}{\Delta x}, \qquad (5.25)$$

where x_i is the particle position, X_j and X_{j+1} are the positions of j-th and $(j+1)$-th gridpoints respectively, and $\Delta x = X_{j+1} - X_j$. One could also use higher-order weighting schemes to further smooth the grid effects, however this would also increase the computational cost. In our simulation we use the first-order weighting scheme for collecting the grid quantities from particles.

- Integration of field equations on grid: using the grid quantities $(\rho, \mathbf{j})_j$, the electromagnetic field is calculated at the gridpoints $(\mathbf{E}, \mathbf{B})_j$ from the Maxwell's equations. This is done by a special solver, either electrostatic (which solves the Poisson equation (1.5) to find the electrostatic field and potential) or electromagnetic (which solves the Maxwell's equations (1.3-1.4) for the electromagnetic field). The detailed description of these solvers can be found, for example, in [59].

- Weighting of forces from grid to particles: from the calculated fields on the grid $(\mathbf{E}, \mathbf{B})_j$ we calculate the force exerted by these fields on the particles. This calculation is analogous to weighting of quantities from particles to grid. For example, in one-dimensional case the electric field acting on i-th particle can be calculated using the first-order weighting scheme as

$$E(x_i) = \frac{X_{j+1} - x_i}{\Delta x} E_j + \frac{x_i - X_j}{\Delta x} E_{j+1}, \qquad (5.26)$$

where E_j and E_{j+1} are the values of the electric field at the j-th and $(j+1)$-th gridpoints, respectively. The force on the i-th particle due to this electric field is simply $q_p E(x_i)$.

- Acceleration of particles by EM field: given the forces acting on particles, we advance particle velocities in time according to equation of motion

$$m_p \frac{d\mathbf{v}_i}{dt} = q_p \left(\mathbf{E}(x_i) + \frac{1}{c}\mathbf{v}_i \times \mathbf{B}(x_i) \right). \tag{5.27}$$

  The optimal time-centered energy-conserving scheme for advancing particle velocities according to this equation of motion is given in [59].

- Collisions: calculate the change of particle velocities due to $e-n$ and $e-e$ collisions, as discussed above (see Collisions, p. 95).

- Moving particles: advance particle positions according to the total particle velocity change due to acceleration by EM field and collisions:

$$\Delta\mathbf{x}_i = \left(\Delta\mathbf{v}_i + \Delta\mathbf{v}_i^{\text{e-n}} + \Delta\mathbf{v}_i^{\text{e-e}} \right) \Delta t. \tag{5.28}$$

5.1.4 Diagnostics

At each timestep of our simulation, we need to output diagnostic data to monitor the plasma system being simulated. In PIC simulations the accessible physical quantities are the positions and velocities of all superparticles, so the most straightforward way to save the information about the state of plasma during the simulation would be to save the positions of all particles in coordinate-velocity phase space. However, this is not an option for systems of many particles being simulated over many timesteps, not only because it requires huge storage capacities, but also because this "raw" information does not provide any physical insight. Therefore we need to extract some meaningful physical quantities out of the information about particle positions and velocities. The evolution of most plasma systems is described by macro quantities such as mass and charge density, flow, current, temperature, kinetic energy of particles, electrostatic and electromagnetic field and energy. Therefore in the diagnostic part of the simulation program we output these grid quantities $(n, \rho, \mathbf{j}, T)$ and the fields at the gridpoints at each timestep. It is also useful

to know a velocity distribution function of particles $f(\mathbf{x}, \mathbf{v}, t)$. Basically all information about plasma is confined in $f(\mathbf{x}, \mathbf{v}, t)$: the appropriate macroscopic quantities can be calculated as corresponding moments of $f(\mathbf{x}, \mathbf{v}, t)$ as

$$
\begin{aligned}
n(x, t) &= \int f(\mathbf{x}, \mathbf{v}, t) d^3 v, \\
\mathbf{j}(x, t) &= \int q_p \mathbf{v}\, f(\mathbf{x}, \mathbf{v}, t) d^3 v,
\end{aligned}
$$
and so on...

The velocity distribution is determined by counting particles within bins on a 3-dimensional velocity grid.

To monitor the heating of plasma by the electromagnetic wave we also calculate and output at each timestep the total kinetic energy of all particles as

$$
KE = 1/2 \sum_{i=1}^{N_p} m_i \left| \mathbf{v}_i \right|^2, \tag{5.29}
$$

where N_p is the number of superparticles in the simulation.

5.2 Simulation Setup

Our simulation code is designed for modeling plasma heating in ICP discharge in nonlocal regime, to verify the results of our theoretical model (see Chapter 3). Therefore we use the idealized one-dimensional planar plasma model (see Fig. 1.3) in our simulation, with three particle velocity components (1d3v).

The simulation setup is the following: the plasma, consisting of immobile cold ions and mobile warm electrons, occupies the region $0 < x < L$ and is confined by two walls. The electrons are reflected specularly off these walls. The simulation is started with uniform density of electrons; the initial velocity distribution of electrons is Maxwellian. The electromagnetic field enters the system from $x < 0$, i.e. from the left.

To simplify the simulation, we use the same assumption of exponentially decaying electromagnetic field as we used in our theory (ref. Chapter 3). With this assumption, we do not have to solve for the self-consistent electromagnetic field in our simulation (ref. Fig. 5.2). Just as for our theory, the appropriate skin depth δ and the imaginary part κ of the wave vector $\gamma = 1/\delta - i\kappa$ enter the simulation as input parameters. They can be calculated in one of the ways discussed in Chapter 3 (see p. 59). The skin depth that we use in our simulation is calculated by solving Eqs. (3.18-3.19) simultaneously (this is done separately from the simulation process), and κ is taken to be equal to zero (see Appendix A). We should note that even if non-zero κ is used in the simulation, the heating varies less than by approximately 25% of its value when κ is changed from 0 to $\sim \delta^{-1}$, i.e. the heating is rather insensitive on κ.

Our theoretical model considers semi-infinite plasma, therefore, in order to setup our simulation so that it is as close to our theoretical model as possible (to be able to compare the results of the simulation and the theory), and to eliminate the effects of the second (right) wall, we set the length of the plasma $L \gg \delta$. In our simulation we use $L = 100$ cm.

The electrostatic field (directed along x) is calculated from the charge density on the grid using the Poisson's equation (1.5); however, to compare the results with our theoretical model which does not account for the electrostatic field, we toggle the electrostatic solver off.

The electrons are accelerated by the electromagnetic field, and therefore are heated. By toggling the $e - n$ collisions off and on we can observe the collisionless heating and study the influence of collisions on heating in nonlocal regime. Also, by toggling the magnetic field on and off in the equation of motion of electrons (5.27) we can study the influence of the electromagnetic field on plasma heating (note that in most theoretical approaches to plasma heating the influence of the RF magnetic field is not accounted for).

Below we consider the typical simulation results on plasma heating in nonlocal regime. We consider two cases: heating due to RF electric field only (no

magnetic field), and heating due to full electromagnetic field.

5.3 Simulation: Heating due to RF Electric Field only

Let us first simulate the electron heating in ICP in nonlocal regime due to the prescribed RF electric field $E_y = E_0 \exp(-x/\delta) \cos \omega t$ only (no RF magnetic field). As we have seen from our theory (Chapter 3), the heating in nonlocal regime is a result of two heating mechanisms: collisional and collisionless. In our simulation we can toggle the $e-n$ collisions on and off, in order to observe the purely collisionless heating and to compare the total heating due to both collisional and collisionless heating mechanisms with the purely collisional heating, as we did theoretically in Chapter 3 (see Fig. 3.5).

5.3.1 Evidence of Collisionless Heating

Since the resonant heating of plasma electrons by electromagnetic wave is proportional to $(\partial f_{0e}/\partial v_y)_{v_x=\omega/k}$ (see Eq. 3.24), it should occur in plasma with warm electrons (as in such plasma there is a substantial number of resonant electrons with velocities close to the wave phase velocity), and should not occur in cold plasma. To see the evidence of collisionless heating in PIC simulation of plasma with warm electrons, we plot the time evolution of total kinetic energy of plasma electrons in the electric field $E_y = E_0 \exp(-x/\delta) \cos \omega t$ for different electron temperatures, in the absence of collisions (Fig. 5.3). It is seen that in cold collisionless plasma (Fig. 5.3 (a)) the average total kinetic energy of electrons does not change over time, and thus electrons are not heated by the wave field, as expected. In warm collisionless plasma (Fig. 5.3 (b)) we see that the total kinetic energy grows in time, i.e. electrons are indeed heated collisionlessly. The estimated total absorbed power for the collisionless heating is calculated as $(KE_{final} - KE_{initial})/t$, where $KE_{initial}$ and KE_{final} are the
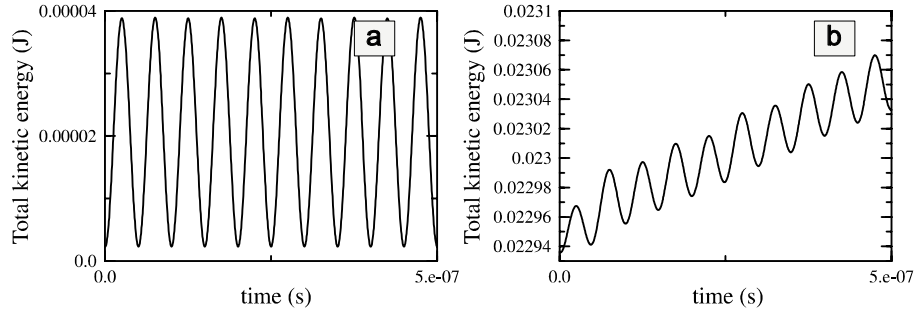
Figure 5.3: Time evolution of total kinetic energy of electrons in collisionless plasma with (a) cold electrons and with (b) warm electrons ($T_e = 10$ eV).

initial ($t = 0$) and final total kinetic energy of electrons, and t is the time of the simulation. For the case plotted in Fig. 5.3 (b) ($T_e = 10$ eV, $n_0 = 10^{10}$ cm^{-3}, $\omega/2\pi = 10$ MHz, $\nu_e = 0$, $E_0 = 2$ V/cm, $\delta \approx 5.6$ cm) the total absorbed power measured in the simulation is approximately 190 W, while our theory predicts 170 W (from Eq. 3.13) for the same parameters. We see that the discrepancy between our theory and the simulation is rather small (relative error is about 10%). Thus the results of the PIC simulation of collisionless heating confirm our theoretical model.

5.3.2 Comparison of Simulation Results with Linear Theory. Evidence of Heating Reduction at Low Frequencies

In Chapter 3 we studied the influence of electron thermal motion on plasma heating in nonlocal regime (see Fig. 3.5). To do this, we introduced the parameter $\eta = S_{tot}/S_{coll}$ which is the ratio of the total power absorption in nonlocal regime (3.13) to the purely collisional power absorption (3.15). This parameter compares the actual heating in nonlocal regime to the heating that would have occurred if only the collisional mechanism of power absorption was active, with all other conditions being the same. Studying the dependence of η on the

driving frequency we have shown theoretically (Fig. 3.5) that the heating in nonlocal regime is enhanced significantly (compared to the purely collisional heating) at frequencies near a resonance (when $|s| = 1$, or $\sqrt{\omega^2 + \nu_{en}^2} = v_{Te}/\delta$), and is reduced significantly at low frequencies $\omega < \nu_e$ (effective reduction of heating).

Now that we have the tool for PIC simulation of plasma heating in nonlocal regime, let us study the same dependence of $\eta = S_{tot}/S_{coll}$ on the wave driving frequency, and compare it to the theoretical curve (Fig. 3.5). Particularly we will be looking at the enhancement of heating at resonant frequencies, and at the effective reduction of heating at low frequencies.

We conducted a series of numerical experiments using our PIC code with collisions described above, with the prescribed exponentially decaying electric field $E_y = E_0 \exp(-x/\delta) \cos \omega t$ that heats the plasma. In these simulation runs we measured the total heating of electrons S_{tot} from an increase of the total kinetic energy of electrons, and compared it to the purely collisional heating calculated from (3.15). The purely collisional heating was calculated using the same mean collision frequency ν_{en} as that used in the simulation. In our setup, this collision frequency entered the simulation as an input parameter, and its value was taken from the experiment [32].

The parameters for which the simulations were carried out were chosen to match the experimental parameters [32] and were the following: plasma density $n_0 = 2.7 \cdot 10^{10}$ cm^{-3}, $e - n$ collision frequency $\nu_{en} = 1.5 \cdot 10^6$ s^{-1}, electron temperature $T_e = 10$ eV, the driving frequency ranged from 10^{-2} MHz to 10^2 MHz, which corresponds to a transition from strongly nonlocal regime to local regime of electromagnetic phenomena in plasma. The dependence of the ratio $\eta = S_{tot}/S_{coll}$, measured in the numerical experiments on the driving frequency, is compared to the according theoretical dependence for the same parameters in Fig. 5.4. We see from Fig. 5.4 that there is a very good match between the results of PIC simulation without RF magnetic field and our linear theory. Namely, the simulation justifies the novel phenomenon of the
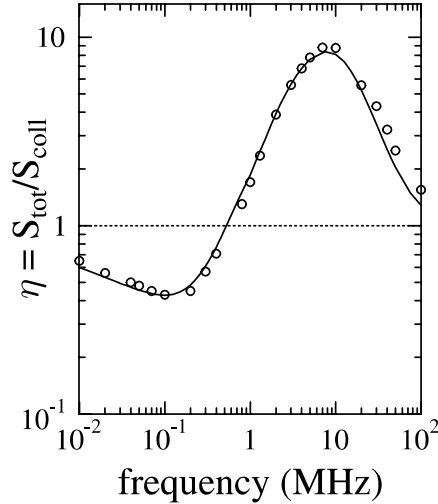
Figure 5.4: Ratio $\eta = S_{tot}/S_{coll}$, measured in PIC simulation (no RF magnetic field), for different driving frequencies. Results of the simulation are represented by circles. The theoretical (linear) result for the same parameters (solid line) is plotted for comparison.

effective reduction of heating at low frequencies; it also confirms the resonant enhancement of heating at moderate frequencies, when $|\omega + i\nu_{en}| \approx v_{Te}/\delta$.

This match between the simulation results and our linear theory is not very surprising as these simulations are performed at conditions that are very close to the assumptions made in our theoretical model. Most importantly, we have switched the RF magnetic field off in these simulations. Taking the RF magnetic field into account might change the heating, especially at low frequencies, when the nonlinearity due to the Lorentz force is significant. In Chapter 4 we developed the quasilinear theory which accounts for the effect of weak electromagnetic (mainly RF magnetic field) on electron heating. This theory predicts a small nonlinear enhancement of electron heating at low frequencies, followed by a reduction at higher frequencies, in case of weak heating field. However, it is interesting to study the effect of RF magnetic field on electron heating for arbitrary field strength. This can be done by means of the numerical experiment.

112

5.4 Simulation: Nonlinear Effect of RF Magnetic Field on Heating

To study the effect of the induced RF magnetic field on plasma heating by means of numerical experiment, we calculate the RF magnetic field B_z from the electric field $E_y = E_0 \exp(-x/\delta) \cos \omega t$ using (1.3), and move particles (electrons) taking into account both the electric field force $-e\mathbf{E}$ and the Lorentz force $-e/c \, [\mathbf{v} \times \mathbf{B}]$. The Lorentz force imposes nonlinearity into the problem, as the electron trajectories are not "straight" anymore. The kinetic equation for the electron distribution function generally becomes nonlinear, and the heating may deviate significantly from predictions of the linear or even the quasilinear theory.

When simulating plasma heating with an account for the RF magnetic field, we will study two cases. First is a case of weak nonlinearity, when the electromagnetic field is weak; by simulating this case we will be able to justify our quasilinear theory that predicts (for the cold collisional plasma) a nonlinear enhancement of heating at low frequencies compared to the linear heating, followed by a nonlinear reduction of heating at higher frequencies, vanishing as the frequency grows (see Fig. 4.1, Chapter 4). Second is a case of strong nonlinearity, when the magnetic field is strong enough to significantly alter electron trajectories. This case is described by a nonlinear kinetic equation, which generally can not be solved analytically. Therefore the usage of numerical simulations for studying the case of strong nonlinearity is very attractive.

We will start with the case of weak nonlinearity.

5.4.1 Weak Nonlinearity

Here we consider the case of plasma heating by weak field, when the electron oscillatory velocity in the electric field E_y is small compared to their thermal
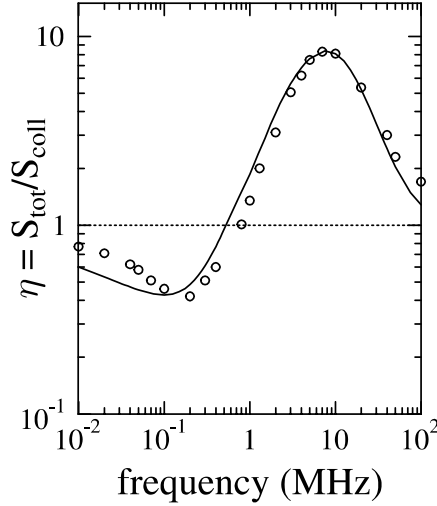
Figure 5.5: Ratio $\eta = S_{tot}/S_{coll}$, measured in PIC simulation (weakly non-linear case), for different driving frequencies. Results of the simulation are represented by circles. The theoretical (linear) result for the same parameters (solid line) is plotted for comparison. The parameters are $E_0 = 0.05$ V/cm, $T_e = 10$ eV.

velocity,

$$\frac{e}{m_e}\frac{E_0}{\sqrt{\omega^2 + \nu_{en}^2}} = v_E \ll v_{Te}. \tag{5.30}$$

This condition is the same as (4.23), which implies that the nonlinear perturbation of the electron distribution function from the background Maxwellian distribution is small, $\delta F \ll f_M$ (see Chapter 4). Hence this is the case of weak nonlinearity, and it is described by our quasilinear model, developed in Chapter 4. Thus one might expect to see a similar picture as was predicted in Chapter 4 for the case of cold collisional plasma. This picture, however, can be modified by the electron thermal motion, as now we have a warm plasma with collisions.

The effect of weak nonlinearity on plasma heating in case of warm plasma with collisions is well seen in Fig. 5.5. Here again we plot the parameter $\eta = S_{tot}/S_{coll}$ against the wave driving frequency, taking into account the magnetic field in the case of weak fields, and compare it to the linear case,

114

without the magnetic field. As we see from Fig. 5.5, there is a nonlinear deviation of the simulation results for heating from the prediction of our linear model at low frequencies, as expected. Moreover, this deviation is in qualitative agreement with the predictions of our quasilinear theory for the case of cold collisional plasma. Namely, we see a slight enhancement of heating (compared to the linear value) at low frequencies, followed by a slight reduction of heating at higher frequencies, vanishing as the frequency goes up, just as in Fig. 4.1 (Chapter 4). This qualitative agreement of the results of numerical experiment for warm plasma with collisions with the prediction of our quasilinear theory for cold collisional plasma suggests that the electron thermal motion does not significantly alter the nonlinear modification of heating.

Note that the value of the electric field $E_0 = 0.05$ V/cm used in this case is rather small; it is smaller than typical values of the electric field in real discharges. However, we used such a field to illustrate the effect of weak nonlinearity on plasma heating, which leads to a somewhat enhancement of heating at low frequencies compared to the linear case.

Next we will consider the case of strong nonlinearity with field values that are close to the typical experimental values.

5.4.2 Strong Nonlinearity

Let us now consider the case of plasma heating with strong fields, when the electron oscillatory velocity is of the order of the electron thermal velocity,

$$v_E \simeq v_{Te}. \tag{5.31}$$

For such fields the electron distribution function can deviate significantly from isotropic (Maxwellian), and therefore a significant deviation of heating from the predictions of both our linear and quasilinear theories is expected. Indeed, we see such deviation at low frequencies from Fig. 5.6, where the ratio $\eta = S_{tot}/S_{coll}$ is calculated from the results of PIC simulation in the case of strong fields, and compared to the result of the linear theory. The electric
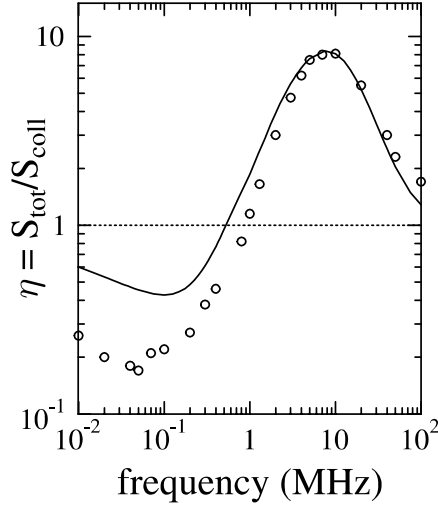
Figure 5.6: Ratio $\eta = S_{tot}/S_{coll}$, measured in PIC simulation (strongly non-linear case), for different driving frequencies. Results of the simulation are represented by circles. The theoretical (linear) result for the same parameters (solid line) is plotted for comparison. The parameters are $E_0 = 0.5$ V/cm, $T_e = 10$ eV.

field amplitude in the simulation of this case is 0.5 V/cm, which is close to the actual experimental values at low frequencies. We see from Fig. 5.6 that at low frequencies, when the ratio of electron cyclotron frequency in the RF magnetic field to the wave frequency, which characterizes the nonlinear influence of magnetic field, is large, $\omega_c/\omega > 1$, there is a significant deviation of heating from the prediction of the linear model. Namely, we see even greater reduction of heating compared to the purely collisional value (in linear case) than that predicted from our linear theory. This additional reduction of heating could be related to several nonlinear effects that have been previously discussed theoretically in literature. One of the effects responsible for this additional reduction is the depletion of plasma density in the skin region due to strong ponderomotive effect at low frequencies predicted by Cohen and Rognlien [7, 15]. Indeed, the ponderomotive force is greatly enhanced at low frequencies (see Eqs. 3.28, 3.32), and it shifts the plasma away from the skin region, thus reducing the

plasma density in the skin region. As a consequence, the plasma current induced by the electromagnetic field is reduced, and therefore the plasma heating is also reduced compared to the case without magnetic field (linear case). This is a nonlinear effect that requires strong fields, which is the case here. Another effect that can possibly cause the nonlinear deviation of heating from heating in the linear case is the nonlinear trapping of electrons by the electromagnetic field in the skin region [71].

As in the case of weak nonlinearity (see Fig. 5.5), the nonlinear deviation of heating from the linear case in the case of strong nonlinearity diminishes as the wave frequency increases, i.e. as the nonlinearity parameter ω_c/ω becomes small (see Fig. 5.6).

It should be noted that in the simulations of both weakly and strongly nonlinear cases we did not account for the electrostatic field, as we designed our numerical experiment to have as close setup with our theoretical model as possible, and our theoretical model does not account for the ambipolar electric field. However, one might expect that in the case of strong nonlinearity the ponderomotive depletion of plasma density in the skin region would create a significant electrostatic field which would keep the plasma quasineutral. This field might also influence the heating. However, as it was discussed by Cohen and Rognlien [15], this field does not lead to any significant change of heating, moreover, the heating rate calculated with account of this field is slightly lower than the heating rate without the electrostatic field. It is difficult to verify this statement using our PIC code which uses a Poisson equation to calculate the electrostatic field, as for this we would need a timestep small enough to resolve the plasma frequency. With typical plasma densities of the order of $10^{10} - 10^{12}$ cm^{-3} the problem of simulating plasma heating at low frequencies (below 0.1 MHz) with account for the electrostatic field requires from hundreds to thousands of hours of computational time per each point on the plot of $\eta = S_{tot}/S_{coll}$ versus frequency ω. A remedy for this could be a usage of a different technique for calculating the self-consistent electrostatic

field based on plasma quasineutrality [72] (page 66), [73], [74]. This technique allows to not resolve the plasma frequency, therefore being more adequate in simulations of slow-timescale phenomena (compared to period of plasma oscillations), such as plasma heating. Also this technique is characterized by much lower noise than that using the Poisson solver. Implementing this technique and simulation of plasma heating in nonlinear case with account for the electrostatic field could be one of the directions of the future work.

Chapter 6

Conclusions and Suggestions for Future Research

The modern ICP discharges typically operate in the regime of the anomalous skin effect, when the thermal motion of plasma electrons is essential, i.e. plasma is warm, $v_{Te} > \omega\delta$. This regime, also called a nonlocal regime, is characterized by such features as nonlocal Ohm's law, nonmonotonic profile of the electromagnetic field in plasma, and increased depth of the electromagnetic field penetration into plasma compared to the case of cold plasma (regime of classical skin effect).

The experimental measurements of ponderomotive effect and plasma heating in ICP at conditions of the anomalous skin effect, conducted by Godyak *et al.* [17, 31, 32], demonstrated some interesting features. Namely, it was shown that the actual ponderomotive effect in the nonlocal regime is significantly smaller than that predicted by the classical Miller theory of ponderomotive effect in cold plasma [22]. Also, the measurements of plasma heating in nonlocal regime demonstrated an importance of resonant wave-electron interaction, leading to significant collisionless heating of plasma, as well as an importance of thermal diffusion of the electron current in plasma, leading to negative absorption of the electromagnetic wave power by plasma electrons.

The discrepancy between the measured ponderomotive force and the prediction of the Miller theory, occurring due to the thermal effects, has not been previously explained. Moreover, the whole notion of thermal modification of the ponderomotive force has not been discussed theoretically. Most previous investigations implicitly or explicitly dealt with situations of weak nonlocality and weak time dependence of field amplitude. These works treated the problem of calculating the ponderomotive force perturbatively, by using small parameters $1/\tau \ll \omega$ (here τ is a characteristic timescale of weak time dependence of field amplitude, ω is the frequency of field oscillations), and $kv_{Te} \ll \omega$ (here k is the characteristic wave vector of the field). Under these assumptions the thermal effects result only in small correction to the standard cold plasma formula for the ponderomotive force.

The case of ICP in nonlocal regime is opposite: $kv_{Te} > \omega$, therefore it can not be treated by the perturbative technique typically used in other theoretical works on ponderomotive effect. This motivated us into development of the linear kinetic model of electron dynamics in ICP in nonlocal regime, which accounts for electron thermal motion and collisions in non-perturbative manner. This model describes both ponderomotive force and plasma heating, showing a good agreement with the experimental data of Godyak *et al.* In particular, it predicts the reduction of ponderomotive force compared to the Miller expression as it was observed experimentally in [17], which is one of our main results. Our model also describes correctly the resonant absorption of the electromagnetic field in plasma [32]. It also yields the negative absorption of the heating wave power by plasma electrons, in good agreement with the experimental picture and earlier theoretical work [31]. Another important accomplishment of our model is the prediction of the reduction of total plasma heating compared to the purely collisional heating at low driving frequencies, which has not been previously reported. In other words, this effect means that, at low driving frequencies, the total plasma heating due to both collisional and collisionless (resonant) mechanisms becomes smaller than it would have been

if only the collisional mechanism was active. This is contrary to the general belief that the resonant absorption always increases the total plasma heating as compared to heating due to collisional mechanism alone.

Our linear theoretical model, developed in Chapter 3, does not account for nonlinear modification of the electron distribution function and subsequent modification of plasma heating. To account for the nonlinear effect of the weak electromagnetic field, we developed the quasilinear kinetic theory. Within this theory, equations for the nonlinear perturbation of the electron distribution function and for the subsequent nonlinear modification of plasma heating were derived, and they were solved analytically in the approximation of cold collisional plasma. It was shown that the nonlinear effect of the electromagnetic field on plasma heating is mainly due to the RF magnetic field, and occurs at moderate collisionality of plasma electrons, $\nu_{en} \lesssim \omega$. For highly collisional plasma, when $\nu_{en} \gg \omega$, the electron distribution function is highly isotropic, and the nonlinear effect of the RF magnetic field vanishes, leaving only the nonlinear effect of the RF electric field. In the moderately collisional regime $\nu_{en} \lesssim \omega$ the magnetic component of the RF electromagnetic field leads to a nonlinear enhancement of heating at low frequencies, followed by a nonlinear reduction of heating at higher frequencies; this nonlinear modification of plasma heating, however, does not eliminate the effect of heating reduction at low frequencies predicted by our linear theory. The nonlinear effects vanish at high frequencies of the electromagnetic wave, $\omega \gg e/m_e E_0 \nu_{en} \delta / v_{Te}^2$, and the plasma heating at these frequencies is well described by the linear kinetic theory developed in Chapter 3.

In order to verify the effect of reduction of plasma heating at low frequencies, as well as to investigate the nonlinear effects of the RF magnetic field on plasma heating for arbitrary field amplitude, we developed the 1d3v PIC code with electron-atom and electron-electron collisions as a tool for numerical simulations of ICP discharge in nonlocal regime. This code is not fully self-consistent, as it uses the prescribed electromagnetic field profile, instead

of calculating it self-consistently from the Maxwell's equations with the charge and current density measured during the simulation. The electron-atom collisions, that are the primary collisions in ICP discharges, were implemented into the code using the direct Monte-Carlo technique, and the electron-electron collisions, that drive the electron distribution towards Maxwellian, were implemented using the stochastic Langevin equation (see Chapter 5, p. 99 for more details). The simulation results confirmed the results of our linear theory. In particular, the effect of relative reduction of plasma heating compared to the purely collisional value at low frequencies has been confirmed. The nonlinear effect of the RF magnetic field on plasma heating was investigated using the PIC code for the cases of weak and strong nonlinearity, that correspond to the weak and strong electromagnetic field, respectively. It was shown that in the case of weak nonlinearity the effect of the RF magnetic field on heating of warm plasma qualitatively agrees with the prediction of the quasilinear theory for cold collisional plasma, suggesting that the electron thermal motion does not have a significant impact on the nonlinear effect in case of weak fields. In the case of strong nonlinearity, which is beyond the scope of the quasilinear model, the nonlinear effects lead to a further (compared to the linear model) reduction of plasma heating at low frequency, thus enhancing the effect of relative heating reduction at low frequencies predicted by the linear theory.

One of the directions of the future research is the modification of the linear theoretical model to account for the nonhomogeneity of plasma density, making the ICP model more realistic. Also it would be desirable to account for the ion motion in the PIC simulation code when studying the low frequency modes of discharge operations, since the dynamics of ions, especially at low frequencies, may play a significant role on plasma heating and ponderomotive force.

The further development of the PIC simulation code should include implementation of the Maxwell's equations solver for the electromagnetic field in order to make the field profile self-consistent. A more sophisticated procedure for electron-atom collisions could also be included, using the realistic atom

cross-sections for various gases. To reduce the noise, inevitably occurring in electrostatic plasma potential due to using of the Poisson solver, as well as to reduce the computational time for high plasma densities of the order of $10^{10} - 10^{12}$ cm^{-3}, a different technique for calculation of the electrostatic field, based on the plasma quasineutrality, should be implemented (see, for example, [72] (page 66), [73], [74] for more details).

Correct value of the ponderomotive force in warm inductive plasmas is of practical importance for operation and modeling of ICP discharges. As it was shown, for typical parameters the ponderomotive potential in ICP in nonlocal regime is of the order of plasma electron temperature, therefore it can significantly modify ambipolar potential. Note that the classical cold plasma expression predicts the ponderomotive potential of the order of 80 V, which would have a major impact on the plasma density profile. Therefore, in order to have a correct plasma density profile, the effect of the thermal reduction described by our theory should be included in models of ICP discharges in nonlocal regime. Also, the newly predicted effect of reduction of total heating compared to the purely collisional heating at low frequencies in nonlocal regime should be kept in mind when designing the low-frequency discharges with strong electric field inhomogeneity.

Another result of our work is analysis of importance of the nonlinear effect of the RF magnetic field on plasma heating, which is usually neglected in theoretical descriptions. We have shown that the plasma heating is well described by the linear theory at high frequencies $\omega \gg e/m_e E_0 \nu_{en} \delta / v_{Te}^2$, while at lower frequencies the nonlinear effects become significant and should be accounted for. Our results indicate that further analytical and numerical studies of strongly nonlinear regimes are warranted.

An important result of this work is also the development of the 1d3v PIC code with collisions, which is a powerful tool for conducting numerical experiments. This PIC code can be applied for other problems where the simulation of one-dimensional warm plasmas with collisions is required. It can also be fur-

ther developed to perform simulations of two-dimensional plasma discharges with realistic conditions.

References

[1] F. Chen, Phys. Plasmas **8**, 3008 (2001).

[2] E.S. Weibel, Phys. Fluids **10,** 741 (1967).

[3] V.I. Kolobov, and D.J. Economou, Plasma Sources Sci. Technol. **6,** R1-R17 (1997).

[4] V.A. Godyak, R.B. Piejak, and B.M. Alexandrovich, Phys. Plasmas **6,** 1804 (1999).

[5] M.A. Lieberman, and V.A. Godyak, IEEE Trans. Plasma Sci. **26**, 955 (1998).

[6] N.S. Yoon, S.S. Kim, C.S. Chang, and D-I. Choi, Phys. Rev. E **54**, 757 (1996).

[7] R.H. Cohen and T.D. Rognlien, Plasma Sources Sci. Technol. **5**, 442 (1996).

[8] B.B. Kadomtsev and O.P.Pogutse, Sov. Phys.-JETP **39**, 269 (1984).

[9] L.D. Landau, Sov. Phys. JETP **10**, 25 (1946).

[10] R.A. Demirkhanov, Sov. Phys. JETP **10**, 25 (1946).

[11] G.E.H. Reuter and E.H. Sondheimer, Proc. Roy. Soc. (London) **A195,** 336 (1948).

[12] Yu.S. Sayasov, Helv. Phys. Acta **58,** 288 (1979).

[13] J.P. Matte, and K. Aguenaou, Phys. Rev. A **45**, 2558 (1992).

[14] S. Rauf, and M. Kushner, Plasma Sources Sci. Technol. **6**, 518 (1997).

[15] R.H. Cohen and T.D. Rognlien, Phys. Plasmas **3**, 1839 (1996).

[16] T. Shoji, Y. Sakawa, K. Tsuji, T. Watari, and K. Finken, J. Nucl. Mater **220-222**, 483 (1995).

[17] V. Godyak, R. Piejak, B. Alexandrovich, and A. Smolyakov, Plasma Sources Sci. Technol. **10,** 459 (2001).

[18] C. Chung, S-H. Seo, and H-Y. Chang, Phys. Plasmas **7,** 3584 (2000).

[19] T.W. Johnston, RCA Rev. **20**, 571 (1960).

[20] G. Schmidt, *Physics of High Temperature Plasmas*, 2nd ed. (Academic, New York, 1979), p. 47.

[21] V.A. Godyak, R.B. Piejak, and B.M. Alexandrovich, Phys. Rev. Lett. **83,** 1610 (1999).

[22] M.A. Miller, Radiophysics **1**, 110 (1958) (in Russian).

[23] A.N. Kondratenko, *Penetration of Electromagnetic Field into Plasmas* (Atomizdat, Moscow, 1979), p. 43 (in Russian).

[24] K.C. Shaing, Phys. Plasmas **3,** 3300 (1996).

[25] A.B. Pippard, Proc. Roy. Soc. **A191,** 395 (1947).

[26] A.B. Pippard, Physica **15,** 45 (1949).

[27] A.B. Pippard, Proc. Roy. Soc. (London) **A224,** 273 (1954).

[28] V.P. Silin, Trans. Phys. Inst. Acad. Sci. USSR **6,** 199 (1955).

[29] P.L. Bhatnagar, E.P. Gross and M. Krook, Phys. Rev. **94**, 511 (1954).

[30] V.A. Godyak, and R.B. Piejak, J. Appl. Phys. **82,** 5944 (1997).

[31] V.A. Godyak, and V.I. Kolobov, Phys. Rev. Lett. **79,** 4589 (1997).

[32] V.A. Godyak, R.B. Piejak, B.M. Alexandrovich, and V.I. Kolobov, Phys. Rev. Lett. **80,** 3264 (1998).

[33] G.G. Lister, Y-M. Li, and V.A. Godyak, J. Appl. Phys. **79,** 8993 (1996).

[34] V.A. Godyak, R.B. Piejak, and B.M. Alexandrovich, J. Appl. Phys. **85,** 3081 (1999).

[35] M.A. Liberman and A.J. Lichtenberg, *Principles of Plasma Discharges and Material Processing* (Wiley, New York, 1994), pp. 390, 555.

[36] V. Vahedi, M.A. Lieberman, G. DiPeso, T.D. Rognlien, and D. Hewett, J. Appl. Phys. **78**, 1446 (1995).

[37] G.W. Kentwell, and D.A. Jones, Phys. Rep. **145**, 319 (1987).

[38] H. Akama and M. Nambu, Physica **116A**, 155 (1982).

[39] H. Schamel and Ch. Sack, Phys. Fluids **23**, 1532 (1980).

[40] R.E. Aamodt, and M.C. Vella, Phys. Rev. Lett. **39**, 1273 (1977).

[41] H. Schamel, and G. Schmidt, J. Plasma Phys. **24**, 149 (1980).

[42] H. Schamel, Phys. Rev. Lett. **20**, 1339 (1979).

[43] P. Mora, and R. Pellat, Phys. Fluids **22**, 2408 (1979).

[44] F.A. Haas, Plasma Sources Sci. Technol. **10**, 440 (2001).

[45] Yu.O. Tyshetskiy, A.I. Smolyakov, V.A. Godyak, Plasma Sources Sci. Technol. **11**, 203 (2002).

[46] Yu.O. Tyshetskiy, A.I. Smolyakov, V.A. Godyak, Phys. Rev. Lett. **90,** 255002 (2003).

[47] A. Smolyakov, V. Godyak, and Y. Tyshetskiy, Phys. Plasmas **8**, 3857 (2001).

[48] G. Schmidt, Phys. Lett. A **74**, 222 (1979).

[49] I.D. Kaganovich, Sov. Tech. Phys. Lett. **19**, 276 (1993).

[50] A.I. Akhiezer, I.A. Akhiezer, R.V. Polovin, A.G. Sitenko, and K.N. Stepanov, *Plasma Electrodynamics* (Pergamon Press, Oxford, 1975), Vol. 2.

[51] Yu.M. Aliev, V.Yu. Bychenkov, A.V. Maximov, and H. Schlüter, Plasma Sources Sci. Technol. **1**, 126 (1992).

[52] Yu.M. Aliev, I.D. Kaganovich, and H. Schlüter, Phys. Plasmas **4**, 2413 (1997).

[53] U. Kortshagen, H. Schlüter, and A. Shivarova, J. Phys. D: Appl. Phys. **24**, 1571 (1991).

[54] A.B. Langdon, Phys. Rev. Lett. **44**, 575 (1980).

[55] J.P. Matte, M. Lamoureux, C. Moller, R.Y. Yin, J. Delettrez, J. Virmont, and T.W. Johnston, Plasma Phys. Controlled Fusion **30**, 1665 (1988).

[56] V.A. Godyak, and V.I. Kolobov, Phys. Rev. Lett. **81**, 369 (1998).

[57] O.V. Batishchev, V.Yu. Bychenkov, F. Detering, W. Rozmus, R. Sydora, C.E. Capjack, and V.N. Novikov, Phys. Plasmas **9**, 2302 (2002).

[58] A.A. Batishcheva, O.V. Batishchev, M.M. Shoucri, S.I. Krasheninnikov, P.J. Catta, I.P. Shkarofsky, and D.J. Sigmar, Phys. Plasmas **3**, 1634 (1996).

[59] C.K. Birdsall, and A.B. Langdon, *Plasma Physics via Computer Simulation*, IoP, 1998.

[60] J.M. Dawson, *Particle Simulation of Plasmas*, Rev. Mod. Phys. 55(2), 403-445 (1983).

[61] J.P. Boeuf, and E. Marode, J. Phys. D. **15**, 2169 (1982).

[62] M. Kushner, *Monte Carlo Methods for Electron Transport*, ICOPS Minicourse on Plasma Modeling, 29th IEEE International Conference on Plasma Science, Banff, Canada (2002).

[63] L.G.Christophorou, and J.K. Olthoff, J. Chem. Phys. Ref. Data **27**, 1-29 (1998).

[64] M.N. Rosenbluth, W.M. MacDonald, and D.L. Judd, Phys. Rev. **107**, 1 (1957).

[65] D.C. Montgomery, and D.A. Tidman, *Plasma Kinetic Theory* (McGraw-Hill, New York, 1964), pp. 15-24.

[66] N.A. Krall, and A.W. Trivelpiece, *Principles of Plasma Physics* (McGraw-Hill, New York, 1973), Chap. 6.

[67] S. Chandrasekhar, Astrophys. J. **97**, 255 (1943).

[68] M.E. Jones, D.S. Lemons, R.J. Mason, V.A. Thomas, and Dan Winske, Journal of Comput. Phys. **123**, 169 (1996).

[69] S. Chandrasekhar, Rev. Mod. Phys. **15**, 1 (1943).

[70] W.H. Press, S.A. Teukolsky, W.T. Vetterling, B.P. Flannery, *Numerical Recepies in C: The Art of Scientific Computing* (Cambridge University Press, ISBN 0-521-43108-5), Chap. 7.

[71] I.D. Kaganovich, Phys. Rev. Lett. **82**, 327 (1999).

[72] F.F. Chen, *Introduction to Plasma Physics* (Plenum, New York, 1974).

[73] G. Joyce, M. Lampe, S.P. Slinker, and W. Manheimer, J. Comput. Phys. **138**, 540 (1997).

[74] F. Detering, Ph.D. Thesis, University of Saskatchewan, 2002.

Appendix A

Parameters of the Electromagnetic Field Profile in Plasma

In our theoretical model (Chapter 3) we have assumed an exponentially decaying profile of the electromagnetic field $E, B \sim \exp\left(-x/\delta + i\kappa x\right)$ with free parameters δ and κ that should be given "externally". The ratio κ/δ^{-1} is defined by the surface impedance $Z_H = E_y(0)/B_z(0)$, namely $\kappa/\delta^{-1} = \mathrm{Re}\left(Z_H\right)/\mathrm{Im}\left(Z_H\right)$. In the case of collisionless skin effect the ratio $\kappa/\delta^{-1} = 1/\sqrt{3} \approx 0.58$ (see Eq. (2.21)), i.e. κ and δ^{-1} are of the same magnitude in collisionless nonlocal regime. However, if the collisions are taken into account, the ratio κ/δ^{-1} becomes significantly smaller for $\omega \lesssim \nu_e < v_{th}/\delta$ (this condition is typically satisfied in ICP discharges in nonlocal regime), as follows from the surface impedance calculated self-consistently [2, 23, 24]. This is consistent with the estimate of κ/δ^{-1} from the experimental data described below.

To estimate the actual ratio κ/δ^{-1} in the experiment we calculate κ from the discharge absorbed power, and compare it to δ^{-1}, where δ should be taken from the experimental data (typically a few cm). The relation between κ and the discharge power can be obtained from consideration of the Poynting flux of

the wave in plasma $S = c/4\pi \langle E_y B_z \rangle = (c/8\pi)(\kappa/\omega)|E_y|^2$, which is absorbed by the plasma. The discharge absorbed power is $P = S \cdot A$, where $A = \pi R^2$ is the surface area of the discharge (R is the chamber radius). Then we get

$$\kappa = \frac{8\pi\omega}{c^2 E_0^2} \frac{P}{A},$$

where E_0 is the electric field amplitude. For example, taking the discharge power $P = 100$ W, the driving frequency $\omega = 6.78$ MHz, the amplitude value of electric field $E_0 = 1.87$ V/cm, the chamber radius $R = 10$ cm, we get $\varkappa \sim 0.1$ cm^{-1}, while $\delta \sim 2.44$ cm (experimental value), and thus $\varkappa/\delta^{-1} = 0.25$ (note that in this experiment the collisions are not negligible, $\nu_{en} \sim 4 \cdot 10^6$ s$^{-1} \sim \omega$). With a typical discharge power of 50-100 W, magnitude of electric field of 1 V/cm, chamber radius of 10 cm, driving frequency of few MHz and δ of a few cm, the ratio κ/δ^{-1} is a small number, in the range 0.1-0.3.